Benchmarking of the Biomechanical Characteristics of Normal and Degraded Articular Cartilage to Facilitate Mathematical Modelling

Hayley Moody

B.Sc (Physiology)

B.Ed (Secondary)

This thesis was submitted as a requirement for the degree of

Masters by Research

School of Engineering Systems

Faculty of Built Environment and Engineering

Queensland University of Technology

Brisbane 2006

Keywords

Articular cartilage; Enzyme Degradation; Compression; Hyperelasticity; Fracture Mechanics

Abstract

In order to validate the appropriate functional characteristics of cartilage, we need to systematically study and understand what constitutes normality and degradation in cartilage. This thesis provides an important step in this direction.

To understand the mechanical repercussions of disruption to the matrix properties, cartilage is often artificially degraded using common enzymes. Although the process of artificial degradation does not provide an accurate representation of osteoarthritis, it can provide insight into the biomechanical properties of single matrix components by examining the behaviour of the tissue following its removal. Through histological analysis utilising the optical absorbance measurements of Safranin O stain, this work has demonstrated that for a given time and enzyme concentration, the action of Trypsin on proteoglycans is highly variable and is dependent on:

- The initial distribution and concentration of proteoglycans at different depths

- The intrinsic sample depth

- The location in the joint space, and

- The medium type.

These findings provide initial data towards a mathematical model which researchers can use to optimise Trypsin treatment of articular cartilage, and therefore model degeneration in vitro with a better degree of certainty.

The variability noted in the distribution and concentration of proteoglycans, and most likely the collagen network, creates a large variation in the compressive and tensile stiffness of all samples, and total failure strain energy. The average values for each of these tests indicate that a loss of proteoglycan through Trypsin treatment results in

decreased compressive stiffness, increased tensile stiffness, and little change to the failure strains or total failure strain energy. Conversely, disruption to the collagen network shows increased compressive and tensile stiffness, as well as failure strain and total failure strain energy. Due to the large variation in the results for each treatment group, the average values for the treated samples fall within the range of results for normal cartilage. These values cannot therefore be used as dependable parameters to benchmark cartilage, since the parameters for artificially degraded cartilage are within the normal levels. The Yeoh and Polynomial hyperelastic laws were found to best represent the material characteristics of cartilage across the range of tested samples, regardless of differences in health and strength.

The results presented here provide important insight into the biomechanical outcomes of artificial degradation and provide direction for future research in this area.

Table of Contents

List of Figures

List of Tables

List of Symbols and Abbreviations

PLM	=	Polarised Light Microscopy
λ	=	bulk ratio of stretches
σ	=	strain energy per unit volume
W	=	strain energy potential
μ	=	initial shear modulus
φ	=	swelling constant
I	=	deviatoric strain invariant
C_{ij}	=	material constants for the hyperelastic strain energy equations
D_i	=	material constants for the hyperelastic strain energy equations
a_i	=	material constants for the hyperelastic strain energy equations
$\sum$	=	sum

Publications

Moody H.R., Oloyede A.O., Bowden J.C., Brown C.P., McElwain D.L.S, Crawford R.W. (2006) In vitro degradation of articular cartilage – does Trypsin treatment produce Consistent Results? *Journal of Anatomy*, **209**. 259-268.

Moody H.R., Oloyede A.O., Nugent, T., McElwain D.L.S. Assessment of common hyperelasticity constitutive equations for normal and degraded articular cartilage. *Submission imminent*.

Brown C., Oloyede A., Moody H., Crawford R. (2005) New directions for the characterisation of cartilage health in vivo. *In Proceedings Third IASTED International Conference on Biomechanics*, pp. 307-310, Spain.

Nugent T.C., Oloyede A.O., Moody H.R., McElwain D.L.S. Mathematical modelling of the mode of action of Trypsin. *Submission imminent*.

Statement of Original Authorship

The work contained in this thesis has not been previously submitted for a degree or diploma at any other higher education institution. To the best of my knowledge and belief, the thesis contains no material previously published or written by any other person except where due reference is made.

Signature……………………………..
Date………………………………..

Acknowledgments

This work has required a multidisciplinary approach, and as such has demanded the assistance of many generous people from different faculties and departments.

To my principal supervisor, Associate Professor Kunle Oloyede, I extend my sincere gratitude for this tremendous opportunity to prove to myself, that I am capable of anything I put my mind to. You have provided me with a great deal of support and trust in my ability to achieve anything, and I will always be grateful for that.

Thank you also to my associate supervisors, Professor Sean McElwain, Professor Ross Crawford and Dr Prasad Gudimetla, who provided me with assistance along the way, and challenged my findings and analyses to make me a more critical and thoughtful researcher.

Thank you to Christina Theodoropoulos and Deb Stenzel for their help and support with histology. Your friendly smiles and conversations made this one of the most enjoyable parts of my work. Also to Don Geyer and Joseph Kan, thank you for your histology training and continued technical advice. A special thank you to Sally Gardner and Josh Bowden, for your collaboration. And, Greg Tevelen, Kimble Dunster and Melissa Johnston, without whom no work could ever be done!

A big thank you to Cameron Brown who not only provided me with a lot of technical knowledge and assistance, but also brought me back down to reality every day with a delicious hot chocolate and made this whole experience a much more enjoyable one! My sincere thanks to Thanh Nugent who provided me with much needed

mathematical support, and always with a smile. Also a thank you to Helen Cunningham and Katrina McDonald for your help with my work.

Finally to my family. Ian, who has provided me with the most amazing support and encouragement I could have ever asked for. Mum and Dad, Dan and Ang for always supporting my decisions and being proud of absolutely everything I do. And Fay and Allan for your continued support.

1 Introduction

The general day to day functions of mammals including walking, lifting, and most conceivable movements about an articulating joint, are made smooth and pain free through the presence of a complex soft tissue designed to cover and protect the ends of articulating bones. Articular cartilage plays this functional role despite its very small thickness of 2-4mm, through an intricate structural arrangement and matrix properties (Figure 1.1).
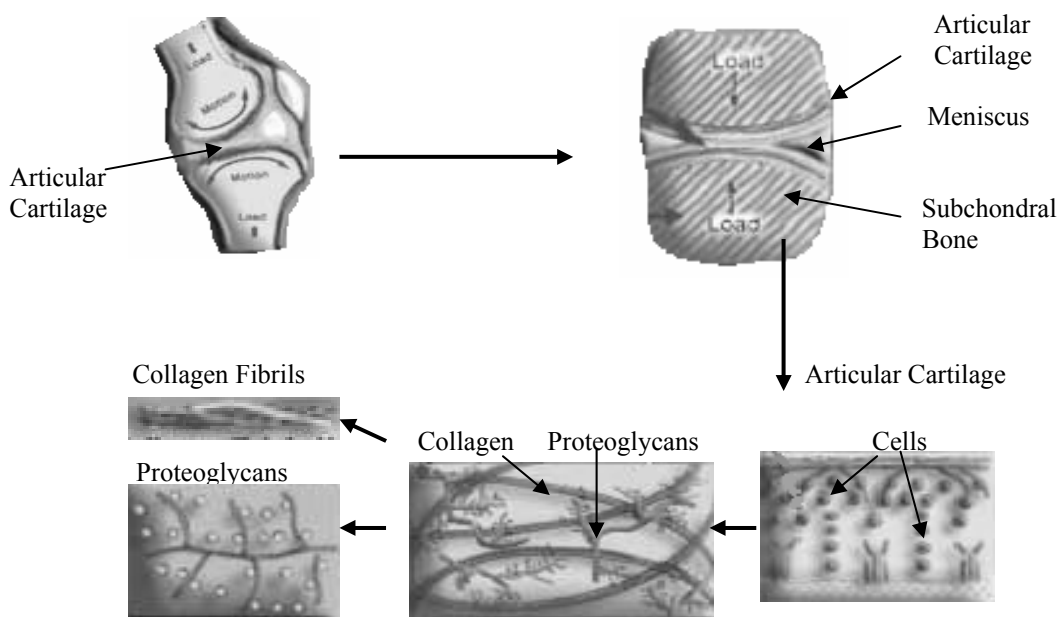
Figure 1.1 The constituents of Articular Cartilage. Articular cartilage in the knee joint (clockwise from top left), closer view of synovial joint, the distribution of cells across the entire cartilage thickness (representative of the collagen arrangement), interaction of the main matrix constituents, and the individual collagen fibrils and proteoglycan branches (adapted from (1)).

The precise arrangement of collagen fibrils and water bound proteoglycans throughout the different depths of cartilage, allow this tissue to provide a well lubricated, low friction bearing surface that is able to distribute loads across a greater area onto the underlying subchondral bone. During static or slow loading, this

function is achieved through a spreading of energy across a taut network of collagen fibrils in the surface area of the cartilage and the deeper zones, and the gradual exudation of the fluid within the tissue. Under sudden impact, the fluid is trapped by the immediate tension in the collagen fibrils, resulting in a small elastic deformation.

Articular cartilage undergoes millions of cycles of these static, squasi-static and impact loading regimes over a person's lifetime. However due to sudden impact blows, ageing or disease, a cascade of degenerative changes may begin to take place, eventually resulting in a complete wearing away to bone causing great pain to the individual. The affects of this degenerative process is of particular importance due to the large population affected. According to the National Health Survey (2), there were 1.39 million people reported to have osteoarthritis in 2001, that is 7.3% of Australia's population, and was reported to have increased to 7.8% in 2004 (3). Osteoarthritis alone was reported to have accounted for $1.4 billion of the total national health expenditure in Australia in 2004, for direct costs (3). This does not include indirect costs associated with Osteoarthritis, or costs from pain and suffering. With an ageing population, and prevalence of osteoarthritis reaching almost 32% in Australia's population over 75, the impact of this disease will become increasingly greater, with an expected 26% increase in the prevalence for all ages by 2020 (3).

Due to the great economic and burdening impact on the population, the study of osteoarthritis and other degrading processes in articular cartilage has been explored extensively. As a result, there have been great advancements in the understanding of the biochemical, anatomical, physiological and biomechanical properties of the tissue, which has lead to the development of artificial tissue models, neocartilage for replacement of damaged cartilage, and analytical instruments for the determination

of cartilage health in vivo. However due to the highly anisotropic nature of the articular cartilage, there is still much to discover about the tissue.

Previous research has explored the biomechanical properties of cartilage for both normal and degenerate states of health. In order to accomplish this, researchers have used osteoarthritic or artificially degraded cartilage using collagen and proteoglycan specific enzymes. Although osteoarthritic samples provide realistic models of cartilage degeneration, it is often difficult to obtain samples from similar stages of degeneration. To overcome this problem, many researchers use enzymes to artificially degrade specific properties of the cartilage. This may produce a more uniform and therefore less realistic degradation across entire surfaces than would be expected in osteoarthritic samples. Artificial degradation is merely an idealisation of what can happen in-vivo due to disease processes; however, it does provide the advantage of allowing degradation of specific matrix components, to a desired level of degradation. This enables a greater specificity in distinguishing between the roles of each matrix component and how they relate to other components, and an ability to observe these factors at different structural depths throughout the cartilage.

Although there has been extensive work conducted in artificial degradation of cartilage, there is great variation in the enzyme use, leading to the question of what is the desired enzyme and concentration to obtain the desired degradative effects. This is the first question that requires attention in order to apply this method to exploring the biomechanical properties of cartilage in laboratory simulated degradation. The work presented here shows the effect of two different mediums used for degradation, and exposes the variability in the mode of action of the enzyme, determined by the

3

variation in the matrix properties, which act as a rate limiting step. This mode of action can be represented mathematically to allow for more accurate and cost effective methodologies for researchers. Work towards this modelling is presented here.

The biomechanical properties of interest to articular cartilage researchers include the stiffness of cartilage due to dynamic and static loads, porosity and permeability during consolidation/deformation and the stiffness in tension and related behaviour during crack propagation. The data obtained from these experiments provide information to aid in understanding the behaviour of cartilage mechanics, to be able to create mathematical models and obtain tissue parameters, for example numerical analysis. Although there has been extensive work performed on crack propagation in normal cartilage, there has been none on degenerate cartilage.

Crack propagation has previously been studied using fracture mechanics. This provides information on the behaviour of the matrix properties in tension, and insight into how cracks grow throughout the different depths of cartilage. Previous research into fracture mechanics has explored the propagation of cracks in normal cartilage. The fracture toughness of all materials and tissues are determined by their specific composition. Due to the anisotropic and heterogeneous nature of the cartilage, the toughness varies throughout the depths of tissue, depending on the concentration and alignment of the matrix properties. Given that the propagation of surface cracks has been associated with the development and progression of osteoarthritic cartilage, it is of great importance to determine how fractures propagate in diseased tissue, with an alteration in these toughness determining matrix properties. This thesis is aimed at

determining the effects of collagen disruption and proteoglycan degradation through artificial enzyme degradation, in order to understand how these properties alter the propagation of cracks. It is expected that this information should provide insight into the development of cracks in diseased tissue where collagen fibrillation is prominent, and proteoglycan numbers are depleted.

In order for the data obtained from this work to be useful in providing a holistic model of the intricate biomechanical functions, this thesis will also report on the comparative analysis of the response of normal and degenerate cartilage samples subjected to compressive loading, and thereby determine the hyperelastic relationships describing these types of tissue. Hyperelasticity describes the large non-linear response of a tissue to loading, and it is this behaviour that may influence the cracking mechanism, through the limiting of the speed at which the cracks grow by altering the local energy available at the crack tip.

The objectives of this thesis are to present and compare parameters that can be used to benchmark the biomechanical characteristics of normal and degraded articular cartilage through:

- The development of a methodology for controlling and quantifying the artificial degradation of cartilage to study the biomechanical effects of levels of particular types of degradation and the effects of structural integration on articular cartilage properties (Chapter 3)
- Studies of elastic deformation mechanics of normal and artificially degraded articular cartilage to determine the representative existing stress-strain law(s) that describe the tissue (Chapter 4)

- The determination of the effects of artificial degeneration on cartilage fracture properties (Chapter 5)

2 Articular Cartilage Structure and Biomechanics – A Literature Review

2.1 Introduction

Articular Cartilage is a soft, translucent tissue covering the ends of articulating bone in the synovial joints of mammals for the purpose of transmitting high loads with very little frictional resistance (Figure 2.1). Human cartilage varies in thickness from approximately 2-4mm (4) depending on the joint, location on the bone, the size of the individual, species and the health state of the tissue. The cartilage remains virtually intact throughout a lifetime of activities, and requires mechanical stimulation for development and homeostasis (5). However, once damaged the cartilage has limited ability to repair itself due to an absence of nerves, blood vessels and lymph nodes, and may undergo degenerative pathological changes, leading to diseases such as osteoarthritis.

This figure is not available online.
Please consult the hardcopy thesis available from the QUT Library

Figure 2.1 Articular cartilage of the knee joint (6)

Articular cartilage is a highly complex, anisotropic material, differing in its component concentration, distribution and arrangement in every direction. It is therefore important to first understand the architecture of the tissue in order to understand how the tissue responds biomechanicaly to stimuli.

2.2 Articular Cartilage Architecture

Articular cartilage is made up of a gel like matrix containing up to 80% water content and specialised cells called chondrocytes. Although the matrix and the cells are structurally separate, they rely on each other to function. The chondrocytes are responsible for the synthesis of the matrix, and the matrix in turn maintains the homeostasis of the cells' environment. The mechanical properties and therefore the function of cartilage are determined by the entrapment of fluid swollen proteoglycans by collagen meshwork which makes up the bulk of the matrix.

2.2.1 The Matrix

The matrix is composed mainly of proteoglycans, a meshwork of collagen fibrils, and water (Figure 2.2). It is the interplay between these that form the stiff gel-like structure and is responsible for the mechanical properties of cartilage (7). The matrix also contains small amounts of inorganic chemicals and lipids (4).

The matrix components are not uniformly distributed throughout the tissue, but rather vary according to depth beneath the surface and distance from the chondrocytes. The highly anisotropic structure of zonal and compartmental differentiation of the physico-chemical properties of the matrix, account for its stress dispersing properties.

8

This figure is not available online.
Please consult the hardcopy thesis
available from the QUT Library

Figure 2.2 The Articular Cartilage matrix largely contains collagen fibrils, proteoglycans and water. The properties and relationship of these components determines the mechanical response of the cartilage (8).

2.2.1.1 Anatomical Classification

2.2.1.1.1 Zonal Classification

Based on the development of joints (9) and the distribution of chondrocytes and matrix components throughout the tissue, articular cartilage can be divided into four parallel zones. The superficial or tangential zone (10-20% of the total thickness) lies at the surface of the cartilage, adjacent to the joint cavity. An abundance of collagen fibrils arranged in a multidirectional plane (10), parallel to the surface (11) makes up most of the matrix in this layer, with only a small amount of proteoglycans visible. Chondrocytes appear small and oval in appearance, and are concentrated throughout the layer in an undefined pattern (Figure 2.3).
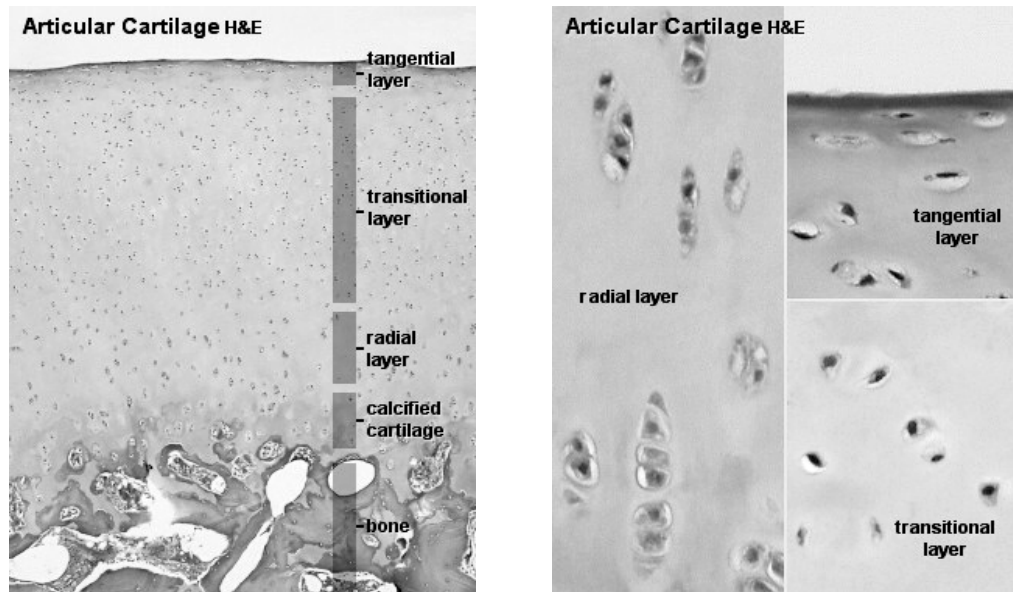
Figure 2.3 Articular cartilage stained with Haematoxylin and Eosin stain, showing the cell distribution and size in each of the four zones. Cells are flattened and small in the articular surface (tangential layer), and increase in size towards the deeper zones, while forming horizontal clusters (12).

As the tissue merges into the intermediate, transitional or midzone (40-60% of the total thickness), the collagen fibrils begin to change from a lateral to a more radial orientation, and become less dense. The architecture of the collagen is commonly known as the Benninghoff arcade (13) (Figure 2.4). Conversely to the collagen, the proteoglycans increase in number as they move towards the subchondral bone. The chondrocytes become larger and spherical, and more equally spaced throughout the matrix, however the cell numbers decrease dramatically between the articular surface and the intermediate zone (14) (Figure 2.3).

In the third, deep or radiate layer (30% of the total thickness), the collagen fibrils are arranged in a radial orientation (11), encapsulating the many proteoglycans. The chondrocytes begin to arrange into columnar groups of 4-8 cells (4) (Figure 2.3).

This figure is not available online.
Please consult the hardcopy thesis
available from the QUT Library

Figure 2.4 The Benninghoff arcade describes the arrangement of the collagen network throughout the 4 zones, denoted by I, II, III and IV. The line indicated by the arrow represents the tidemark (15).

The fourth layer or calcified zone connects the cartilage to the subchondral bone and is distinct by its calcification, compared to the uncalcified layers above. This zone is marked by a basophilic line, designated the tidemark, which is proposed to help prevent the shear fatigue fracture of collagen (11, 16). It contains few cells, and the matrix is concentrated with crystals of calcium salts.

2.2.1.1.2 Compartmental Classification

Within the different zones of the tissue, cartilage can further be classified into compartments dependent upon the proximity to the chondrocytes. The tissue closest to and surrounding the cells is the pericellular matrix, which is devoid of regular collagen fibrils, containing only finely textured filaments. The pericellular matrix is encapsulated by a fine meshwork of collagen fibrils. During histological preparation, the cells are often lost leaving behind holes in the tissue called lacunae. Histological studies show dark staining in the cell lacunae walls (11), suggesting that collagen is densely organised around this area in what looks like a cell protecting mechanism

(14). Further away from the cell is the intercellular or territorial and inter-territorial matrix, which forms the bulk component of cartilage. The fibrils are considerably larger and coarser within this matrix, and account for the mechanical properties of the tissue.

The properties of the different compartments are not uniform across the different zones, but instead change depending on the depth from the surface and therefore the zone with which they are located. For example the fibrils found in the territorial matrix in the superficial zone have a diameter that is only a quarter of those found in the territorial matrix in the deep zone (17). The number of cells within lacunae also varies with respect to the zones, increasing in number and aligning radially towards the deeper zones.

2.2.1.2 Matrix Components

2.2.1.2.1 Collagen

There are at least 20 known types of collagen making up the different connective tissue within biological tissue including cartilage, tendons and ligaments, skin and muscle (18). Within cartilage, collagen type II is the most abundant form, accounting for 90-95% of the collagen in the matrix, and is responsible for its great tensile strength. This strength is attributed to the triple helical structure (18) (Figure 2.5) consisting of three left handed $\alpha 1$(II) polypeptide helices wound around each other in right handed twist (19). The oppositely twisting direction of the helices prevents the unravelling of the molecule under tension (18). Type XI collagen interacts with type II and is possibly involved in forming the fibril meshwork, and may control fibril diameter. Type X contains interrupted triple helices which are thought to form

bridges between the collagen and proteoglycans and is also found mineralised in the calcified zone of cartilage. Type VI collagen is microfibrillar, forming elastic fibrils that are in higher concentration surrounding the periosteum.
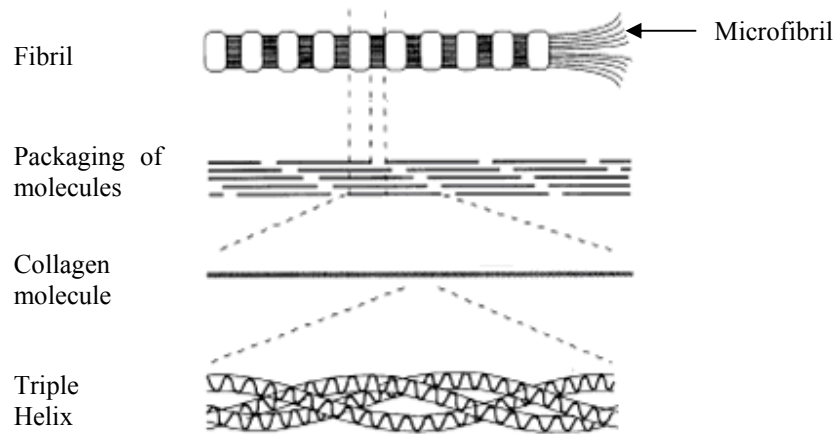
Figure 2.5 Structure of the collagen fibril. The collagen molecule is made up of three collagen threads wound in a triple helix. These microfibril molecules are then packaged to form strong fibrils, which appear as striated bands due to the overlap and hole zones in the packaged molecules (20).

Normal collagen is structurally characterised by an amorphous structure of fibrils of varying diameter. As the collagen fibrils extend throughout the matrix the fibrils are occasionally observed to run in parallel bundles over long and short distances, randomly entwined (21).

In the superficial zone, the collagen fibrils run parallel to the surface (11, 22). The study of split line direction has been used to determine the directional orientation of the collagen fibrils in the superficial zone (10, 11, 22-25). When the surface is pierced with an Indian ink charged pin, a longitudinal split line forms along this surface indicating the predominant direction of collagen fibrils in the surface layer.

There have been many contrasting interpretations of split line results as to the directional organisation within the articular surface. Studies involving split line propagation have reported definite alignment along split line direction (22), while

13

others have noted multidirectionality (10, 11). The articular surface is most strain limiting in tension along the split line direction, and least strain limiting across the split line (10, 26, 27). This means the tissue exhibits greatly increased stiffness along the split line than across it, with increasing strain or deformation. Some researchers have interpreted this result as an indication of the alignment of the fibrils within the articular surface (26, 27), while others hypothesise that the split line direction provides a measure of the ability of the fibrils to rearrange under loading (10).

2.2.1.2.2 The Proteoglycans

The predominant proteoglycan in articular cartilage consist of a protein core of hyaluronic acid covalently linked by link proteins to aggrecan monomers. The aggrecan consists of a core protein, attached to two types of glycosaminoglycans, keratin sulphate and chondroitin sulphate, giving aggrecan its bottle-brush form (Figure 2.6). The primary role of the aggrecan is to provide the cartilage with compressive stiffness (28). This is achieved by drawing positively charged water osmotically into the negatively charged proteoglycan branches, causing them to swell and resist compressive forces.

Perlecan is a large heparin sulphate proteoglycan found prominently in the pericellular matrix surrounding the chondrocytes and is suggested to promote cell adhesion, chondrocyte differentiation, cartilage and extracellular matrix maintenance (29). The small leucine-rich proteoglycans include fibromodulin, epiphycan, lumican, decorin and biglycan. These are thought to aid in cartilage maintenance through their interaction with the collagen network in binding growth factors and

contributing to the fixed charge density. In normal cartilage, proteoglycans are heterogeneous, varying in size and composition (30).
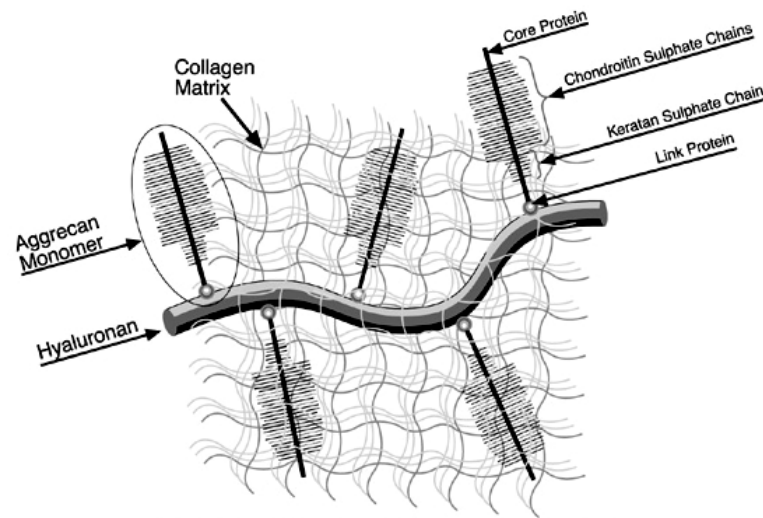
Figure 2.6 Partial proteoglycan molecule entangled in the collagen matrix. The proteoglycan consists of a Hyaluronic backbone, attached to many aggrecan monomers by link proteins. The glycosaminoglycans chondroitin sulphate and keratin sulphate are the glycosaminoglycans that result in the bottle brush form (31).

2.2.1.2.3 The Lipids

Lipids are found on the surface of articular cartilage, within the extra-cellular (32), and intra-cellular matrix, contributing to about 0.5 to 1.0% of the wet weight (33). Extensive research has explored the role of surface lipids in providing a boundary lubricant within the synovial joint, decreasing the frictional resistance and providing the hydrophobic properties of the articular surface (34-36). Also, intra-cellular lipids have been shown to have an effect on the stiffness of cartilage, with delipidization found to decrease strain of the matrix by 15-20% (37, 38).

2.2.1.2.4 The Chondrocytes

Chondrocytes account for between 3-10% of the cartilage volume, and are in no physical contact with each other, which in addition to the avascular, aneural and alymphatic properties of cartilage, results in a tissue that has a very limited and slow response to damage (39).

The primary role of the chondrocyte is to synthesise the matrix, and continue to remodel and replace the matrix of collagen and PG. During mechanical stimulation of articular cartilage, the matrix transmits signals to the chondrocyte to maintain the normal composition of the matrix. The synthetic activity of the chondrocytes also appears elevated in the presence of matrix fragments. When the joint is immobilised, the chondrocyte responds with the secretion of proteinases which breakdown the proteoglycans and collagen fibrils. This process of synthesis and degradation continues for many decades, until age, disease or environmental impacts lead to an imbalance in the chondrocytes breakdown of the matrix.

2.3 Biomechanics of Cartilage

2.3.1 Zonal Variations in Mechanical Properties

Articular Cartilage is anisotropic and therefore the mechanical response to loading is different in each zone. The superficial zone has an abundance of collagen fibrils aligned parallel to the surface (11), and a limited number of chondrocytes and proteoglycans, with limited interactions between macromolecules. This allows for greater fibril realignment during loading, creating a surface that is highly resistant to wear and tear. The parallel alignment of fibrils also strengthens the layer, greatly increasing the energy required for crack propagation through this layer (23, 40).

The change in collagen orientation and increase in proteoglycans sees a change in the deeper layers, to that of a load bearing role. Due to the orientation of the collagen fibrils, enclosing proteoglycan molecules, this zone responds to loading through the consolidation model.

The collagen fibrils are anchored into the calcified zone, which is thought to influence the nutrition of cartilage and increased stability to overcome shear stress (11, 16).

2.3.2 Variation across the Joint

Different areas of the joint are subject to different magnitudes of loading. We therefore see different concentrations of collagen and proteoglycans in areas under heavier/more direct loading than those with less. For example in areas with higher levels of compressive stress, there is a higher content of proteoglycans and therefore increased compressive stiffness.

2.3.3 Load Carriage

In normal, everyday activity the cartilage is subject to stresses in shear, compression, and tension. Shear stress is overcome by the concentrated arrangement of collagen fibrils in the articular surface. Stress caused by compression and tension are resisted by the interaction between the collagen fibrils and the proteoglycans.

Collagen fibrils form an intense meshwork, binding to and entrapping the proteoglycans into a structural gel. The highly negative concentration within the proteoglycans creates an osmotic pressure, causing the molecules to swell and resist

the initial compression of a load. As the stress increases, the cartilage deforms, causing the pores within the matrix to narrow, and the hydrostatic pore pressure to increase until equilibrium is reached. Over the next few minutes known as the creep phase, the remaining fluid is slowly squeezed out of the tissue until the load is carried by the collagen network. Once the load is removed, water is osmotically driven back into the negatively charged matrix.

Articular cartilage is a poroviscoelastic material, meaning it is saturated with fluid that flows relative to a deforming solid matrix. Therefore, cartilage responds differently to slow and impact loads (41). When a load is applied slowly to the tissue, the resultant deformation or strain is defined by a nonlinear elastic response. This is due to the consolidation of the tissue, where the initial load is carried by the water content, which gradually exudes out of the cartilage. The collagen fibrils also have time to realign in the direction of the stress in order to cope with a greater stress once the water has dissipated. However when cartilage is subjected to dynamic loading, there is an instantaneous load carriage by the stiffness, which is caused by the swelling of the proteoglycans. This more closely resembles a linear elastic model because the fluid cannot be released in the limited time available for deformation due to low permeability in the tissue.

2.3.4 Force Transmission

In healthy cartilage the surface layer is stretched across the curvature of the underlying subchondral bone. This creates a constant tensile pre-tension within the layer, which acts to transmit and dissipate stress during tensile, compressive and shear loading (42). When a load is applied in compression, the tissue deforms

laterally, increasing the load bearing contact areas and more evenly distributes the load being transferred to the underlying bone. Articular cartilage is then subjected to greater tensile stresses as it conforms to the newly exaggerated surface area.

As loads are applied to cartilage, the energy is stored within the superficial layer by the collagen type II fibrils. Due to the tensile pre-tension properties of this layer, the energy can be transmitted and dissipated to other parts of the matrix and the underlying bone (42). This also allows for the fluid to be expelled from the cartilage more uniformly during loading. However the exudation of fluid is also the major factor in decreasing the total amount of stored energy within the matrix.

2.3.5 Fracture Mechanics

Materials that are subjected to cyclic compressive and tensile forces over an extended period of time may at some point fail in the way of a crack in the material surface. The factors that generally lead to material failure include negligence in the design, construction, or operation of the material, and the application of new materials or designs with unexpected results (43). The same factors may be applied within biological tissue such as articular cartilage. Failure may be due to problems with the biological construction and maintenance, including inadequate nutrition, and genetic disorders, or negligence in the operation of the material such as repetitious heavy loading over long periods of time or impact blows.

In articular cartilage, failure is believed to be caused by abnormal loads on normal cartilage, and/or normal loads on abnormal cartilage (44). Fracture mechanics is a tool that provides information on how cracks may form, or how existing cracks

propagate through a material. This enables researchers to understand the properties of a material subject to tensile loading, and therefore gain further insight into how the components of the tissue effect the biomechanical functioning of the material. It is therefore important to investigate fracture mechanics of both healthy and osteoarthritic cartilage in order to gain a greater understanding of how failure occurs in this material.

2.3.5.1 Behaviour of Cracks in Normal Cartilage

Once a split or crack has been introduced into a material, the strength required for failure is greatly reduced. Stress will concentrate around the crack tip (Figure 2.7) so that even when the material is under low stress, the tip stress of the crack is much larger. This excess in stress at the tip may be enough to propagate the crack even under normal safe loads, leaving the material susceptible to failure. As a crack propagates, it creates a new surface (Figure 2.7), requiring strain energy stored in the bulk of the stressed specimen. The amount of energy required to create the given area of surface is dependent on the toughness of the material. As a result, cracks may propagate rapidly without any increase in stress and are said to exhibit unstable behaviour. Alternatively, cracks can propagate slowly with either an increase, decrease or no change in stress, which is termed stable behaviour.
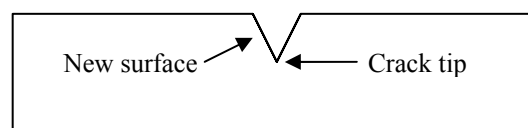
Figure 2.7 Stress concentrates around the crack tip, increasing the chance of propagation. As the crack propagates, a new surface is created.

Cartilage is an anisotropic material, consisting of 4 horizontal zones separated by a changing concentration and architecture of the matrix properties. As a crack propagates through the matrix from the articular surface, it develops in a non-

uniform behaviour, determined by the arrangement and concentration of the matrix properties. This can be seen in stress strain curves of crack growth in articular cartilage (Figure 2.8), which can be broken down into 5 stages (40):

1. Rapid opening by stretching

2. Prolonged steady (stable) opening of articular surface

3. Rapid (unstable) propagation through general matrix

4. Temporary cessation of unstable propagation, followed by brief period of stable propagation

5. catastrophic failure

This figure is not available online.
Please consult the hardcopy thesis
available from the QUT Library

Figure 2.8 Stress-Strain curve of crack growth in articular cartilage (40)

The articular surface appears to be the toughest zone for crack growth (23, 40, 45), denoted by the prolonged steady opening of the surface (stage 2). In this zone, the collagen fibrils are aligned parallel to the surface, rearranging in a predominant direction during tension (10). This arrangement of collagen constitutes the main resistance against tensile forces and the propagation of radial cracks. For a crack to grow, it must break through the large number of fibrils lined perpendicular to the

growth direction. The greater compliance of the articular surface therefore makes it more difficult for energy to be available for the crack root in the early stages, providing some protection against the propagation of minor surface cracks.

The crack growth becomes more rapid through the midzone and deep zones where collagen concentration is decreased, and the alignment of fibrils turns to a transverse and finally a radial direction towards the tidemark, and propagates until final failure. The predominantly radial direction of the fibrils enables the rapid growth through these deeper zones because the growth mainly involves the breaking of the increasing interfibril connections deeper down rather than the collagen type II fibrils (23). The toughness of the cartilage and therefore the resistance against crack growth appears to be primarily dependant upon the orientation and alignment of the collagen fibrils, in that cracks propagate more easily in the direction of the collagen fibrils (23, 40, 46, 47).

During normal loading, articular cartilage undergoes indentation, causing compression of the tissue towards the bone. However the tensile pre-tension causes lateral strain, causing the collagen fibrils in the surface zone to pull in tension, stretching the surface. If a small crack exists in this surface due to a high impact blow, or fibrillation from disease, the lateral spread of the surface will input energy to the crack, allowing it to propagate, leading to an eventual failure of the tissue over time.

Previous work has described the propagating crack and how the matrix components influence this growth; however there has been no research conducted on the

influence of the underlying bone with respect to crack propagation in cartilage, or on degenerate models of crack propagation. Diseased and damaged cartilage exhibits fibrillation, and impact blows may occur in the elderly following falls from instability. It is therefore important to determine how disruption to the collagen network and proteoglycan loss may influence the growth of cracks, and gain a realistic perspective of crack propagation in cartilage on bone.

2.4 Articular Cartilage Degeneration

2.4.1 Articular Cartilage Disease In Vivo

Cartilage is a highly resilient tissue which can withstand great stresses throughout a lifetime of activity. Like most tissues in the body, cartilage undergoes normal changes due to ageing, wear and tear, and disuse. However, because of its aneural, alymphatic and avascular properties, it has a limited ability to repair damaged tissue.

There is no known definitive cause of osteoarthritis, and research suggests that there may not be one or a set combination of biochemical and biomechanical causes that leads to the progression of the disease. Damage to cartilage may be induced by the natural wear and tear of the matrix from decades of use, change in the general activity or lifestyle, disuse, or rapid high energy impacts causing large cracks. Structural and biochemical changes may also occur in surrounding tissue, altering the mechanical loading of the cartilage. This may include damage to the subchondral bone, or joint instability from the rupture of the anterior cruciate ligament (48), causing a redistribution of loading and stress attenuation. These changes in cartilage may lead to a cascade of degenerative processes (49), involving the eventual alteration and loss of collagen, proteoglycans, chondrocytes and other non-

collagenous proteins. These degenerative symptoms are often classified as osteoarthritis, which is the most common form of arthritis, affecting 1.6 million Australians in 2004, almost half the total number of people affected by arthritis (3).

2.4.1.1 Biochemical Mechanisms of Cartilage Degeneration

Cartilage health is maintained by the regulation of equilibrium between the rate of synthesis and rate of degradation of the matrix by the chondrocytes (20). As a result of early stage disease, or as the first stage of disease itself, the chondrocytes send out signals to increase the synthesis of proteinases, and decrease proteinase inhibitors, causing an increase in matrix degradation and decrease in synthesis respectively.

In various levels of degenerate cartilage, there are often areas of normal, healthy looking tissue throughout the cartilage. While it may appear macroscopically healthy, the metabolic activity of the healthy tissue is actually similar to the diseased area, suggesting there is no healthy cartilage in a diseased joint (17). This suggests that once a lesion evolves either through biochemical or biomechanical causes, the spread of degradation may be facilitated through biomechanical signalling.

2.4.1.2 Mechanical Changes in Degenerate and Osteoarthritic Cartilage

Osteoarthritis is characterised by an early onset of surface fibrillation, increased swelling, a decrease in stiffness, loss in tensile strength, and an increase in tissue hydration and permeability, hypercellularity, followed by increased fissures, splitting, and hypocellularity, penetration of blood vessels through the tidemark region(50), until the eventual wearing away to bone. These characteristics have been

linked to degradation in collagen, proteoglycans (51), chondrocytes (52), and lipids(35).

In its degenerate state, the articular surface varies from that of a smooth, amorphous structure, to fibrillation, exhibited by rough crimping in the surface. In the early stages of degeneration, it appears that the destruction of the synovial fluid/lipid layer, and hence loss of the waxy, hydrophobic surface, accelerates the wear and progression of degeneration (35).

In contrast to normal, healthy tissue, osteoarthritic cartilage displays areas of transition between the normal directionless meshwork of fibrils to areas of strongly radial directed fibrils, with many fibrils aligning in parallel bundles, forming intense knotting and exposing large areas of open network (21). This may be caused by the loss of smaller collagen and proteoglycan molecules that function to bind collagen together, forming a tightly woven meshwork. The collagen fibrils are therefore less able to align in the direction of an applied stress, which in addition to the already fibrillated surface, decreases the tensile strength of the tissue. With a decrease in tensile strength, there is a diminished capacity for the superficial zone to distribute the energy across the entire tissue, and instead focuses the energy on specific points directly beneath the applied stress. This increases the stress normally applied to areas of tissue, increasing the chance of further damage here.

The degree of swelling in osteoarthritis is linearly correlated to the decrease in collagen (53). With the decrease of the swell limiting meshwork provided by the collagen fibrils, more water is able to bind to the proteoglycans, increasing tissue

hydration and therefore the amount of swelling. The open spaces formed by the tangled collagen meshwork also provide for an increased permeability that is less frictionally resistant against the exudation of fluid. These factors lead to a decrease in matrix stiffness (21, 53). Mechanically, the cartilage would not be able to support the same static and dynamic forces as healthy tissue.

2.4.2 Fracture of Degenerated Articular Cartilage

Osteoarthritis is characterised by a loss in proteoglycans and disruption to the collagen network, apparent as fibrillation and the appearance of microcracks in the surface. Once a crack appears in the cartilage, the constant loading through daily activities will increase the energy available to allow the crack to grow. Although crack propagation has been investigated extensively, there is no data on the behaviour of cracks in artificially degraded articular cartilage.

The propagation of cracks in articular cartilage is greatly determined by the changes in matrix constituents throughout the depths, therefore diseased cartilage will behave differently from normal cartilage due to the disruption of the collagen fibrils, and degradation of the proteoglycans. As osteoarthritis is thought to initially occur in the articular surface, the disruption to the superficial collagen network could have an enormous impact on the tissues ability to stop or even slow the progression of small cracks. Proteoglycan loss has also been shown to reduce the tensile stiffness through an increase in available space for the collagen fibrils to realign in the direction of tensile loading (54). It can therefore be expected that any disruption to the matrix will have an effect on the fracture toughness of articular cartilage, and so the ability of the tissue to resist fracture propagation.

2.4.3 Artificial Models of Degenerate Articular Cartilage

Artificial degradation through enzyme treatment has been shown to produce models that resemble early stage osteoarthritis, including loss of superficial collagen fibrils and proteoglycans (55-57). Although artificial degradation can replicate these predominant symptoms of osteoarthritis, it cannot exhibit true osteoarthritic traits including entanglement of collagen fibrils, localised diseased areas surrounded by mechanically healthy tissue to name a few. Therefore, it is important to note that artificial degradation cannot demonstrate all of the intricacies of the symptoms of osteoarthritis; instead it can only provide information on collagen disruption and proteoglycan loss.

An important benefit of artificial degeneration is that the level of degradation can be controlled through the choice of enzyme solutions and duration of exposure of the tissue to these enzymes. For this reason, enzyme treatment has been widely used to investigate the structure-function relationship of matrix constituents and chondrocytes (54, 55, 58, 59) and to model aspects of articular cartilage degeneration. A major purpose of modelling degeneration is to understand the biomechanics of cartilage in health and in different stages of disease (37, 38, 54-56, 58-61), and also to validate the use of diagnostic instruments (62-66).

In order for the biomechanical properties of the matrix and diagnostic instruments to be validated, the variation in the intrinsic characteristics of articular cartilage samples must be controlled. Like most biological tissue, the physical and morphological properties of cartilage are unique to each individual. Depending on the location from

which a sample is removed and the stress it encounters due to an individuals body weight, skeletal structure and alignment, muscle attachment, lifestyle, etc., the tissue may vary in total thickness, and in the distribution of matrix components and chondrocytes in each zone to allow the individual to function and perform. The study of enzymatic modification of cartilage therefore begins with greatly varied samples even before the enzymatic degradation has begun.

2.4.3.1 Artificial Enzyme Degradation of Matrix components

2.4.3.1.1 Enzyme Degradation of Collagen In Vitro

Degradation of collagen is considered the irreversible step in articular cartilage leading to failure (20). The matrix metalloproteinases include at least three collagenase types that are capable of degrading collagen, namely, MMP-13 and to a lesser extent MMP-1 and MMP-8. In vivo, the triple helical collagen molecule is cleaved by collagenases approximately a three-quarter way from the N-terminus, resulting in ¾ and ¼ fragments. These fragments denature at body temperature and are then further degraded by gelatinases and non-specific proteinases (20).

In vitro, a collagenase originally isolated from Clostridium histolyticum is commonly used to mimic the natural degradation of collagen. The procedure for collagen disruption is less varied than for proteoglycans. Researchers use concentrations of $30U\ ml^{-1}$ for 24 hours (62) and 44-48 hours (55, 56, 62, 67) for minor disruption to the superficial collagen network (24 hours), through to complete disruption of the superficial collagen network (44-48 hours). This has been shown to result in minor proteoglycan loss, possibly due to leaching through the damaged collagen network (55).

2.4.3.1.2 Enzyme Degradation of Proteoglycans In Vitro

Unlike collagen, depletion in proteoglycan numbers is reversible through its constant secretion from chondrocytes. However due to its protective role in preventing collagen degradation (68), loss of proteoglycans may be an important early step in cartilage disease.

There are many cleavage sites along the glycosaminoglycan protein core, with a range of MMPs and aggrecanases binding to specific peptide bonds along its length (Figure 2.9). In vitro, a range of enzymes have also been very popular in cleaving the proteoglycan molecule. These include Trypsin (57, 59, 61-63, 65-67, 69-73), chondroitinase ABC (54, 55, 74), Cathepsin D (58), Elastase (55), or combinations of proteinases (54). Of the aforementioned, Trypsin and chondroitinase are the most commonly used enzymes to degrade proteoglycans in articular cartilage in vitro.

This figure is not available online.
Please consult the hardcopy thesis available from the QUT Library

Figure 2.9 Structure of cartilage aggrecan and the multiple bonds cleaved in situ in articular cartilage by aggrecanases or MMPs (75). The specific sites of cleavage by MMP and aggrecanases are indicated by arrows, along with the position of these sites within the aggrecan core protein.

Chondroitinase ABC catalyses the degradation of chondroitin 4-sulfate, chondroitin 6-sulphate, dermatan sulphate, and acts slowly on the hyaluronate backbone. Trypsin

is a serine protease which cleaves peptides on the C-terminal side of lysine and arginine amino acid residues. Trypsin has also been reported to cause minor degradation to collagen fibrils (67), which contains three possible sites for Trypsin cleavage. Due to its accessibility, extensive use by researchers in this field of work, and desirable effect on cartilage matrix, Trypsin was chosen for the tests conducted in this research.

2.4.3.1.2.1 Trypsin

It is widely accepted that Safranin O staining for proteoglycans demonstrates a proteoglycan depletion front where there is a distinct digested/undigested interface (57, 62, 63, 69). This suggests that Trypsin moves as a wave front from the surface through to the cartilage-bone interface, digesting all of the proteoglycans in its path. It has however been noted that the decrease in safranin staining, and therefore Trypsin penetration, is non-linear (63, 69). It appears that Trypsin penetration is rapid through the superficial zone where proteoglycan concentration is lowest while its action and penetration rate slow down in the deeper zones due to the greater concentration of proteoglycans (63). However other research has shown that staining after Trypsin digestion demonstrates an inhomogeneous pattern, where the penetration wavefront of Trypsin does not result in complete depletion of proteoglycans but instead a decrease in stain intensity (61). Following these results, it could be argued that Trypsin penetrates the layers of cartilage at a faster rate than its rate of proteoglycan digestion along its path. That is, proteoglycans remain within the matrix following Trypsin passage.

The two modes of Trypsin penetration mentioned above raise important questions. What is the exact action of Trypsin on proteoglycans, and how is its effect altered by

different parameters such as enzyme concentration, medium and initial cartilage physical properties? These questions require attention if the accuracy of in vitro modelling of cartilage degeneration for biomechanical/chemical assessment is to have sufficient scientific merit and data integrity, and are therefore the subject of the present investigation. Despite the vast body of work that has been done in this area, there is no protocol for the use of Trypsin as to the optimum Trypsin concentration, or the required length of time of exposure to the enzyme necessary to result in a specimen of fixed loss in proteoglycan-depth with respect to the specific parameters of that tissue.

3 Artificial Degradation of Articular Cartilage for Biomechanical Evaluation Strategies

3.1 Introduction

Osteoarthritis and related diseases are often characterised by loss of proteoglycans and/or disruption of the collagen meshwork. In order to understand how this degenerative process is developed and the progression of the disease, it is important to study the characteristics of both healthy and degraded tissue, by comparing and assessing their differences. Ideally, naturally degraded cartilage samples would be studied to determine the effects of disease and/or degeneration; however, the disparate manifestations of the disease and the cascade of multiple degenerate processes occurring in the joint, make it impossible to conduct a quantitative assessment of matrix disruption and determine the specific contributions from the load carrying components of this biological gel. Consequently, researchers apply methodologies of in vitro degradation aimed at targeting and controlling the level of disruption to the matrix to study the structure-function relationship of the components. For this methodology to be meaningful, and allow differentiation, for example, between the biomechanical responses of proteoglycan-depleted or collagen-disrupted samples relative to the effect of loading rate, it is necessary to first establish that the tissues are in the same preloaded condition with the same amount of proteoglycan loss or collagen disruption.

Researchers use enzymes such as Trypsin and Collagenase to artificially degrade and disrupt the proteoglycans and collagen fibrils respectively, with the intention of understanding the biomechanical consequence of disruption to individual matrix constituents. Although this methodology does not provide a realistic example of diseased tissue, it does enable insight into the effects of individual matrix constituents on the tissue function and secondary effects on other matrix components during disease processes. This methodology is approached with the assumption that a similar degradation process will result in similar levels of matrix degradation. However preliminary tests in our laboratory have resulted in greatly varied samples degraded under the same conditions, for the same exposure time, leading to the supposition that in vitro degradation of articular cartilage produces inconsistent results. This raises the question as to the accuracy of in vitro degradation having any scientific merit and data integrity, in determining the functional consequence of matrix disruption.

Consequently, the following steps need to be taken:

- Develop a methodology for controlled proteoglycan depletion,

- Develop a methodology for controlled collagen disruption, and

- Study individually, the biomechanical manifestations of proteoglycan and collagen disruption.

The study of the combined degradation of the matrix properties would also provide useful insight into the disease processes; however this is outside of the scope of this current investigation.

This study aims to expose the degree of variability in Trypsin penetration action when carried in common solvents like PBS (56, 65, 67, 70-73) at two well published concentrations of 1.0mg/ml (59, 66, 67, 69, 71) and 0.1mg/ml (65, 70, 73), and in a less commonly used 0.15M saline solvent (66, 69). PBS was chosen as the medium for the main focus of this study, as it is a commonly used buffer with Trypsin for degrading cartilage proteoglycans. The variability of Collagenase will also be tested here, as it is predicted that the causes of variability during Trypsin treatment may also affect the variability of the mode of action of Collagenase.

These findings have lead to the acceptance of a manuscript entitled 'In Vitro Degradation of Articular Cartilage Produces Inconsistent Results', soon to be published in the Journal of Anatomy. This work has also provided data for a second paper, soon to be submitted, which presents a mathematical model which researchers can use to pre-determine, and then apply with a better degree of certainty, Trypsin and Collagenase treatment of articular cartilage when modelling degeneration in vitro.

3.2 Material description and Justification

3.2.1 Proteoglycan Quantification

Through the extensive work performed in the area of enzyme degradation of articular cartilage, there has also been a range of in-depth studies into the quantification and orientation of the matrix components. Immunohistochemical techniques using monoclonal antibodies (developed by Pearce 1980), enables an accurate estimation of the distribution of specific components within histological specimens. However digital densitometry provides information on the spatial distribution of matrix

components, and it is much more cost effective and has been widely used to provide accurate quantification of proteoglycans, and will therefore be the method used here.

3.2.1.1 Staining

There are a number of histological stains used in the quantification of proteoglycan concentration including toluidine blue and alcian blue, however Safranin O is the most commonly used on articular cartilage, and has been found to produce the most reproducible results (76).

Safranin O is a cationic dye that binds stoichiometrically to mucopolysaccharides, that is, one positively charged dye molecule binds to one negatively charged carboxyl or sulphate group (76-79). Safranin O is a metachromatic dye, whereby the colour or absorption spectra of the dye changes due to the bonding of a dye molecule to a polyanion. In histological preparation Safranin O is dehydrated prior to mounting, which destroys the metachromatic dye-dye interactions and transforms Safranin O to an orthochromatic form (76, 77), where the colour of the stained polyanions is the same colour as the dye. The colour of permanently mounted slides will remain unchanged for a considerable period of time (77). The stable orthochromatic properties make this stain useful in quantitatively evaluating the concentration of mucopolysaccharides within a sample, however it does not differentiate between chondroitin 6-sulphate and keratan sulphate (77). Safranin O is therefore a useful dye in determining levels of disease in osteoarthritic cartilage, or artificially degenerate specimens.

Following enzymatic digestion, Safranin O stains the remaining glycosaminoglycans, with the end result an advancing front of unstained cartilage from the articular surface. It has been observed in extensive states of disease and digestion, that Safranin O is not sensitive when the remaining glycosaminoglycans concentration is small (78).

3.2.1.2 Optical Absorbance Measurements

Optical Absorbance provides spatial information about the concentration of proteoglycans, based on the stoichiometric binding of Safranin O to the negatively charged glycosaminoglycans (79). The measuring device consists of a polarised light microscope (PLM), with a modified blue light source of 495nm attached to increase the light absorption of the red coloured Safranin O (80) (Figure 3.1). As Safranin O concentration increases linearly, so too does the light absorbance. Therefore, the light absorbance of the orthochromatic Safranin O stained slide can be quantified under monochromatic light to determine the quantity of the stoichiometrically bound glycosaminoglycans to the stain.
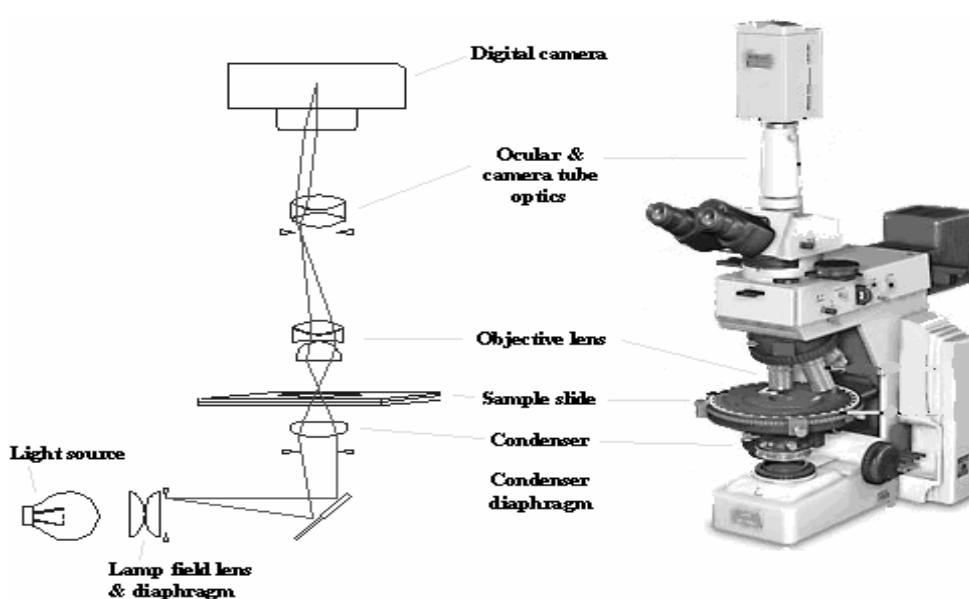
Figure 3.1 Polarised Light Microscope set up for optical absorbance measurement

3.2.2 Collagen Quantification

Unlike proteoglycans, collagen fibrils cannot be quantified through staining procedures because stains such as Van Gieson do not distinguish between intact fibrils and disrupted collagen networks. Instead, unstained sections of cartilage can be viewed under a special microscope to determine the orientation and presence of intact collagen fibrils.

3.2.2.1 Polarised Light Microscopy

Within the last ten years, PLM has been increasingly used to describe the orientation and density of collagen fibrils. In PLM (Figure 3.2), light is first filtered through a polarizer, which converts the electron field vectors of light waves vibrating in all perpendicular planes, to a single plane. As this light moves through an anisotropic material such as cartilage, the light waves are refracted or split, due to the orientation of the fibril's crystalline lattice axis with respect to direction of light. The two waves, called the ordinary ray and extraordinary ray, then travel in an orientation at right angles to each other, and at different velocities, until they pass through a second polariser called the analyser. This filter recombines the waves into one plane again, which is then seen through the eyepiece. This affect of anisotropic material on polarised light is termed birefringence, or double refraction.

When the analyser is positioned at right angle to the initial polariser (cross polarised), no light passes through the system and the view in the eyepiece is dark. Maximum contrast is achieved when the cartilage specimen is rotated 45° to the initial state of polarisation (81), allowing equal amounts of the two rays oriented at right angles. The resulting image displays brightest zones at the superficial zone (81),

and the radial zone, reaching maximum intensity at the tidemark. In contrast, the transitional zone appears most dark due to the random orientation of fibrils (81, 82).
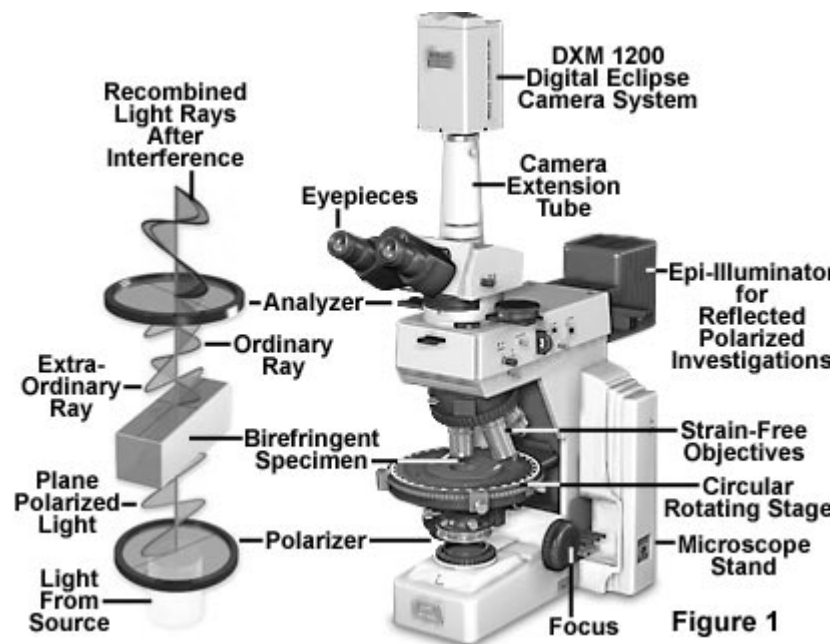
Figure 3.2 Polarized Light Microscope. Multiplanar light rays are converted to a single plane as they pass through the polariser. The light is split into two rays as it passes through the cartilage (birefringent specimen) and again converted to one plane as it passes through the analyser, and is seen through the eyepiece.

PLM is sensitive to a number of parameters, and therefore specimen preparation and the microscopic variables such as light intensity, alignment, lens aberrations etc, must be kept constant to maintain reproducibility and quantify the total content of collagen accurately (24, 81). Specimen preparation is also a very important variable that must be kept constant. The retardation value of the superficial zone is highly dependent on the direction of specimen sectioning thickness, therefore it is necessary to prepare the specimens by sectioning parallel to the split line direction, and maintaining a consistent thickness (24, 81).

3.3 Method

3.3.1 Specimen Preparation

Macroscopically normal and intact bovine patellae were harvested from a local abattoir within 24 hours of slaughter and wrapped in a 0.15M saline soaked cloth and stored at -20°C. Prior to treatment, the patellae were thawed in saline for up to one hour. Following enzyme treatment, all biopsy specimens were immediately placed in individual specimen jars after removal from the joint and placed in the freezer for up to 1 week until required for histological examination.

3.3.1.1 Saline Solutions

Trypsin is most active in a solution of pH 7 to pH 9 (83). Consequently we have chosen two types of saline solution in this study, namely 0.15M saline solution, and phosphate buffered 0.15M saline solution, with pH 6.3-7.0 and pH 7.5 respectively, in order to study the actions of Trypsin on proteoglycans within and outside the published range.

3.3.1.1.1 Trypsin – Saline Solution Test

During preliminary tests, the action of Trypsin in saline solution was examined by immersing one whole patella in a solution of 0.1mg/ml of Trypsin (from bovine pancreas T4665, Sigma-Aldrich) in 0.15M saline, and placed in an incubator at 37ºC for up to 24 hours. After 2 hours, the patella was removed from the solution, and 6 small biopsies approximately 2mm by 4mm were taken from various locations across the patella. The patella was then returned to the solution within 5 minutes, and the process was repeated after 4 hours, 6 hours, 8 hours and 24 hours. This process was repeated on a second patella, removing 3 small biopsies for each exposure time

group, to obtain samples for optical absorbance measurements. A control group was placed in saline only, under the same conditions as the Trypsin treated group.

3.3.1.1.2 Trypsin – PBS Solution Test

To measure the variation of Trypsin action across a joint in PBS, one whole patella was divided into 8 separate specimens. Four specimens from various locations across the patella were placed into a Trypsin solution containing PBS, pH 7.5 (P4417, Sigma-Aldrich), and 0.1mg/ml of Trypsin, while the remaining four specimens from the various locations were placed in the same solution, but at a Trypsin concentration of 1.0mg/ml to measure the variation of proteoglycan loss due to Trypsin concentration. Each specimen was removed after 2 hours to take a biopsy approximately 2mm by 4mm, and returned within 5 minutes. This process was again repeated after 4 hours. A control group was immersed in PBS only, under the same conditions as the Trypsin treated group.

3.3.1.2 Collagenase Test

Seven cartilage specimens were harvested across four patella. Small biobsies were taken from each specimen before treatment to compare the effect of collagenase. The specimens were then placed in collagenase solution containing PBS, pH 7.5 (P4417, Sigma-Aldrich), and 30U ml^{-1} collagenase (Sigma C0773 protease free, Sydney, Australia) for 40 hours. Biopsies were again taken for histological comparison after treatment.

3.3.1.3 Trypsin – Compression Test

To measure the relationship between proteoglycan content and stiffness, three patellae were sectioned into approximately 20mm squares and labelled according to their position on the patella groove. Cartilage specimens were embedded in Palapress® (Heraeus Kulzer GmbH & Co. Kg) dental resin and mounted on stainless steel plates. A fine felt tip pen was used to mark the point of compression. Embedded cartilage-on-stainless steel was left to set, and placed in saline for at least 90 minutes and measured to ensure thickness had recovered to that prior to preparation. Following the first round of indentation tests, cartilage samples were degraded for 1, 2, or 3 hours in 0.1mg/ml Trypsin in PBS to obtain a range of degradative levels.

3.3.2 Compression Test

The cartilage-on-stainless steel were attached to the moveable gantry on a 5-kN Hounsfield Testing Machine (model H5KS, Hounsfield Testing Equipment, Salsford, England) and loaded at 1.5mm min^{-1}, to 33% strain. Multiple sites of indentation on each specimen were separated by a lateral dimension of $R_{plug} > 4R_{ind}$ (84) to simulate an infinite sheet of tissue. Following testing a section was removed from the area directly beneath the site of indentation with a sharp scalpel and stored for histology. The remaining sites of indentation on all specimens were artificially digested with Trypsin and tested in compression, under the same conditions as before, and in the same position. After the second set of compression testing, the remaining areas under the site of indentation were removed as before for histology.

3.3.3 Microscopic Techniques

Each specimen was placed on a metal mount and embedded in optimal cutting temperature (OCT) medium (IA018, ProSciTech) and rapidly frozen in liquid nitrogen to limit damage to the tissue samples. The sample was then placed within the cryostat and sectioned at 7µm in the transverse direction. The sections were immediately picked up by a microscope slide and left to dry within a sealed container, at 4°C overnight. Before staining, a soldering gun was used to apply a small amount of wax at either end of the cartilage section on the slide. This decreased movement of the specimen during the staining process.

For staining, slides were fixed in 95% alcohol for 30 seconds and left to dry in air. Proteoglycans are hydrophilic and easily extracted during conventional histological aldehyde fixation (85), hence the use of a less disruptive fixative regime. The slides were then hydrated in distilled water, rinsed in 1% Acetic Acid for 8 dips and then stained in 0.1% Safranin O for 5 minutes. Finally, the slides were dehydrated in 95% alcohol for 6 dips, followed by 8 dips in 100% alcohol. Following the optical absorbance measurements of stained sections, colour pictures were captured by light microscope.

3.3.3.1 Optical Absorbance Measurements

Optical Absorbance provides spatial information about the concentration of proteoglycans, based on the stoichiometric binding of Safranin O to the negatively charged glycosaminoglycans (79). Sections were examined unstained and then after Safranin O staining using a Nikon Labophot-pol microscope, fitted with a blue 1W LED monochromatic light source, with a (nominal) wavelength of 470nm and

spectral half-width of 25nm (Lumileds Lighting, San Jose, California). Images were captured by a 10-bit CCD camera (S.V. Micro, Sound Vision Inc.) and stored as 16 bit greyscale TIFF files. The unstained images were acquired first and stored. Images were then collected after Safranin O staining, maintaining the exact position and orientation of the two images. These two images were processed as outlined below to obtain the absorbance due to Safranin O stain on a per pixel basis. Shutter speed and light intensity were optimised and set to be identical for the unstained samples and their stained counterparts so that the experimental parameters were the same for all sections.

3.3.3.2 Calibration of Image Processing

Linearity of the microscope system was confirmed using solutions of Safranin-O in a concentration range of 1.78×10^{-5} to 7.12×10^{-4} mol L^{-1} in a 120 micrometer deep reservoir covered by a cover-slip to keep constant depth of solution. Absorbance values were calculated using the methodology in section 3.3.3.3, and a linear function was fit to the concentration versus absorbance data and resulted in an R^2 value of 0.9974, indicating a highly linear response. The slope of the response gave a molar absorption coefficient of 33270 $mol^{-1}cm^{-1}$. Change in linearity due to the possibility of metachromasia in concentrated samples was minimised by using the technique of alcohol fixation which is known to minimise this effect (76, 77).

3.3.3.3 Image Processing

Image processing for optical absorbance measurements has been validated to show a highly linear relationship between optical absorbance and proteoglycan concentration for Safranin O stained sections (76). Images of the unstained and matching stained

sections were imported into ImageJ software (1.33u, Wayne Rasband) and converted to 32 bit floating point format. The unstained images were then pasted into the stained images, registered to match features and divided with the paste control function. The log of each pixel was determined and multiplied by -1 to express the intensity of the staining in absorbance units. Profiles were then taken from the superficial zone to the tidemark. The resulting stain absorbance profiles were then compared to each other as a measure of the proteoglycan concentration in each specimen.

3.3.3.4 Polarised Light Microscopy

The polarised light microscope measurements were performed using a Nikon Labo-Phot PLM. To ensure reproducibility, the camera was calibrated to the light intensity of a $\lambda/4$ wave plate, with a known birefringence. The exposure time was then adjusted to the thin section of cartilage and kept constant for the remaining samples. Slides were placed on the moveable stage, with the articular surface facing toward the body of the microscope. The stage was then turned 45° to ensure maximum light emittance through the polarisers and therefore maximum brightness. At this point, the image was captured, and converted to ImageJ software (1.33u, Wayne Rasband) for analysis of the retardance profiles.

3.4 Results

3.4.1 Trypsin-Saline Solution

Cartilage specimens treated with Trypsin in saline solution appeared to degrade proteoglycans rapidly in an advancing front until a specimen-dependent time. After this time, the preliminary test group showed the loss of proteoglycans was greatly

reduced and evenly distributed across the remaining depths. Figure 3.3 demonstrates this as an absence of stain in the superficial layers and a decrease in stain intensity with increasing exposure time in the combined intermediate and deeper zones. Complete loss in staining had not been achieved in some samples after 24 hours.
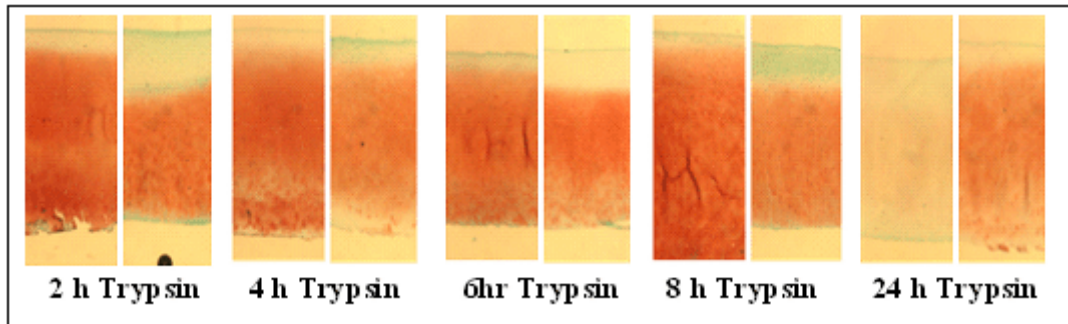
Figure 3.3 Safranin O stained sections of biopsies taken from the preliminary Trypsin-saline test. Each pairing of sections displayed here shows the least and most stained section of the 6 biopsies taken at each interval. The action of Trypsin is hindered in saline, resulting in a slow loss of proteoglycans throughout the entire depth of cartilage.

The second test group displayed a wavefront penetration action throughout the entire depths of cartilage (Figure 3.4), increasing in proteoglycan loss with increasing exposure time. Complete loss in staining was achieved by 24 hours, and so their results were not shown. The control group showed no loss of staining, indicating that depletion of proteoglycans was due to the action of Trypsin alone.
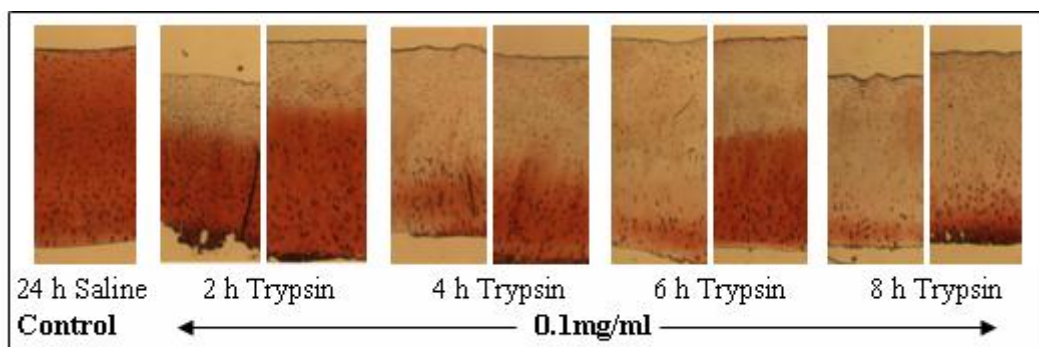
Figure 3.4 Safranin O stained sections of biopsies taken from the 2nd Trypsin-saline test. Each pairing of sections displayed here shows the least and most stained section of the 3 biopsies taken at each interval. With reference to the control section, the comparison here shows Trypsin is responsible for an active and progressive wave-front proteoglycan digestion for up to 8 hours of Trypsin treatment.

Significant variation can be seen between the preliminary test group and the second test group. These tests were performed under the same conditions, but on separate occasions. The only variable would have been a change in pH due to the absence of a buffer in the solution. Marked variation can also be seen between samples from the same patella in each of these test groups, for different time exposure. The Safranin O staining in Figure 3.3 and Figure 3.4, and the optical absorbance measurements shown in Figure 3.5, demonstrates that two specimens exposed for the same time show large variations in their level of depletion. Furthermore, it can be seen in Figure 3.3, that a specimen exposed for two hours was more depleted of its proteoglycans than that exposed for eight hours.

Figure 3.5 Optical absorbance measurements showing variability of proteoglycan distribution across three different Safranin O-stained samples of articular cartilage treated in saline and 0.1mg Trypsin for each of 2 hours (samples 1a, b & c) (i), 4 hours (samples 2a, b & c) (ii), 6 hours (samples 3a, b & c) (iii) and 8 hours (samples 4a, b & c) (iv).

3.4.2 Trypsin-PBS Solution

The behaviour of Trypsin in PBS at pH 7.5 was more consistent in its mode of action to that of Trypsin in 0.15M saline. From the Safranin O stained sections in Figure

3.6, it is evident that the Trypsin remained sufficiently active in PBS to penetrate the cartilage and degrade the proteoglycans as an advancing front throughout the entire depth. The control group for PBS alone showed no loss of staining, indicating that proteoglycan loss was a result of Trypsin alone. These results show that 0.1mg of Trypsin in PBS and the second 0.1mg Trypsin–saline test displayed a similar trend of Trypsin penetration; however, the solutions in both of these tests penetrated through the matrix at a consistently faster rate than the preliminary 0.1mg Trypsin-saline test.
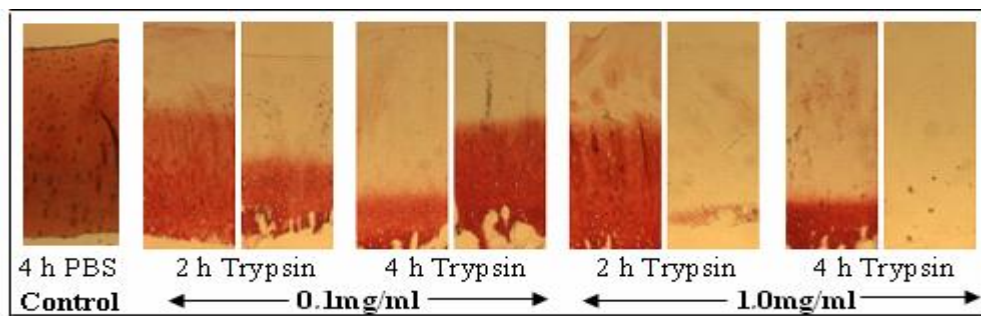
Figure 3.6 Safranin O stained section of biopsies taken from 0.1mg/ml and 1.0mg/ml Trypsin treatment in Phosphate buffered saline after 2 hours and 4 hours. Each pairing of sections displayed here shows the least and most stained section of the 4 biopsies taken at each interval. With reference to the control section, the comparison here shows Trypsin is responsible for an active and progressive wave-front proteoglycan digestion for up to 8 hours of Trypsin treatment.

Proteoglycan degradation appeared most rapid through the surface and intermediate layers (Figure 3.7) where proteoglycan concentration was lowest, which is consistent with previous findings (63, 69). These results support proteoglycan concentration as a limiting factor for Trypsin action. Sixteen samples were used in these tests with 8 each for 0.1mg and 1.0mg Trypsin treatment. After 2 hours, there was a 46.5% ± 11.5% and 71.3% ± 28.8% proteoglycan loss in 0.1mg and 1.0mg Trypsin respectively, while 70.8% ± 32.3% and 82.3% ± 20.3% of proteoglycans were lost in the 0.1mg and 1.0mg Trypsin after 4 hours exposure.
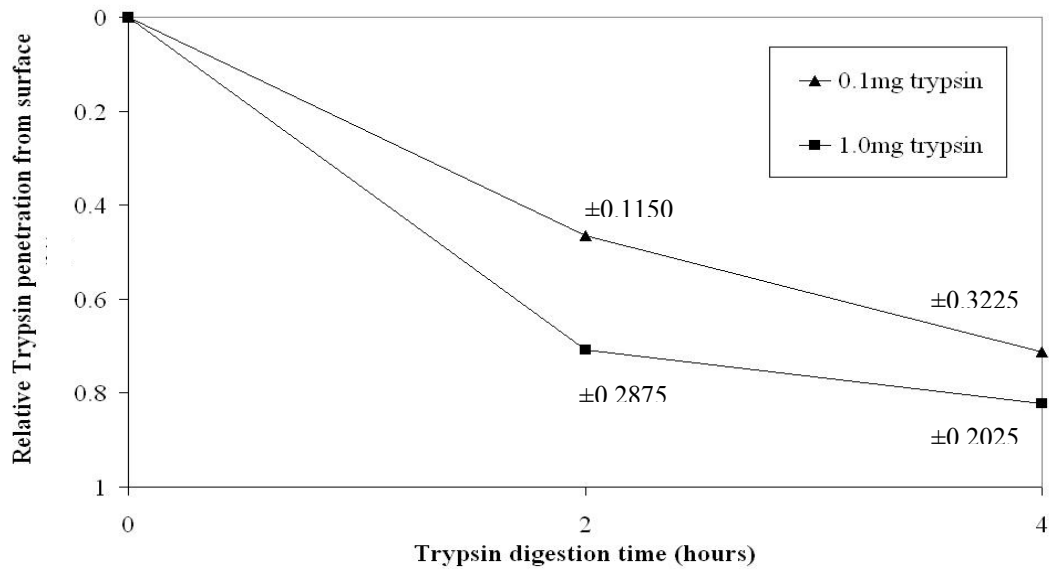
Figure 3.7 Trypsin penetration rate from the surface through to the bone. Depth of proteoglycan loss was greatest in the first two hours and in the surface and intermediate zones, and slowed down during the following two hours throughout the deeper zones.

Optical absorbance measurements of Safranin O stained sections of the samples incubated in PBS displayed significant variability across samples exposed to Trypsin for 2 and 4 hours. This was evident in both concentrations of 0.1mg and 1.0mg of Trypsin (Figure 3.8). The increase in concentration of the Trypsin solution appeared to increase the rate of proteoglycan loss, but did not appear to decrease variability.

Figure 3.8(iii) shows samples with a trend of larger depth of proteoglycan loss and small remaining absorbance value. Alternatively Figure 3.8(i), (ii) and (iv) show specimens with a larger depth of proteoglycan loss, coupled with a higher remaining absorbance value than those with a smaller depth of proteoglycan loss. These findings indicate a large variability in proteoglycan concentration and the uneven and nonlinear increase in proteoglycans through to the deep zones.
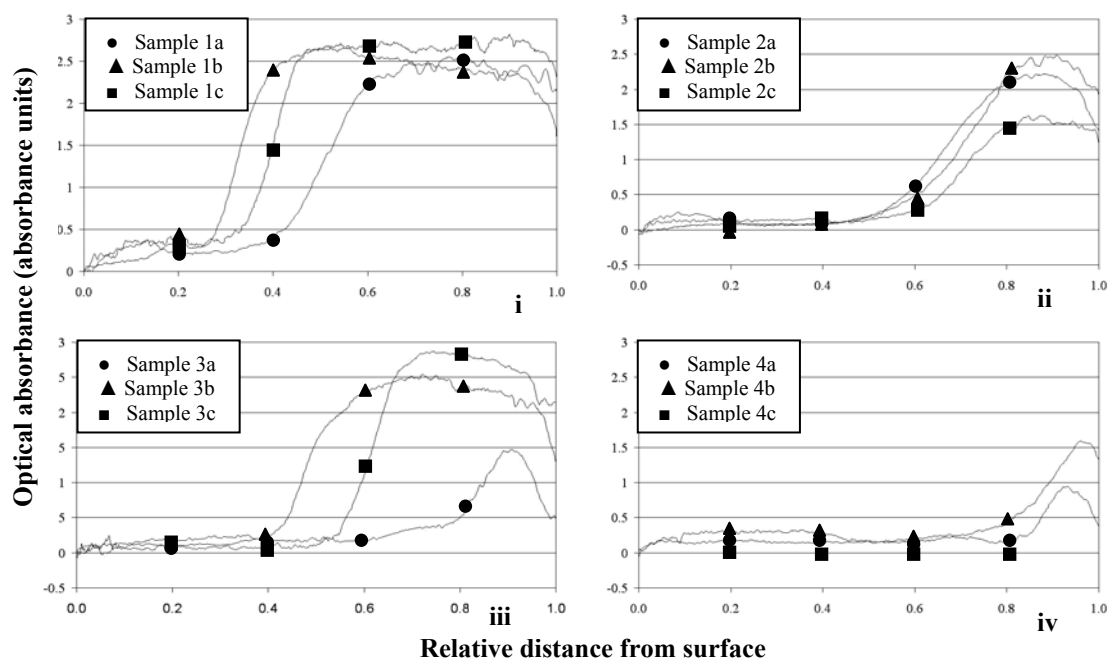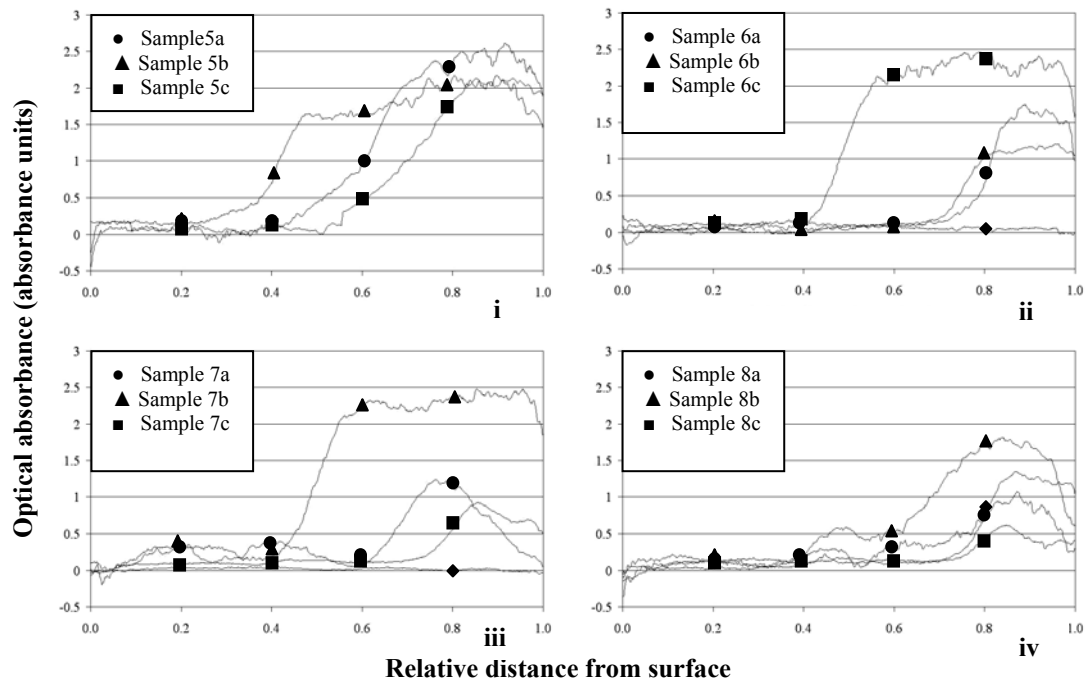
Figure 3.8 Optical absorbance measurements showing variability of proteoglycan distribution across three to four different Safranin O-stained articular cartilage samples treated in PBS and 0.1mg Trypsin for each of 2 hours (samples 5a, b & c) (i) and 4 hours (samples 6a, b, c & d) (ii), and in 1.0mg trypsin for 2 hours (samples 7a, b, c & d) (iii) and 4 hours (samples 8a, b, c & d) (iv).

Figure 3.9(i) and (ii) demonstrate that the proteoglycan distribution in adjacent samples taken from the same patella sample, exhibit a similar pattern of variation across the depths of specimens. However, the concentration of proteoglycans indicated by optical absorbance varies greatly between the specimens. The sections exhibiting greater staining intensity in the non-degraded deep regions were coupled with a smaller penetration depth of Trypsin, while those with a lower peak of proteoglycan content had been penetrated further. Assuming that the initial proteoglycan distribution did not change significantly across the very close proximity of the location from which the measurements were taken, these results also support proteoglycan concentration as a limiting factor for Trypsin action.
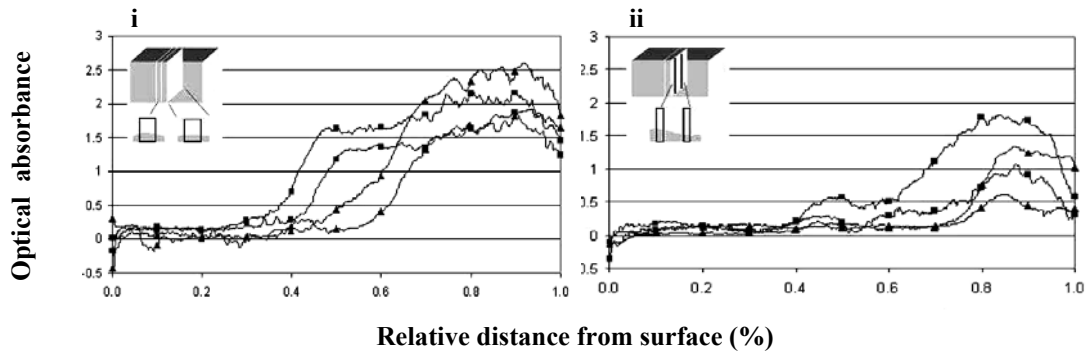
Figure 3.9 Optical absorbance values of proteoglycan distribution across Safranin O stained articular cartilage. The absorbance measures are taken from adjacent sections (a) and from areas of different intensity from the same histology section (b) as illustrated in the schematic. Absorbance values taken from adjacent specimens, or different areas on the same specimen, and within the one sample, are denoted by matching symbols within each graph.

3.4.2.1 Relationship between proteoglycan concentration and compressive stiffness

Analysis of PG concentration and compressive stiffness revealed that there was a linear relationship between the proteoglycans concentration and the compressive stiffness of cartilage (Figure 3.8). This suggests that a sample with a large total concentration of proteoglycans will be stiffer than a sample with a smaller total concentration.
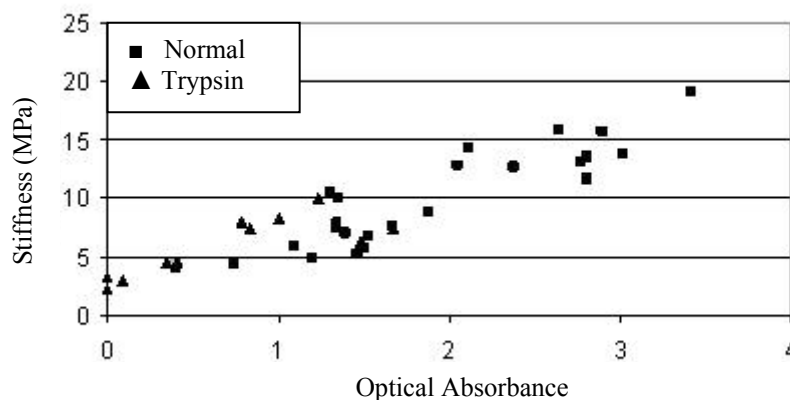
Figure 3.10 A linear relationship is observed between the optical absorbance (proteoglycan content) of a sample and its hardness. A large overlap between normal and Trypsin treated cartilage can be seen here.

The results shown in Figure 3.10 also present the large variation in proteoglycan content and their associated stiffness, and an overlap in the results of the normal samples and those that have been severely degenerated. Therefore, a sample that is tested as a normal sample may contain a lower total PG content and stiffness than a sample artificially degenerated to model osteoarthritis.

3.4.3 Collagenase Solution

To determine the effects of Collagenase on cartilage for 40 hours, and assess the process of measuring the disruption to the collagen network, histological samples were obtained before and after treatment and measured using polarised light microscopy. These samples underwent indentation testing (results not reported here) following treatment, and the biopsies taken for analysis of treated cartilage. The graphs reported here indicate the birefringence of 20% of the cartilage thickness, consisting mostly of the superficial zone, as this is the area reported to be affected by Collagenase after 40 hours of treatment.

The birefringence graphs shown in Figure 3.11 show the variation in the birefringence of normal samples, and the variation in the results of Collagenase treated samples. Collagenase appeared to either cause a disruption to the collagen network in a number of the samples tested, no change, or an increase in the birefringence values. Figure 3.11(iii) shows a false result in the normal sample due to curling of the superficial area of the cartilage. This resulted in approximately the first 10% of the surface bunching up, making its exact quantification unmeasurable.
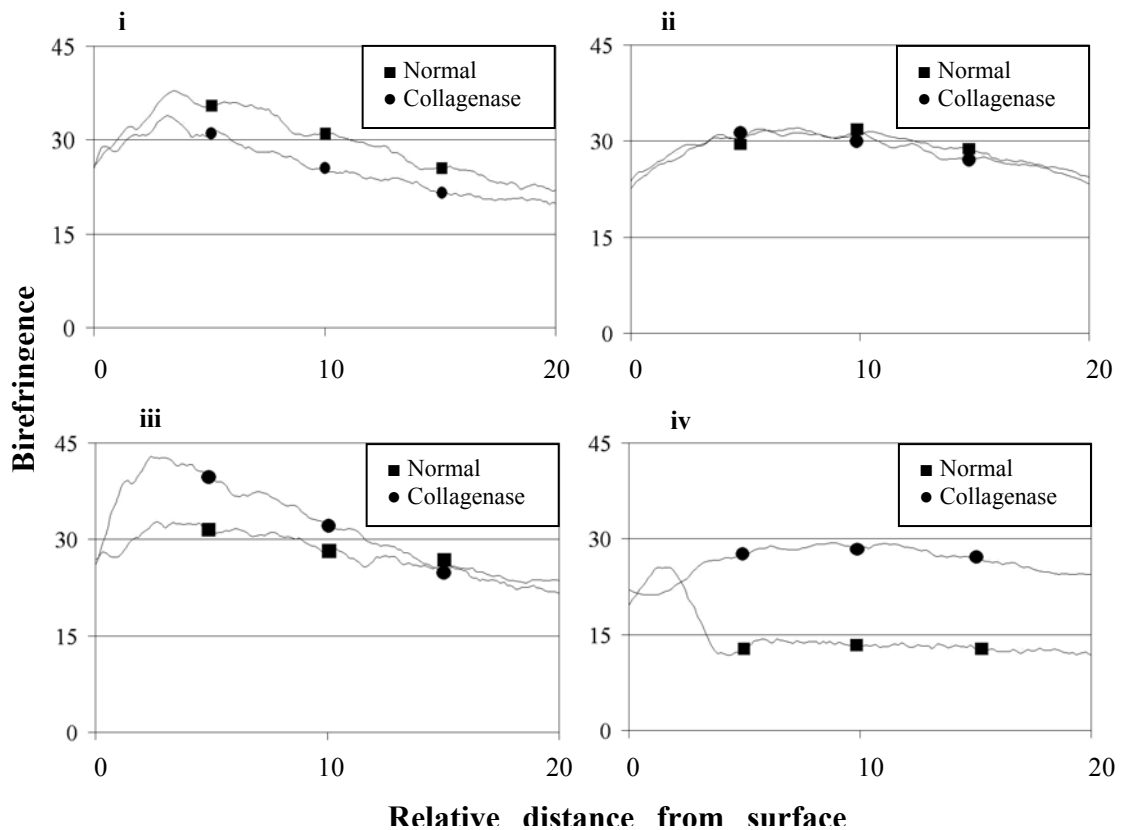
Figure 3.11 Birefringence graphs of normal cartilage and neighbouring cartilage after 40 hr Collagenase treatment. Variation can be seen between graphs, where Collagenase treatment results in decrease birefringence (i), no change (ii), increase birefringence (iii), and false results (iv).

3.5 Discussion

3.5.1 Trypsin and proteoglycans

The methodology for the Trypsin-PBS and Trypsin-saline tests varied slightly, with a whole patella immersed in the saline, while 8 separate specimens of cartilage were immersed in the PBS. This did not influence the results because biopsies were removed at a distance from the edge of the specimens, to ensure that penetration of the Trypsin solution from the side of the cartilage was not evident in these biopsies, and instead, only penetration from the surface through to the bone was observed.

The patterns demonstrated by the samples treated in Trypsin-saline (Figure 3.3 and Figure 3.4) and Trypsin-PBS (Figure 3.6) reveal that regardless of the type of

52

solution used, proteoglycan depletion is always inconsistent. These solutions are characterised by pH values of 6.3-7.0 (Trypsin-saline) and 7.5 (Trypsin-PBS) and therefore infer that the inconsistency in the Trypsin depletion of proteoglycans occurs regardless of whether the pH value of the solution is inside or near the active range of the enzyme (pH 7-9). It should be noted however, that the overall effect of Trypsin over a given duration might have been influenced by a continuation of its action on the sample removed from the solution. We expect this residual action to be limited to a short time from just after removal to freezing, while the Trypsin action can be argued to be much slower than when in the enzyme environment. Despite this probability, it can be expected that any such action will be consistent across samples, thereby producing the same effect, if any, on the stained samples.

In contrast to the mode of action of Trypsin in PBS, exposure to Trypsin-saline solutions resulted in significant changes in the mode of action of Trypsin. Preliminary tests showed localised penetration which was mostly concentrated in the superficial region of the samples, followed by a slow and near uniform decrease in stain intensity in the deeper zones, while the second test displayed a wave front penetration action similar to that of the Trypsin in PBS test. This variation may be attributed to the unstable pH level in the un-buffered saline medium.

For the preliminary saline tests, the less active state caused by an unstable and lower pH level enables the Trypsin to degrade the proteoglycans in the surface zone where there is a lower proteoglycan concentration. In the more highly concentrated deeper zones, there follows a gradual loss of proteoglycans, possibly due to limited enzyme activity and leaching through osmosis. Due to the slow rate at which proteoglycans were lost from the deep zones, the exposure time of cartilage in Trypsin-saline

solution was extended to 24 hours to allow for extensive proteoglycan loss. Over the 24 hours, there is marked variability in the loss of proteoglycans, rather than an expected increase in proteoglycan loss with increasing time, as seen by the large proteoglycan loss after 2 hours compared to the small loss after 8 hours (Figure 3.3). This finding was common for both Trypsin in saline and PBS and supports the proteoglycan rate limiting effect of mode of Trypsin action. The greatly varied Safranin O staining samples treated in Trypsin in an un-buffered saline medium (Figure 3.3 and Figure 3.4) makes the mode of action of Trypsin unpredictable, and therefore not desirable for controlled testing of articular cartilage.

In order for researchers to use enzymatic degradation of cartilage to validate instruments and further understand the components of cartilage in health and disease, the cartilage samples must have similar characteristics in order to produce significant results. To do this, one must first deal with the variability in the distribution and concentration of matrix components, and then the impact of this variation in the progression of Trypsin action throughout the matrix.

The most influential factor in the large variation of treated samples was the initial variation in the intrinsic characteristics of the cartilage samples. The results shown in this study not only indicate a great degree of variation in the depth of proteoglycan loss from the surface and remaining proteoglycan concentration, but also show an inconsistency in the relationship between these two factors. It could be logical to assume that if one were to take a sample with a large remaining proteoglycan concentration and another with a very small concentration, that the first sample may have contained a much higher concentration of proteoglycans across its depths.

However Figure 3.5a-d indicates a lack of uniformity of proteoglycan distribution and concentration across the depths of cartilage. The remaining peak height is therefore not indicative of the action of Trypsin or of the initial proteoglycan content throughout the superficial zone. This variability alone causes great variation in the rate at which Trypsin is able to penetrate through the depth of cartilage if its action is primarily proteoglycan dependent.

The distribution and concentration of proteoglycans from the surface through to the bone is non-linear and unique to each specimen, and more specifically, the geographical location on each specimen. This is perhaps the major factor causing large variability in the Trypsin treated cartilage. If all specimens consisted of the same proteoglycan content in each zone, it may be assumed that the penetration rate of Trypsin would be constant across all samples. With further testing, it may be possible to more accurately determine the rate of Trypsin penetration per unit area concentration of proteoglycan, and to determine if there are any other factors that may be contributing to the penetration rate of Trypsin.

The sample size for the cartilage harvested for each group in the Trypsin-PBS solution showed the large variation that can occur in samples taken from a single patella. The variation seen between the parallel neighbouring areas (Figure 3.7a and b) is also noteworthy, highlighting the large variation that can occur in thickness and proteoglycan concentration, and perhaps collagen content and orientation within an area as small as 14μm (total thickness of two histological sections). Due to such dramatic variations across small distances, it would be advisable for future research to prepare a number of sections from the one sample and average the measurements

to not only reduce the error arising from slight variations in thickness of cartilage sections (55), but to produce a more accurate measurement of the total area under investigation.

Another effect observed which could constitute a source of error was the negative values seen in the optical absorbance graphs (Figure 3.5, Figure 3.8 and Figure 3.9). We argue that this was a consequence of the crinkling of the superficial zone which occurred during the fixing of the sample in alcohol before recording the first image. The crinkles disappeared during the staining process, causing a misalignment of the unstained and stained images of the superficial zone, thereby yielding an image ratio greater than 1. Because of this, the analysis inevitably included taking the negative log of a number greater than 1 and therefore a negative value. It is important for the reader to know that this discrepancy was only applicable to a small portion of the superficial zone in the results presented in this study.

The results from the compression tests indicated a linear relationship between total proteoglycan content and stiffness, in accordance with previously reported tests (28). It would therefore be reasonable to assume that in order to test a group of similar cartilage samples, one could first determine the stiffness of the cartilage samples, and retain those that were within 10% of the mean curve for all the samples for further testing. According to these results, the samples with a similar stiffness should contain a similar total proteoglycan concentration, and therefore degrade to a similar level for a given time. This process should limit the amount of testing required in order to obtain a group of similarly degraded cartilage samples.

The results presented here support the notion that the unique concentration of proteoglycans throughout the anatomical zones of cartilage specimens, as well as experimental variability such as Trypsin solution and concentration, contribute greatly to the determination of the rate at which Trypsin solutions penetrate each individual cartilage specimen.

3.5.2 Collagenase and Collagen network

The analysis of the health of the collagen network is very difficult to determine with the current set of techniques. Birefringence has been shown to indicate the level at which the collagen network is intact by the refraction caused by the collagen fibrils to polymerised light. In this current investigation, a few problems were encountered in the analysis of the treatment of cartilage with Collagenase, and measuring its effect through PLM. To determine the effect of Collagenase, a biopsy of the normal cartilage was taken prior to treatment. Following treatment, indentation tests were conducted to disrupt the orientation of the network fibril that had been destroyed during the Collagenase treatment, and biopsies were taken immediately beneath this area. As it is impossible to conduct these measurements on the one specimen, this process was necessary, resulting in the comparison of two neighbouring specimens. Although the samples cannot be treated as identical to begin with, they are assumed to be similar.

Birefringence graphs indicated that Collagenase does cause variation in the amount of collagen disruption. However some results showed a higher birefringence after treatment. This could either be attributed to the change in matrix properties between the neighbouring samples, which is approximately a few millimetres. Alternatively,

or in addition to, the Collagenase treatment may be causing the increase in birefringence. The view on split line direction is still divided by researchers who believe there is a definite alignment of fibrils in the surface, and those who believe that the definite alignment only occurs during loading. Most researchers however believe that whatever the behaviour, there is some degree of further alignment along the split line during loading. If this is the case, when Collagenase breaks some of the bonds between the fibrils, some of these fibrils may still align during the bulk movement of collagen and water bound proteoglycans under loading. When the load is removed, there may be less bulk movement back to resting position, due to the outflow of water that occurred during compression, leaving the broken fibrils aligned along the split line after unloading. Therefore, when the birefringence is measured along the split line, the treated samples will have an addition of fibrils aligned along the split line, increasing the birefringence here. If this is true, PLM may not be the most appropriate tool to use in measuring collagen alignment in articular cartilage.

4 Stress-Strain Characterisation of Normal and Degenerate Articular Cartilage in Compression

4.1 Introduction

The study of cartilage degradation and its biomechanical impact is important for understanding cartilage disease. Laboratory experiments are undertaken to gain insight into tissue properties, and to develop mathematical and computational models that represent tissue attributes. The main attributes of cartilage with respect to load bearing, are determined relative to the behaviour of its fluid component, which is dependent on its osmotic activity, solid skeleton, stress-strain characteristics and structural cohesion in general.

Under sub-impact loads, cartilage exudes its water to facilitate deformation. Over time the pressure in the water is shared progressively with the solid skeleton leading to stiffening. This stiffness, which is over and above that provided by the osmotic pressure and associated collagen distension, facilitates load bearing. At these velocities the stress-strain relationship for the cartilage matrix is non-linear with a prominent J-shaped pattern and is deformation-dependent. The behaviour is commonly referred to as hyperelastic at higher rates of loading and hyperviscoelastic at impact velocity. The viscous effect reflects the increased level of difficulty for fluid exudation as the pores of the matrix reduce in size with increasing deformation.

This chapter reports results of the mechanical response of macroscopically normal cartilage tested in compression, and observed changes that occur following artificial degradation of normal cartilage. Artificial degradation will determine the effect of proteoglycans depletion and collagen disruption on cartilage mechanical properties, with the principal aim of determining the differences imposed by such alterations on the hyperelasticity of the tissue's matrix with respect to established hyperelastic constitutive (stress-strain) laws (86).

4.1.1 Common Hyperelastic Constitutive Relationships

Materials which exhibit large elastic deformation responses (strain greater than 20%) when loaded, are also referred to as hyperelastic materials. Articular cartilage with its characteristic average compression strain of up to 60% and tensile strain of 20% (87) falls into this category of materials. Consequently the statistical theory of rubber elasticity (88) which forms the basis of the established constitutive laws of rubber like or hyperelastic deformation can be used to account for its biomechanical response in the analysis and modelling of its deformation under various conditions. We therefore assess the representative capacity of common hyperelastic laws that are normally used in the analysis of highly deformable, soft, rubber-like materials with respect to their abilities to describe cartilage deformation. The laws considered are Mooney-Rivlin, Yeoh, Neo-Hookean, Arruda-Boyce, Polynomial and Ogden. These are described as follows.

4.1.1.1 Pertinent Hyperelastic Theory

In accordance with the statistical theory of elasticity, the Cauchy stress-strain invariants relationship for uniaxial compression can be written as,

$$\sigma = 2\left(\lambda^2 - \frac{1}{\lambda}\right)\left(\frac{\partial W}{\partial I_1} + \frac{1}{\lambda}\frac{\partial W}{\partial I_2}\right) \tag{4.1}$$

where σ is Cauchy stress; λ the bulk stretch ratio; W is the strain energy potential per unit volume or strain energy density function; I_1 and I_2 are the first and second deviatoric strain invariants which are defined as:

$$I_1 = \lambda_1^2 + \lambda_2^2 + \lambda_3^2 \tag{4.2a}$$

$$I_2 = \frac{1}{\lambda_1^2} + \frac{1}{\lambda_2^2} + \frac{1}{\lambda_3^2} \tag{4.2b}$$

where

$$\lambda = \lambda_1\lambda_2\lambda_3 \tag{4.2c}$$

Also for one-dimensional uniaxial compression with radial constraint which approximates the loading conditions for articular cartilage in vivo and in vitro with a small indenter of diameter 4mm as used in our experiments,

$$\lambda_2 = \lambda_3 = 1 \text{ and } \lambda_1 = \lambda \tag{4.2d}$$

Therefore substituting (4.2d) and (4.2c) into (4.2a) yields,

$$I_1 = \lambda^2 + 2 \tag{4.2e}$$

While substituting (4.2d) and (4.2c) in (4.2b) gives,

$$I_2 = \frac{1}{\lambda_1^2} + 2 \tag{4.2f}$$

Using these equations (4.1), (4.2e) and (4.2f) it is possible to write the following relationship for the established hyperelastic laws under uniaxial compression and radial constraint.

1. The Arruda-Boyce strain energy potential is

$$W = \mu\sum_{i=1}^{5}\frac{C_i}{\lambda_m^{2i-2}}\left(\overline{I_1^i} - 3^i\right) \tag{4.3}$$

61

Where λ_m is the temperature dependent material parameter which is kept constant here, so the formula becomes

$$W = \mu \sum_{i=1}^{5} C_i \left(\overline{I_1^i} - 3^i \right) \qquad (4.4)$$

Where,

$$\mu C_i = D_i \qquad (4.5)$$

Therefore,

$$W = \sum_{i=1}^{5} D_i \left(\overline{I_1^i} - 3^i \right) \qquad (4.6)$$

Combining equations (4.1), (4.2e) and (4.3) yields,

$$\sigma = 2 \left(\lambda^2 - \frac{1}{\lambda} \right) \left(D_1 + 2D_2 \left(\lambda^2 + 2 \right) + 3D_3 \left(\lambda^2 + 2 \right)^2 + 4D_4 \left(\lambda^2 + 2 \right)^3 + 5D_5 \left(\lambda^2 + 2 \right)^4 \right) \quad (4.7)$$

Where σ is Cauchy stress, D_i is the material constants, and λ is the bulk stretch ratio.

2. The <u>Mooney-Rivlin</u> strain energy potential is

$$W = C_{10} \left(\overline{I_1} - 3 \right) + C_{01} \left(\overline{I_2} - 3 \right) \qquad (4.8)$$

Combining equations (4.1), (4.2e), (4.2f) and (4.8) yields,

$$\sigma = 2 \left(\lambda^2 - \frac{1}{\lambda} \right) \left(C_{10} + \frac{1}{\lambda} C_{01} \right) \qquad (4.9)$$

Where σ is Cauchy stress, C_i is the material constants, and λ is the bulk stretch ratio.

3. The <u>Neo-Hookean</u> strain energy potential is

$$W = C_{10} \left(\overline{I_1} - 3 \right) + C_{01} \left(\overline{I_2} - 3 \right) \qquad (4.10)$$

Combining equations (4.1), (4.2e), (4.2f) and (4.10) yields,

$$\sigma = 2 \left(\lambda^2 - \frac{1}{\lambda} \right) C_{10} \qquad (4.11)$$

Where σ is Cauchy stress, C_{10} is the material constant, and λ is the bulk stretch ratio.

4. The <u>Yeoh</u> strain energy potential is

$$W = \sum_{i=1}^{3} C_{i0} (I_1 - 3)^i \tag{4.12}$$

Combining equations (4.1), (4.2e), (4.2f) and (4.12) yields,

$$\sigma = 2\left(\lambda^2 - \frac{1}{\lambda}\right)\left(C_{10} + 2C_{20}(\lambda^2 - 1) + 3C_{30}(\lambda^2 - 1)^2\right) \tag{4.13}$$

Where σ is Cauchy stress, C_i is the material constants, and λ is the bulk stretch ratio.

5. The <u>Polynomial</u> strain energy potential is

$$W = \sum_{i+j=1}^{2} C_{ij} (\bar{I}_1 - 3)^i (\bar{I}_2 - 3)^j \tag{4.14}$$

Combining equations (4.1), (4.2e), (4.2f) and (4.14) yields,

$$\sigma = 2\left(\lambda^2 - \frac{1}{\lambda}\right)\left(c_{10} + c_{01}\frac{1}{\lambda} + c_{11}(\lambda^{-2} - 1) + c_{11}\frac{\lambda^2 - 1}{\lambda} + 2c_{20}(\lambda^2 - 1) + 2c_{02}\frac{\lambda^{-2} - 1}{\lambda}\right) \tag{4.15}$$

Where σ is Cauchy stress, C_i is the material constants, and λ is the bulk stretch ratio.

6. The <u>Odgen</u> strain energy potential is

$$W = \sum_{i=1}^{3} \frac{2\mu_i}{\alpha_i^2}\left(\bar{\lambda}_1^{\alpha_i} + \bar{\lambda}_2^{\alpha_i} + \bar{\lambda}_3^{\alpha_i} - 3\right) \tag{4.16}$$

$$\frac{\partial w}{\partial \lambda} = \sum_{i=1}^{N} \frac{2\mu_i}{\alpha_i} \lambda^{\alpha_i - 1} \tag{4.17}$$

$$\sigma = 2\left(\lambda^2 - \frac{1}{\lambda}\right)\left(\frac{1}{2\lambda} - \frac{1}{4\lambda^2}\right)\frac{\partial w}{\partial \lambda} \tag{4.18}$$

$$\sigma = \frac{\lambda^{\alpha_i - 1}}{4\lambda^2} 2\left(\lambda^2 - \frac{1}{\lambda}\right)\left(-a_0 + (2a_0 - a_1)\lambda + (2a_1 - a_2)\lambda^2\right) \tag{4.19}$$

Where σ is Cauchy stress, a_i is the material constants, and λ is the bulk stretch ratio.

7. The Continuum model (89) is a one dimensional model described as

$$\sigma = \Phi\left(-\lambda + \frac{1}{\lambda}\right) + \mu\left(-1 + \frac{1}{\lambda^2}\right) \tag{4.20}$$

where Φ is the swelling constant determined by the collagen and proteoglycans; μ is the osmotic constant, which is contributed to significantly by the water bound proteoglycans; σ is Cauchy stress, and λ is the bulk stretch ratio.

4.3 Method

4.3.1 Specimen Preparation

Macroscopically normal and intact bovine patella were harvested from a local abattoir within 24 hours of slaughter and wrapped in a 0.15M saline soaked cloth and stored at -20°C. Prior to treatment, the joints were thawed in saline for one hour. Following enzyme treatment and testing, all biopsy specimens were immediately placed in individual specimen jars after removal from the joint and placed in the freezer for up to 1 week until required for histological examination.

To measure the effect of enzyme degradation on cartilage stiffness, 48 cartilage specimens were sectioned into 20mm squares, attached to 5mm of underlying bone, and labelled according to their position on the patella groove. Cartilage specimens were embedded in Palapress® (Heraeus Kulzer GmbH & Co. Kg) dental resin and mounted on stainless steel plates. A fine felt tip pen was used to mark the point of compression. Embedded cartilage-on-stainless steel was left to set, and placed in saline for at least 90 minutes and measured to ensure thickness had recovered to that prior to preparation.

4.3.2 Enzyme Treatment

Following testing, specimens were artificially digested in Trypsin solution containing PBS, pH 7.5 (P4417, Sigma-Aldrich), and 0.1mg of Trypsin for 1 hour or

collagenase solution containing PBS, pH 7.5 (P4417, Sigma-Aldrich), and 30U ml^{-1} collagenase (Sigma C0773 protease free, Sydney, Australia) for 40 hours. After treatment, the samples were blotted dry and placed in saline.

4.3.3 Compression Test

The cartilage-on-stainless steel were attached to the moveable gantry on a 5-kN Hounsfield Testing Machine (model H5KS, Hounsfield Testing Equipment, Salsford, England). To determine the affect of bone on the indentation results of cartilage, 4 normal samples were tested at 1mm/min and 5mm/min, allowing 2 hours for recovery in saline. Samples were then removed from the bone and tested at the same loading rates as before.

To obtain data for the hyperelastic parameters, normal samples were loaded at 4.5mm min^{-1} to 33% strain. Following testing a section was removed from the area nearby the site of indentation with a sharp scalpel and stored for histology. The remaining tissue were artificially digested with Trypsin and tested in compression, under the same conditions as before, and in the same position. After the second set of compression tests, a section of tissue immediately adjacent to the previous biopsy site was removed as before for histology.

At the completion of testing, split line direction was determined by pin pricking the surface of the cartilage with an Indian ink charged pin. These results were recorded and matched up with the samples stored for histological analysis.

4.3.4 Microscopic Techniques

Cartilage samples underwent the same procedures discussed previously for histology (see section 3.3.3).

4.4 Results

4.4.1 Cartilage on bone verse cartilage on stainless steel

Indentation tests on cartilage are often performed on bone, or on cartilage that has been removed from the bone and glued to stainless steel. In order to make the hyperelastic results meaningful for all research conducted in this field, preliminary tests were conducted to determine the effects of cartilage on bone and on stainless steel. The force-displacement curves obtained from the experiments were converted to stress-strain curves (Figure 4.1) to normalize force and the thickness of the cartilage (38). Figure 4.2 shows that cartilage has a higher strength (hardness) when tested on stainless steel than on bone, at two different loading rates. The relationship between the stiffness of cartilage on bone and stainless steel is shown to be proportional from low strain, up to 30% strain, indicating that compression of cartilage on bone is proportional to cartilage on stainless steel at loading rates of 1.0 and 5.0mm/min.
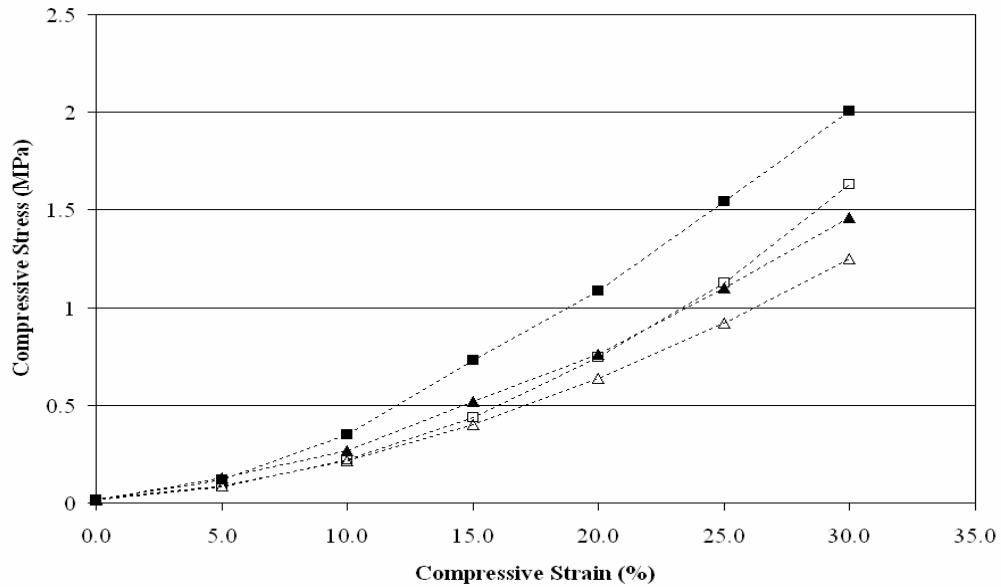
Figure 4.1 Stress-strain response of cartilage on bone at 1mm min^{-1} ($\triangle$) and 5mm min^{-1} ($\square$), and cartilage on stainless steel at 1mm min^{-1} ($\blacktriangle$) and 5mm min^{-1} ($\blacksquare$).
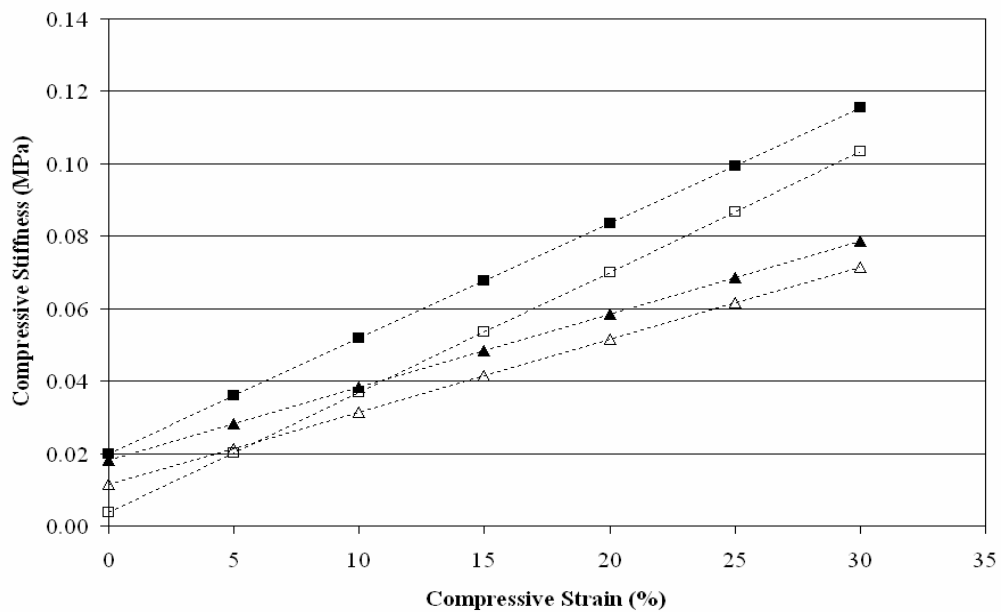
Figure 4.2 Stiffness of cartilage at different strain, on bone at 1mm min^{-1} ($\triangle$) and 5mm min^{-1} ($\square$), and cartilage on stainless steel at 1mm min^{-1} ($\blacktriangle$) and 5mm min^{-1} ($\blacksquare$).

4.4.2 Microscopy

Safranin O stained slides of articular cartilage, provided information on the proteoglycan concentration and distribution throughout the matrix. Variation was evident in the normal cartilage slides, shown by the intensity of the colour and the change in this intensity across the depths of cartilage (Figure 4.3).

67
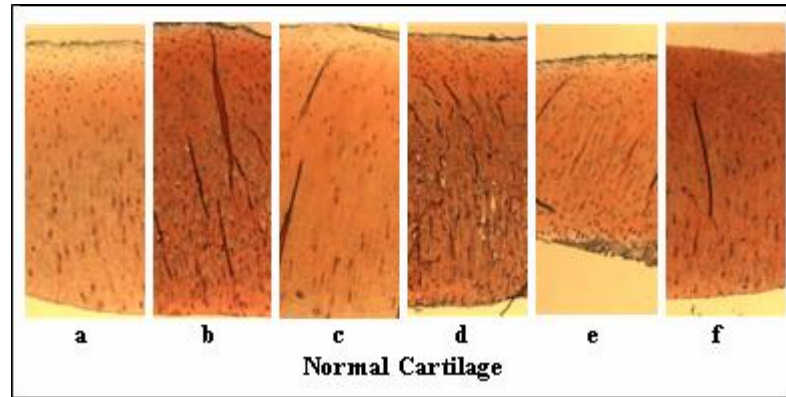
Figure 4.3 Safranin O stained slides of normal cartilage

Artificial degradation of the proteoglycans by Trypsin for 1 hour resulted in a greatly varied level of proteoglycan loss, from 15-85% (Figure 4.4 and Figure 4.5). This was determined by comparing the optical absorbance of Safranin O stained normal sample to degraded samples taken directly adjacent to the biopsy site of the normal sample.
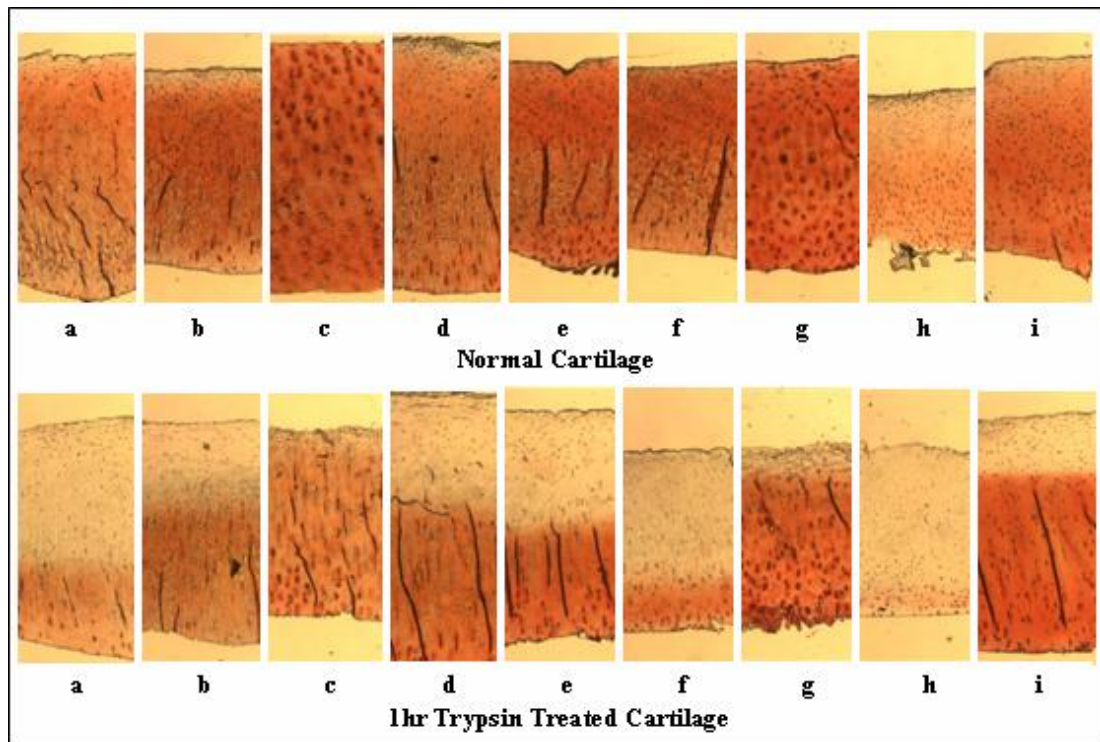
Figure 4.4 Safranin O stained slides of normal and adjacent degraded samples, e.g. samples 'a' in the normal cartilage group is from the region directly adjacent to sample 'a' in the treated group, following 1hr Trypsin treatment.
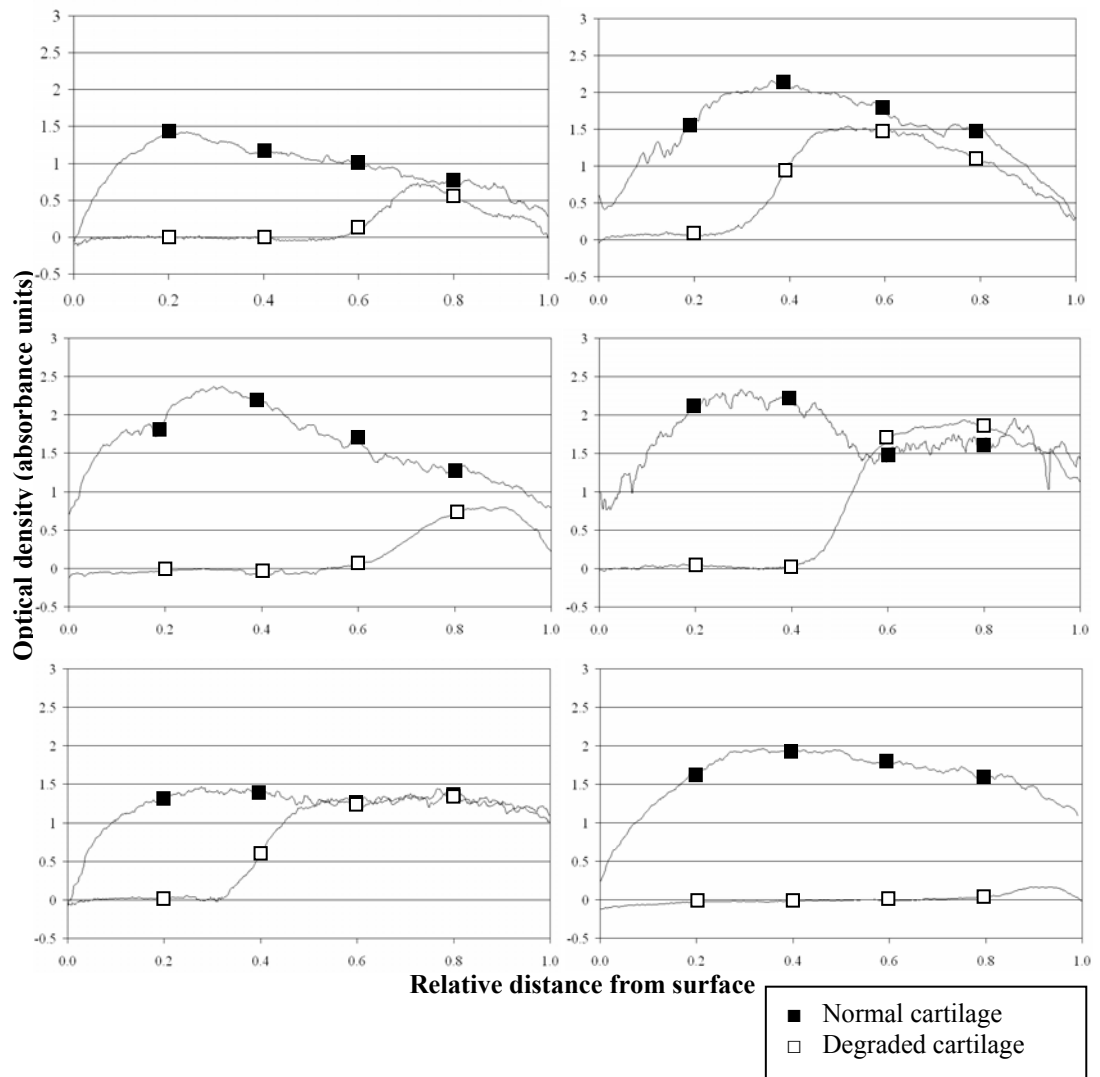
Figure 4.5 Optical Absorbance measurements of cartilage samples taken before (normal) and after (degraded) 1 hour Trypsin treatment.

There was found to be no significant decrease in proteoglycan content as a result of collagenase treatment (Figure 4.6 and Figure 4.7). The birefringence graphs from the PLM were not as reliable as the optical absorbance for proteoglycan, as discussed in chapter 3. Therefore no valid comparison could be drawn between the disruption to the collagen network and stiffness.
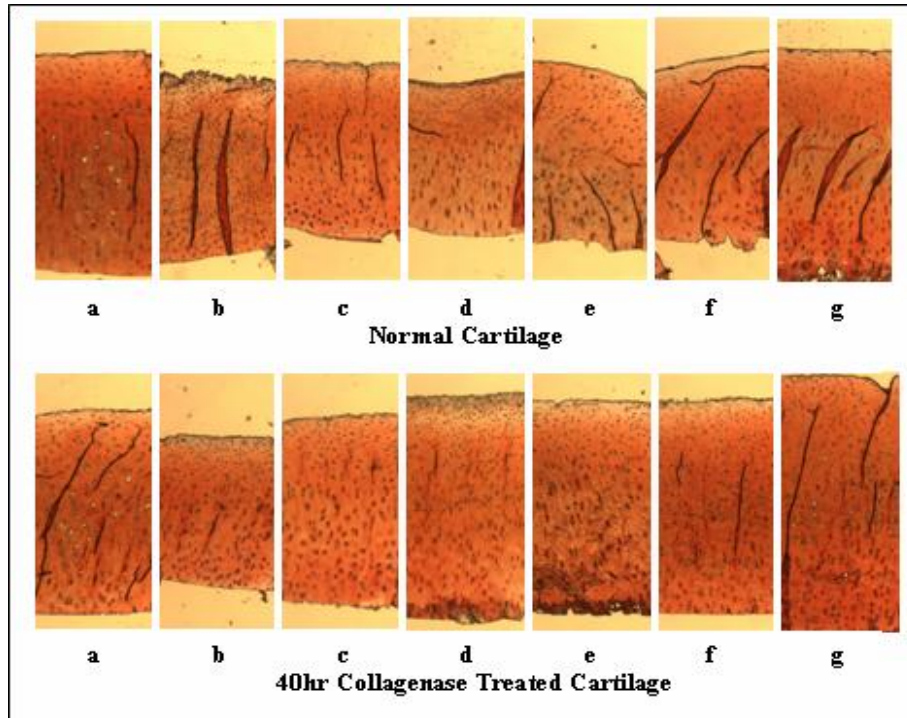
Figure 4.6 Safranin O stained slides of normal and adjacent degraded samples, e.g. samples 'a' in the normal cartilage group is from the region directly adjacent to sample 'a' in the treated group, following 40hrs Collagenase treatment.
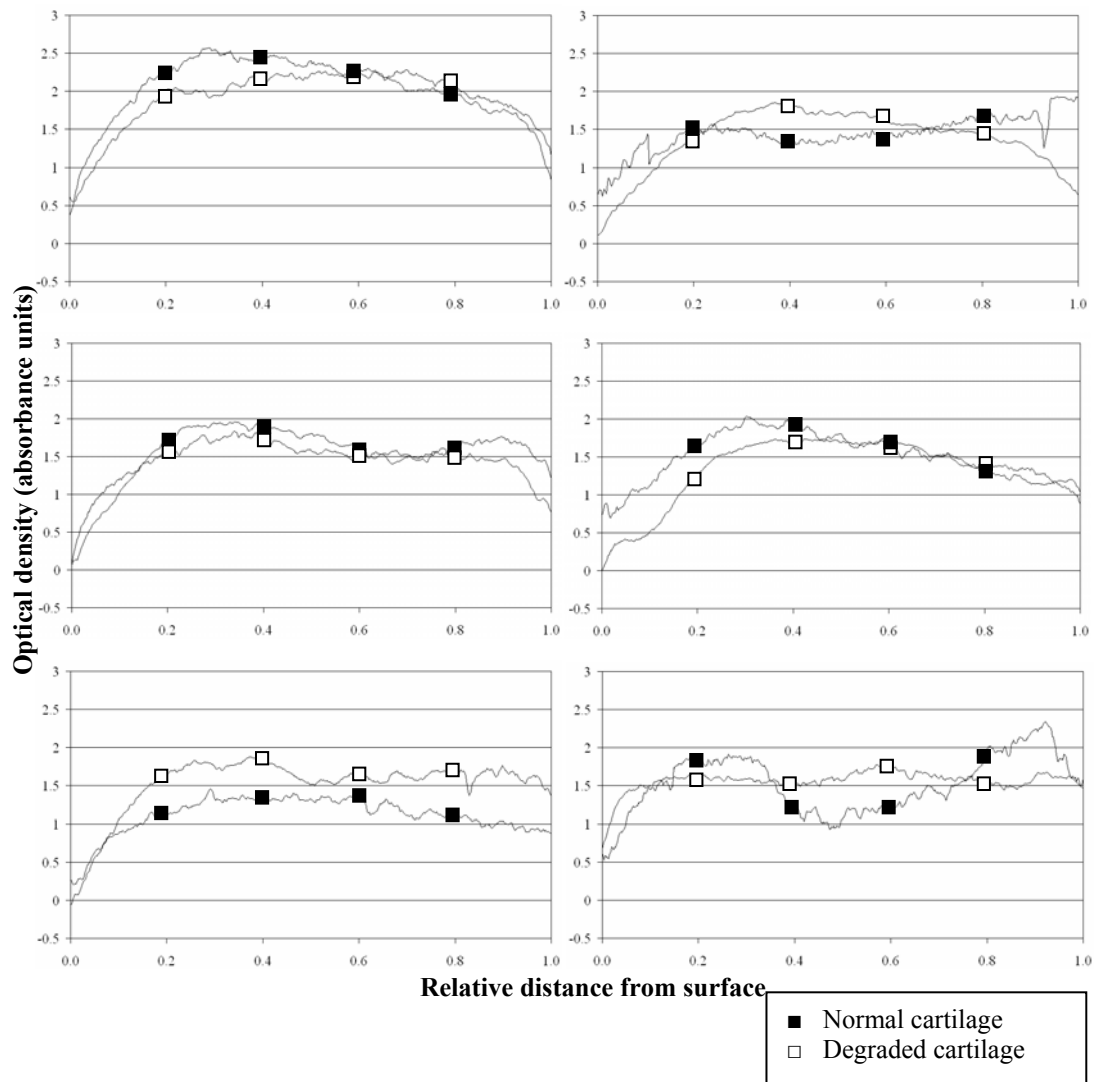
Figure 4.7 Optical Absorbance measurements of cartilage samples taken before (normal) and after (degraded) 40 hours Collagenase treatment.

4.4.3 Mechanical Test Results

4.4.3.1 Choice of experimental curves for analysis – normal intact cartilage

A total of 48 samples from 13 joints were tested in compression at a loading speed of 4.5mm/min. These samples resulted in a large variation in the stress-strain curves (Figure 4.8), with the lowest and highest stress values ranging from 0.4MPa to 5.2MPa at 30% strain. This data does not present well for statistical analysis, therefore we resolved to choose 3 representative curves at the high, average and low stiffness responses as illustrated in Figure 4.8. The average stress value was

calculated to be 1.8MPa (S.D. 1.3MPa) at 30% strain. The hyperelastic curve modelling was therefore carried out with reference to these three curves.
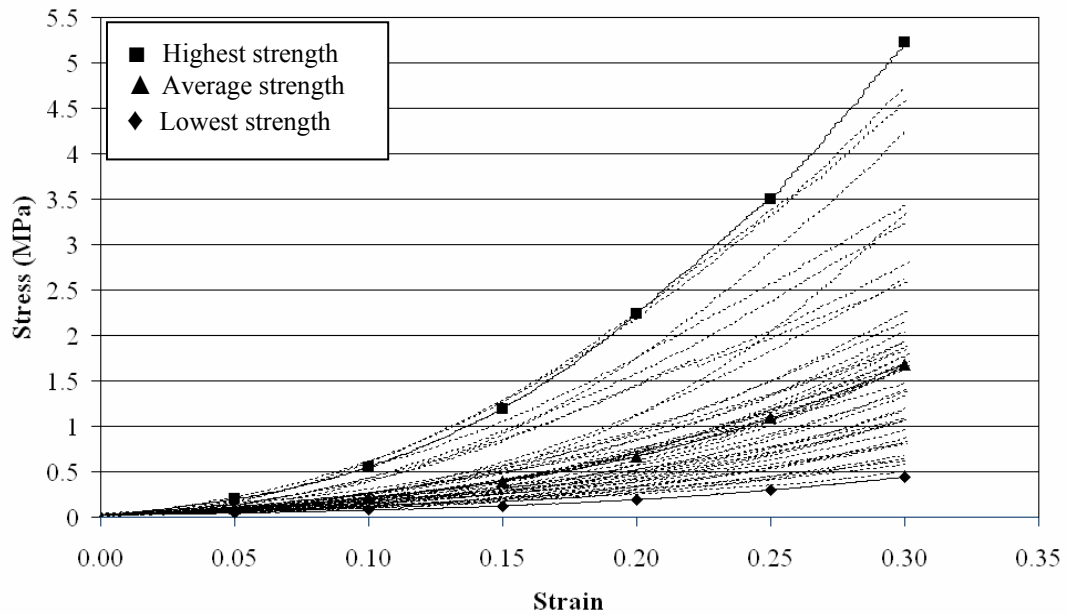
Figure 4.8 Stress-strain curves of all samples tested for hyperelastic experiment.

4.4.3.2 Choice of experimental curves for analysis – proteoglycan depleted cartilage

Following the exposure of normal samples to Trypsin for 1 hour, stress values were shown to increase slightly at larger strains, or more commonly decrease (Figure 4.9). That is, 1 hour Trypsin treatment resulted in a range of stress values with a lowest value of 0.4MPa at 30% strain, a highest value of 3.3MPa, and an average of 1.3MPa (S.D. 1.3MPa) at the same strain. Therefore finding the average of samples degraded by a particular percentage, ± 10% for modelling purposes, would result in a very large standard deviation, and would not provide any significant information.
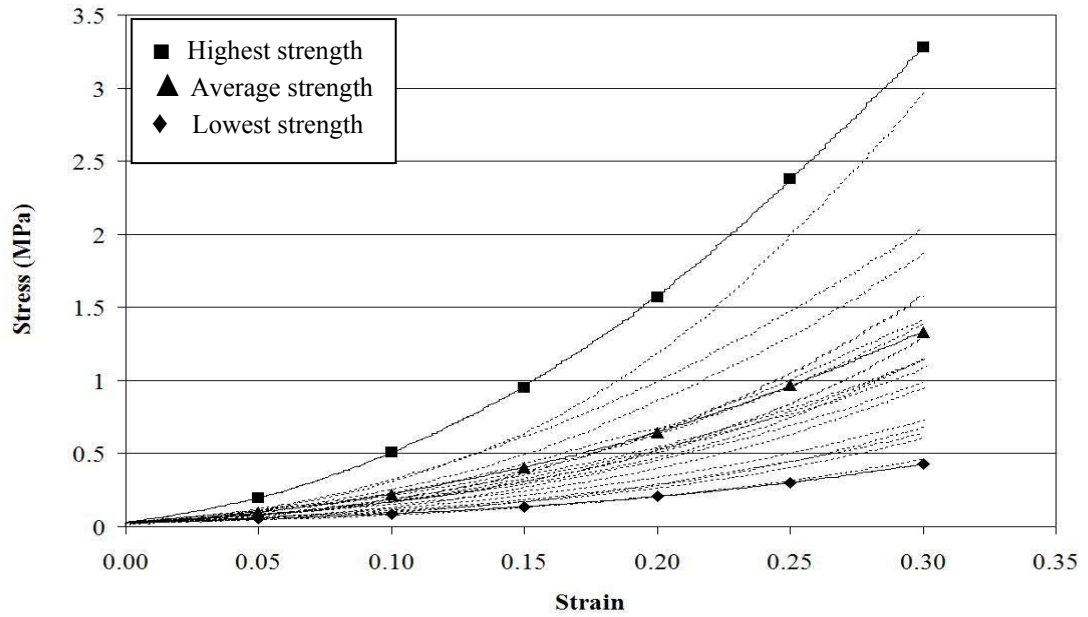
Figure 4.9 Stress-strain curves of cartilage treated in Trypsin for 1 hour.

4.4.3.3 Choice of experimental curves for analysis – collagen depleted cartilage

Collagenase treated samples also showed great variation in stress-strain results. Most of the specimens showed an increase in stress value compared to its normal state following treatment in Collagenase for 40 hours measuring a highest value of 4.7MPa while others showed a lowest value of 0.5MPa at 30% strain. The average value at the same strain was 2.8MPa (S.D.1.2MPa) for all Collagenase treated samples (Figure 4.10).
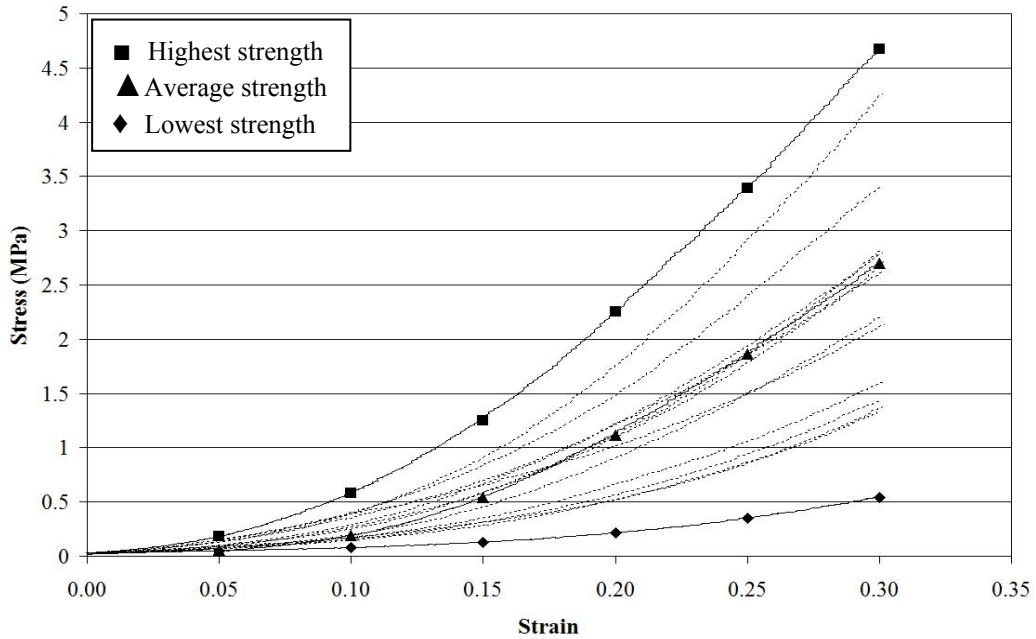
Figure 4.10 Stress-strain curves of cartilage treated in Collagenase for 40 hours.

Due to the large variances in results for the artificially degraded samples, and lack of correlation between the specific decrease in proteoglycans and collagen to change in stress, a similar approach was used here as with the normal samples. That is the smallest, largest, median and mean curves were used to determine the hyperelastic parameters of artificially degraded cartilage.

4.4.4 Modelling

The experimental data was plotted in MATLAB (Version 7.1.0.246), with the curve fitting toolbox (Version 1.1.4). Due to the large variability in the stiffness of the cartilage, the Highest, Lowest, and Average stress-strain curves were chosen to provide a cross section of data from each of the normal, Trypsin and Collagenase treated groups. Each hyperelastic law was applied to the data to determine the coefficients. The value for the coefficients was specified to fall between 1×10^{-7} and 1×10^{7}, in order to return coefficients that were relevant to the material properties of cartilage.

74

The hyperelastic models, along with the coefficients were plotted against the experimental data. Figure 4.11 shows an example of the hyperelastic models plotted against the experimental data, representative of most of the results for the different states of health, levels of hardness, and loading speeds. From this graph, the Neo-Hookean model is shown to be an inaccurate model of cartilage, due to its linearity. Although this model is not representative of the non-linear elastic behaviour of cartilage at loading speeds of 4.5 and 1.5 mm/min, it may provide a more realistic fit for cartilage undergoing impact loading, which displays a more linear shape. The Continuum model and Ogden model also show great deviation from the experimental curve, with the Ogden in particular failing to converge for most of the data.

To distinguish between the remaining hyperelastic models and determine which model provided the most appropriate fit for the mechanical properties of cartilage, three criteria were compared for each model:

- Goodness of fit values,

- The accuracy of the coefficient values in describing the material properties determined by the experimental data, and

- The number of iterations.

A numerical value from 1-6 was assigned to each criteria, where 1 was given to the smallest iteration, the closest goodness of fit values, and the coefficient value closest to the material parameters. These values were then tabulated for each model, and the model with the smallest total sum of values was shown to be the best model. This process was carried out for all of the experimental data, to determine which models best described the experimental data for each level of stiffness, and state of degeneration.

The Mooney-Rivlin model followed a similar trend to the experimental data, and showed a reasonable number of iterations, averaging 46.1, with a standard deviation (S.D.) of. 41.8 (n=18). However the coefficients returned from the curve fitting exercise were most often negative values and so did not correlate well with the material properties. The Arruda-Boyce also showed a very good fit to all experimental curves, with an iteration value averaging 64.6 (S.D. 19.4, n-18). Although this model showed promising results, the relationship of the constants to material parameters was not provided because the constants are known for this model.

The two best models were found to be the Yeoh and Polynomial model. Both exhibited strong goodness of fit values, however the coefficients for the polynomial were often marginally closer to the experimental data material properties, with an average value within 38.2% (S.D. 19.5, n=16) of the material properties, compared to 44.3% (S.D. 22.4, n=16) for the Yeoh. However the Yeoh model required significantly less number of iterations in every test (9.61, S.D. 4.0, n=18) than the Polynomial model (72.89, S.D. 18.6, n=18).
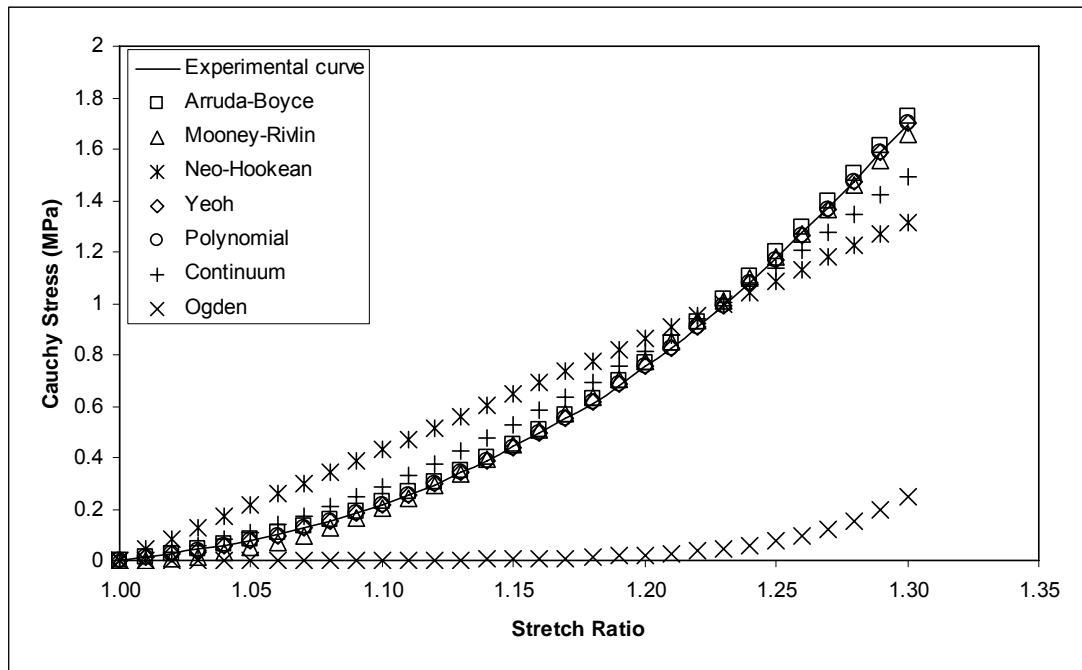
Figure 4.11 Hyperelastic curves plotted against experimental data.

4.4.5 Determination of samples for fracture test

Due to the large distribution in normal stiffness curves, a very large number of cartilage samples would have been required to provide a sample size within a 5-10% stiffness range that was large enough for significant analysis of fracture testing. Because fracture testing leads to the complete failure of cartilage, it would be impossible to test how one specimen behaves normally, and its behaviour following different forms of artificial degradation. Therefore, sample sizes of at least 3 were chosen, whose stiffness values fell within a 10% deviation (Table 4.1), determined by the tangent of the stress-strain curves. It is assumed that samples that behave in a similar way in compression may have a similar matrix composition and therefore degrade to a similar degree. So of the 3 samples in each group, one remained normal, one was treated with Trypsin, and the other with Collagenase. This method produced 5 groups, with some samples being compared across two groups, producing a sample size of 20 for fracture testing.

Strain	Group 1	Group 2	Group 3	Group 4	Group 5
5%	0.41	0.50	0.40	0.36	0.33
10%	0.09	0.19	0.11	0.16	0.04
15%	0.05	0.06	0.03	0.11	0.03
20%	0.06	0.01	0.02	0.10	0.06
25%	0.07	0.06	0.03	0.10	0.07
30%	0.08	0.08	0.05	0.10	0.08

Table 4.1   Variation in stiffness within each group at different strain values

4.5 Discussion

Preliminary tests of cartilage on bone and off bone (on stainless steel) showed a linear relationship at two different loading rates, indicating that at 1mm min^{-1} and 5mm min^{-1}, the bone did not appear to influence the behaviour of the stress processing role of the articular cartilage. For enzyme degradation, the bone is completely enclosed by the Palpress dental resin and the cartilage, protecting it from the actions of the enzymes. Compression tests of cartilage on bone were therefore found to provide reproducible results for determining the mechanical properties of articular cartilage in health and disease and therefore enable the desired mode of enzyme degradation of cartilage attached to bone.

The results for the hyperelastic tests serve to evaluate established hyperelastic laws for their ability to represent stress-strain response of loaded cartilage and the differences imposed by artificial degradation on hyperelasticity of the tissues matrix with respect to these established laws.

The histological and mechanical test results of normal cartilage samples showed a large variation in the matrix constituents, namely proteoglycan concentration and distribution, and in the hyperelastic curves. Similarly, artificial degradation of the normal cartilage using common enzymes Trypsin and Collagenase, lead to further variation in histological and mechanical test results. It should be taken into consideration that the change in stiffness may have been influenced by an artifact of the zero strain position being difficult to define, particularly on degraded tissue which has been substantially softened.

The average hyperelastic value for Trypsin treated samples was shown to be lower than normal samples at the same strain. The action of Trypsin was limited to degrading proteoglycans from the superficial zone toward the bone. Therefore the proteoglycan was lost in varying percentages among samples in the superficial zone through to the midzone and the deep zone. For these samples, the loss in proteoglycans in the more superficial regions would have resulted in a decrease in water in these areas. Consequently, as the indenter compresses the superficial layer, it is met with little resistance from water, resulting in a softer response. Then as the indenter compresses further, the stress would spread into the deeper layers where there is still water bound proteoglycans, and the stress could dissipate more easily through the efflux of water. Compression continues as normal, but at a lower strain than normal cartilage due to the lower concentration of water and subsequently lower pore pressure in the matrix. This finding supports and highlights the importance of the water bound proteoglycans in resisting compression.

The Collagenase treated samples showed increased stiffening at larger strain. This finding is in contradiction to previously published work of the effects of Collagenase on indentation experiments, but does support the local stiffening effect due to collagen fibril collapse (90). As a consequence of Collagenase treatment, the restrictive mechanism of the collagen network in the deeper zones may have become limited due to fibril disruption, allowing water to infiltrate and the tissue to swell. Therefore, as the load was applied, it was met with a large resistance from the increased water content within the tissue, creating a stiffer result. In normal cartilage, the superficial collagen aids in transferring the stress across a greater area of tissue, however with a disrupted network, the stress may be more concentrated beneath the indenter, and so after the initial compression of superficial broken collagen, the stiffness may be further increased due to the more localised distribution and therefore localised stiffening. This could have potential repercussions for the development and propagation of cracks in diseased cartilage.

From the results provided, Trypsin treatment was shown to decrease the stiffness of the hyperelastic curves, while Collagenase treatment was shown to increase the stiffness. However the average hyperelastic curves and the range of the hyperelastic curves for each of the treatment groups fell within the large range of normal samples measured. So, despite the trends observed as a result of artificial degradation, the results do not provide dependable values with which researchers can use to model the stiffness of degraded cartilage, since it falls within the normal range.

Furthermore, although the normal, Trypsin and Collagenase treated groups showed large variation in their hyperelastic curves, all curves maintained similar attributes. In

fact a large proportion of the curves from each group mimicked curves from the other two groups, indicating for example, that a normal sample with a small proteoglycan concentration may behave similarly to a cartilage sample devoid of a large portion of its proteoglycans. It was therefore determined that the resultant choice of hyperelastic laws to best represent cartilage would be consistent for any state of health from normal to artificially degraded, and would only change depending upon its stiffness.

Upon application of the established hyperelastic laws to the experimental data, the large variation in stiffness was also found to have no affect on the best fit of the Yeoh, Polynomial, Mooney-Rivlin and Arruda-Boyce hyperelastic laws for any of the samples. Using the three step criteria to determine the models of best fit, the Yeoh and Polynomial laws were found to best represent the stress-strain response of normal and artificially degraded cartilage.

5 Fracture of Normal and Degraded Articular Cartilage

5.1 Introduction

The study of fracture mechanics provides important information on the formation and propagation of cracks through materials. This methodology can enable researchers to evaluate the resistance of a tissue under load.

This chapter will compare and contrast the propagation of cracks in macroscopically normal articular cartilage and artificially degraded cartilage. These tests will be conducted on and off bone in order to test how the bone influences the propagation of initiated cracks as bone is an unavoidable component of the system in vivo. It is expected that the underlying subchondral bone should create a stiffer response to the lateral expansion and slow the crack propagation (49).

5.2 Method

5.2.1 Specimen Preparation

Cartilage samples were harvested from joints used in the compression tests from chapter 4. This included normal samples, Trypsin treated and Collagenase treated samples. The samples were chosen according to the stiffness measured in the indentation tests, allowing for samples from the normal and degenerate groups whose normal indentation results fell within a 10% stiffness range across the large spectrum

of stiffness results, to show the effects of artificial degeneration on tension and fracture mechanics. Following indentation testing, samples were wrapped in saline soaked cloth and stored in the freezer until required for tension and fracture testing.

Prior to testing, samples were defrosted in changes of saline for several hours. The cartilage samples were cut in half while still attached to the bone, and the cartilage removed from the bone from one of the halves. The thickness W of cartilage was measured using Vernier Callipers to determine the width B required for a B/W ratio of 0.5. Both halves were then sliced with a double blade cutter along the split line (previously determined for PLM in the compression tests), to produce two parallel specimens on each newly cut sample (Figure 5.1). Since the thickness is unique to each cartilage specimen, the width of each specimen varied from 0.5 to 0.9mm. The lengths (L) of the specimens were determined by the separation of the grips on the tensile tester, which was 13 mm, allowing for enough cartilage for the grips at either end. Therefore length was measured to be 17 to 21mm. This process produced 2 samples off bone, and 2 samples on bone, from the area in and around each site of indentation.
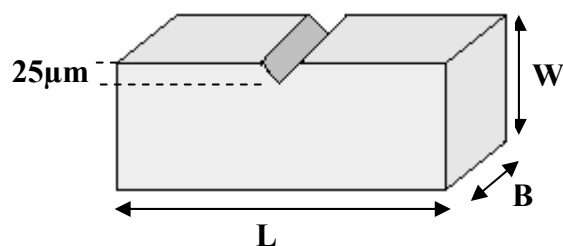
Figure 5.1 Specimen dimensions (not to scale)

The four cartilage specimens from each sample were glued (Locite 454) at both ends to fine sandpaper for greater hold within the grips. All samples were labelled according to their site, and stored in 0.15M saline for testing.

5.2.2 Tensile Test and Fracture Test

For the Tensile tests, specimens (one on bone and one off bone) were placed in the grips of the miniature tensile testing apparatus (Figure 5.2), with a 13mm space between the grips. The apparatus is able to clamp either end of the cartilage within grips that are moved at regulated speeds by a motor and measured by a load cell and linear variable displacement transducer (L.V.D.T). A "black box" controls the power to the motor and sends an amplified and filtered signal to a computer via an analogue-to-digital converter card input into LABVIEW software, specifically written to read the signal from the miniature tensile tester.
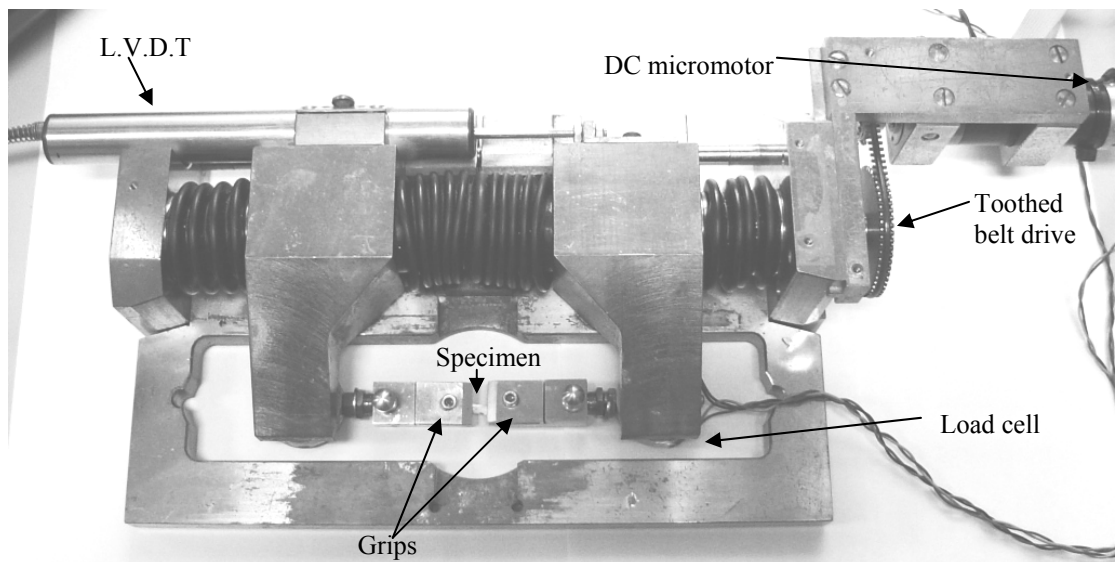
Figure 5.2 Miniature Tensile Tester

Each specimen was placed onto a miniature tensile testing apparatus (40), and tested in tension at an extension rate of 4.5mm min/min until complete failure occurred. These results were recorded and converted into stress strain data for analysis.

For fracture tests, a surface lacerator was used to introduce a radial notch in the articular surface to a depth of 25μm on the remaining specimens (on and off bone) from each sample. The specimens were again placed onto the tensile tester and tested

at extension rates of 4.5mm min/min, to an unspecified strain until complete failure of the tissue. The results were recorded and converted to stress strain data for analysis. Visual data was captured at 5 second intervals using a Canon Eos 20D with a Tamron 90mm f2.8 Macro Lens. At the end of testing, the samples size consisted of normal and degenerate cartilage tested at one extension rate in tension and fracture, on and off bone.

5.3 Results

5.3.1 Fracture of Normal, Trypsin and Collagenase Treated Cartilage

Cartilage specimens were divided into groups of similar stiffness before artificial degradation. Previous tests presented in chapter 3, indicated that the mode of action of Trypsin and Collagenase on cartilage is dependant on the initial matrix composition. It was therefore assumed that three specimens of similar stiffness, should have similar matrix composition, and therefore degrade to a similar state. So, if there were three specimens of similar stiffness, one remained normal, one degraded in Trypsin, and one in Collagenase, it would provide a guide to how one specimen may behave mechanically in its normal state, proteoglycan degraded state, and collagen disrupted state.

The behaviour of crack propagation for normal and degraded cartilage samples was typical of previously published research (23, 40). As the cartilage was loaded, the crack opening (created by the surface lacerator) was pulled in a transverse direction, absent of any crack propagation. This was followed by the radial pulling of the deep matrix toward the surface as the superficial collagen fibrils were loaded laterally.
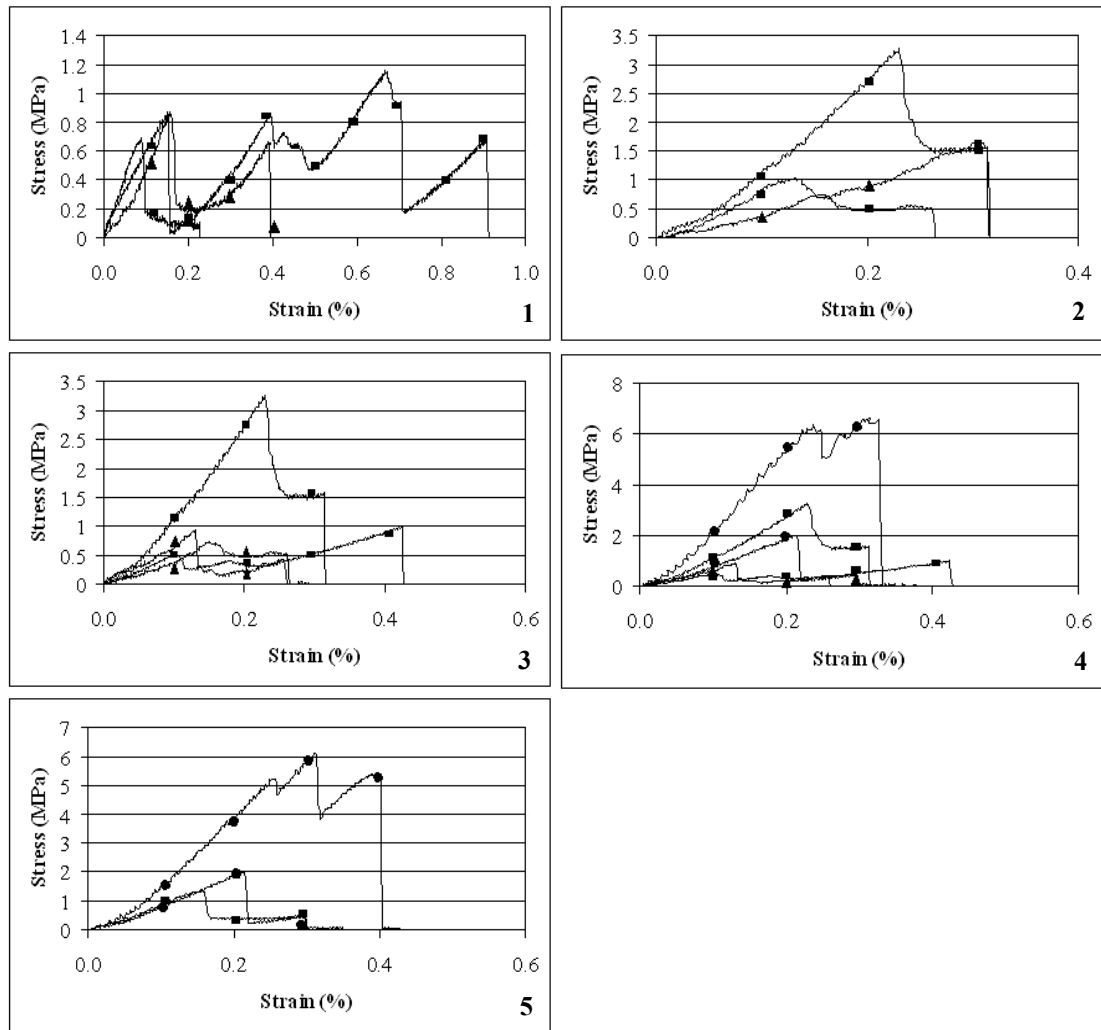
Figure 5.3 Stress-strain curves of articular cartilage undergoing crack propagation. Samples are divided into groups 1 – 5 according to their similar matrix composition determined by compression tests. Symbols denote treatment of each samples including Collagenase treated (●), Trypsin treated (▲) and no treatment, i.e. normal (■).

Figure 5.3 shows the crack propagation of normal cartilage, Trypsin and Collagenase treated cartilage in each group of specimens, divided into groups whose normal stiffness values were within 10% (Table 4.1). From these graphs, it can be seen that less energy was required to initiate crack propagation in Trypsin treated samples. Normal and Collagenase treated samples appeared to require a much larger amount of energy in order to propagate the crack through to tissue failure. A great deal more samples would be required to show a significant trend in the differently treated samples. From this small samples size, a large variation is evident, even amongst normal samples, and those that have undergone the same enzyme treatment.

Curve 1   Curve 2

Curve 3   Curve 4

Curve 5   Curve 6
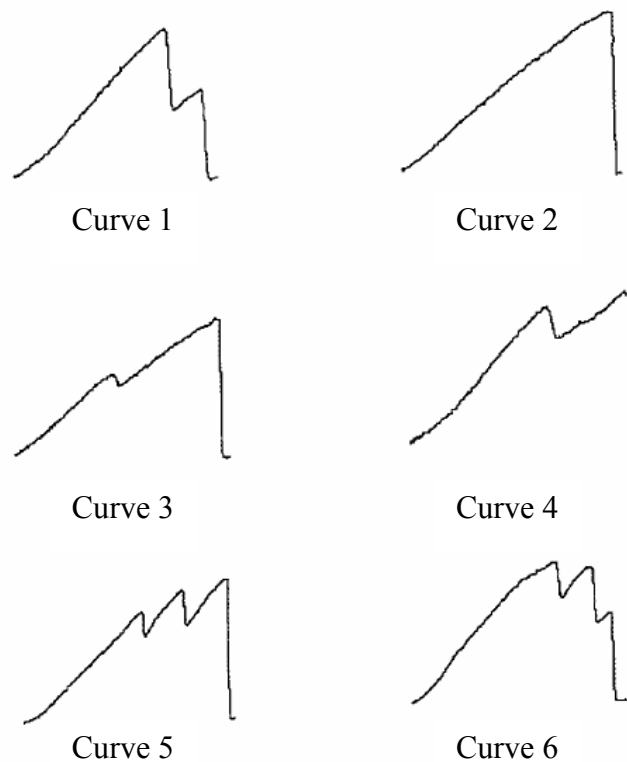
Figure 5.4 Typical stress-strain responses of cartilage pulled in tension through to crack propagation and final tissue failure (40).

Figure 5.4 shows the expected curve types from crack propagation experiments, with curve one the most common representation of crack propagation in normal cartilage(40). Table 5.1 lists the type and occurrence of curves for normal, Trypsin treated and Collagenase treated cartilage. Normal and Trypsin treated cartilage appeared to follow the normal trend of curve one, where as Collagenase treated cartilage was more dispersed across a number of curve types. The three other types of curve displayed by Collagenase suggest a disrupted matrix where complete failure occurred at the first sign of crack propagation (curve 2), and weakened surface zone, where more energy was required to propagate the crack after the surface had been compromised.

Treatment	Curve 1	Curve 2	Curve 3	Curve 4	Curve 5	Curve 6
Normal	6			1		
Trypsin	6	1				
Collagenase	2	1		1	1	

Table 5.1 Distribution of curve types for each normal cartilage, Trypsin treated and Collagenase treated cartilage.

5.3.2 Cartilage on Bone and off Bone

Tensile experiments were performed on cartilage on bone and off bone for all samples. Bone was shown to affect the stress-strain results of the cartilage, with stiffness greater at all strain values for 17 of the 18 samples. Table 5.2 shows the variation in these values. The percentage increase in stiffness was uniform across strain values from 5% through to 20% for every sample.

Treatment	Increase in stiffness					
Normal	0.99	0.09	0.67	-0.53	0.22	0.97
Trypsin	0.39	0.92	0.86	0.92	0.75	0.91
Collagenase	0.59	0.56	0.98	0.72	0.09	0.01

Table 5.2 Increase of tensile stiffness in 18 articular cartilage samples on bone compared to off bone.

Figure 5.5 shows a representative sample of tensile stress-strain graphs of articular cartilage through to failure. These results show that fracture propagation in cartilage on bone samples requires more energy than those off bone, for normal, Trypsin treated and Collagenase treated samples.
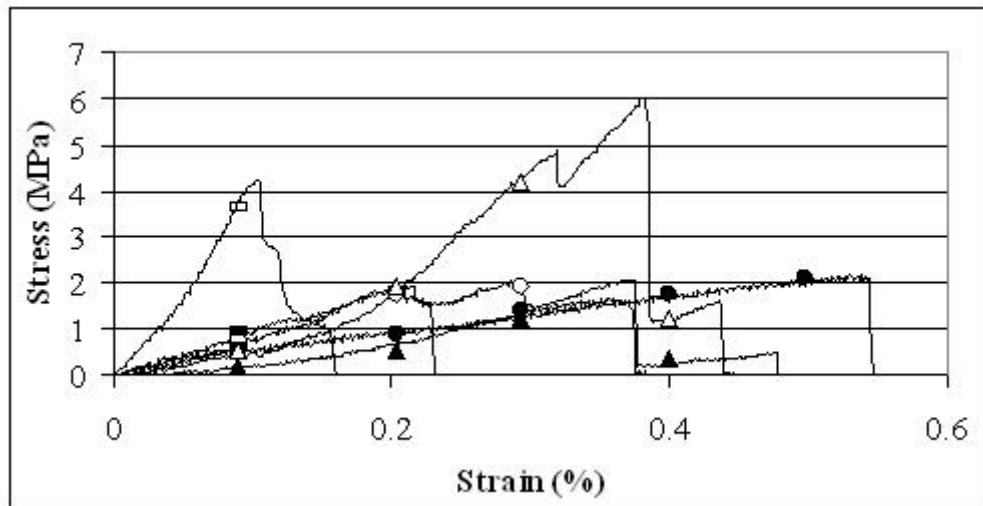
Figure 5.5 Tensile stress-Strain graphs to complete tissue failure of normal (■), Trypsin treated (▲) and Collagenase treated articular cartilage, on bone (outlined shape) and off bone (black shape).

5.4 Discussion

The mechanisms for fracture propagation in cartilage are made more complicated due to the anisotropic and heterogeneous design of the tissue. For most normal cartilage samples, the initial stage of fracture propagation begins with the lateral stretch of the crack opening. To initiate fracture propagation, a large amount of energy is required at the crack notch to break through the perpendicular alignment of the fibrils in relation to the radial crack notch. As the opening increases, there is a rapid cessation of fracture propagation through the surface area, followed by a stabilising effect through the middle zone. As the tissue continues to be pulled laterally, the deep matrix is pulled toward the surface due to the radial anchoring of the superficial fibrils being pulled.

The results presented here demonstrate the effects of enzyme treatment on the fracture propagation of cartilage for the first time. There appeared to be large

variability between samples from the same degradation groups and the normal group, perhaps due to differences between location on a joint (91) or between joints.

Collagenase treated samples appeared to require more energy to initiate fracture propagation than the normal or Trypsin treated samples. The mode of propagation, or type of graph (Figure 5.4), varied from the standard curve as demonstrated by the normal and Trypsin treated groups. This phenomenon may be attributed to the disruption to the cross-linkage of fibrils in the superficial zone, allowing more lateral stretch before fracture initiation. In this case, the superficial zone would no longer provide the greatest resistance to fracture initiation. However, this does not explain the increased energy observed. The disruption to the collagen matrix would have made room for greater swelling ability of the proteoglycans, increasing the pore pressure within the matrix, and therefore increasing the energy required for further lateral expansion.

This phenomenon would also explain the decreased lateral expansion and energy required for crack propagation in Trypsin treated cartilage. Because of the decrease in proteoglycans, and therefore water within the tissue, there would be less escape of energy through efflux of water, leaving energy available to concentrate around the intact collagen network and available to propagate cracks. It has also been shown that although proteoglycans do not appear to significantly affect the tensile stiffness of cartilage, they do have an important function in retarding the rate of stretch and alignment of a sudden tensile load (54). The results presented here also support this theory.

Disruption to the superficial collagen network seems advantageous here in decreasing the likelihood of fracture propagation; however it is the cascade of osteoarthritis and disease events that occurs following this superficial collagen disruption that is of dire consequence. It is not the collagen fibrils alone that are disrupted during disease, but the proteoglycan content and small inorganic chemicals that are also disrupted. Therefore the increased stiffness occurring in the initial stages of degradation, in accordance with other degenerative effects, may lead to the eventual breakdown of the matrix.

Although it was shown here that increasing proteoglycan concentration is coupled with increased total fracture strain energy, analysis of the level of degradation to the collagen network would need to be completed to determine the full effect of both components.

Other difficulties were noticed with the experimental set up procedure in the tensile and fracture tests. It was important to harvest cartilage strips that were taken from flat areas on the cartilage, so that when the cartilage off bone was pulled taut in the mini tester grips, this flat orientation was representative of its natural orientation on bone. Similarly, if the cartilage strips were placed in 0.15M saline for an extended period of time before testing, they began to curl quite severely, which made the cartilage difficult to attach within the grips so that the tissue was taut. The degree of curling is a result of the competition between the severely strain-limiting properties of the articular surface and the swelling of the extensible deeper matrix, which when freed from the constraints of the osteochondral attachment would swell to a degree determined by the tightness of the collagen network when given access to fluid. The

degree of curling may affect the results in that a relaxed collagen network in the deeper matrix may increase the curling than a tight network, so that the cartilage may not be as taut as possible. All efforts were made to ensure that cartilage was as straight as possible without damaging the tissue, and tested soon after submersion in saline to avoid the influence of the swell induced curling.

6 Benchmarking of the biomechanical characteristics of normal and degraded articular cartilage

6.1 Introduction

The primary objective of this thesis was to present and compare parameters that can be used to benchmark the biomechanical characteristics of normal and degraded articular cartilage. This led to the analysis of significant biomechanical consequences of artificial degradation, namely proteoglycan loss and collagen disruption, on normal cartilage.

6.2 Normal Cartilage

Normal, intact and untreated articular cartilage was found to contain a highly variable concentration and distribution of proteoglycans from location to location and joint to joint. Likewise, the compressive hyperelastic curves showed a large variation between samples. For example, at 30% strain the value of stress in some samples was as high as 5.2MPa, while it was as low as 0.4MPa in others at the same strain. The average stress for all samples at this strain was 1.8MPa (S.D. = 1.3MPa) as shown in Figure 6.1. The compressive stiffness of articular cartilage was measured as the gradient at a point on the curve. At 30% strain, the stiffness was as high as 30.5MPa, and as low as 3.6MPa. The average stiffness value was 9.7MPa (S.D. 7.8MPa) for all normal samples.
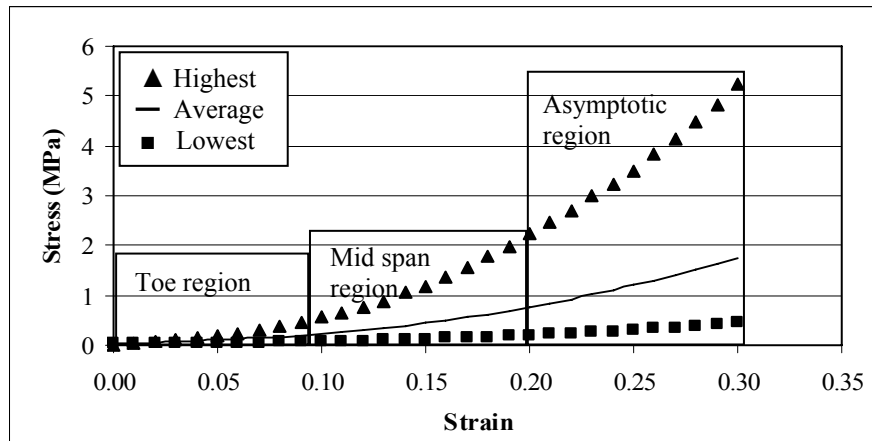
Figure 6.1 Representative compressive stress-strain curves showing highest and lowest and the average curve for normal cartilage.

The tensile stress-strain curves also showed variation for example, at 20% strain the stress in some samples was as high as 3.0MPa, while it was as low as 1.4MPa in other samples. The average stress for all samples at this strain was 1.8MPa (S.D. = 0.6MPa) as shown in Figure 6.2.
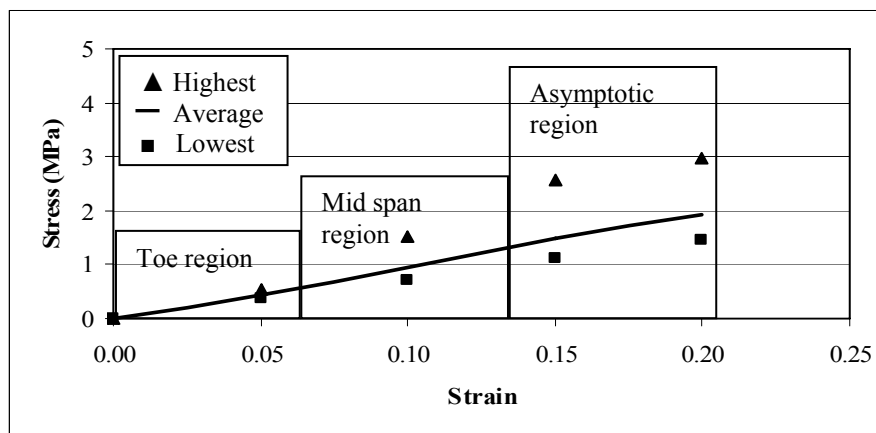
Figure 6.2 Representative tensile stress-strain curves showing highest and lowest levels and the average curve for normal cartilage.

The tensile strength of cartilage was fairly consistent for most samples ranging between 0.04MPa and 0.3MPa at 30% strain; however one of the samples showed a large discrepancy in tensile stiffness, measuring 1.6MPa (Figure 6.3). The average stiffness for all samples, minus the aberrant result was 0.15MPa (S.D. 0.12) at this strain.
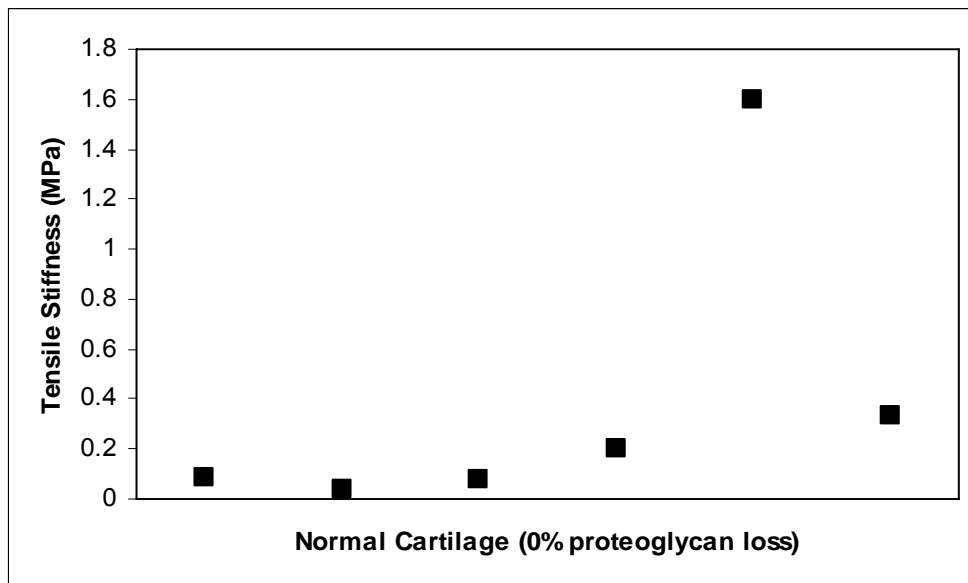
Figure 6.3 Tensile stiffness of normal cartilage at 20% strain

Fracture testing of normal cartilage showed variation in the fracture initiation strain, with strain in some samples as low as 9.3 and as high as 32.1 in other samples (Figure 6.4). The average fracture initiation strain for all normal samples was 19.3 (S.D. 7.8). Final failure strain appeared to follow a similar trend to the fracture initiation strain, with strain as low as 22.9 in some samples, and as high as 50.5 in other samples. The average value for final fracture strain for all samples was 33.5 (S.D. 10.2). Again, there was one sample that showed a large deviation from the rest of the samples, reaching final failure strain at 90.9. The fracture had in fact progressed through the entire tissue at a strain more consistent with the rest of the samples; however the neck of a few remaining fibrils required greater displacement (but very little force) to be drawn out from the divided regions of the matrix, maintaining a very week connection between the two halves. Although this sample provided insight into a possible occurrence in the final stages of fracture propagation, it was not representative of the bulk tissue properties, and was therefore omitted from the calculations of the average value.
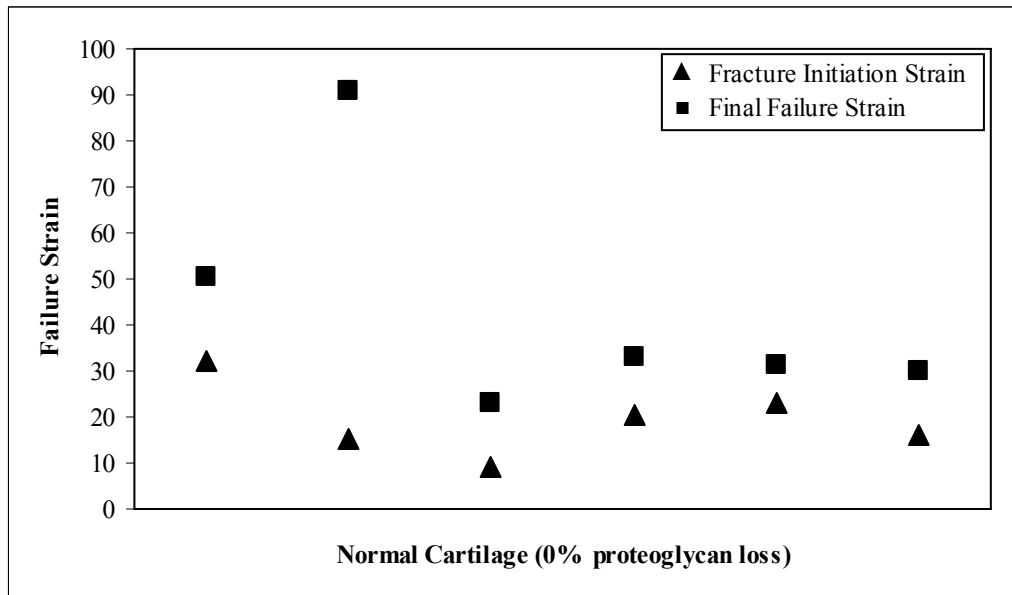
Figure 6.4 Fracture initiation strain and final failure strain for normal cartilage

The total failure strain energy of normal cartilage varied between 0.05Nm and 0.47Nm for all samples tested (Figure 6.5). The average value for all samples was 0.28 (S.D. 0.18). The total failure strain energy was taken to be the area underneath the stress-strain curve for fracture tests, therefore indicating a larger value for tougher tissues.
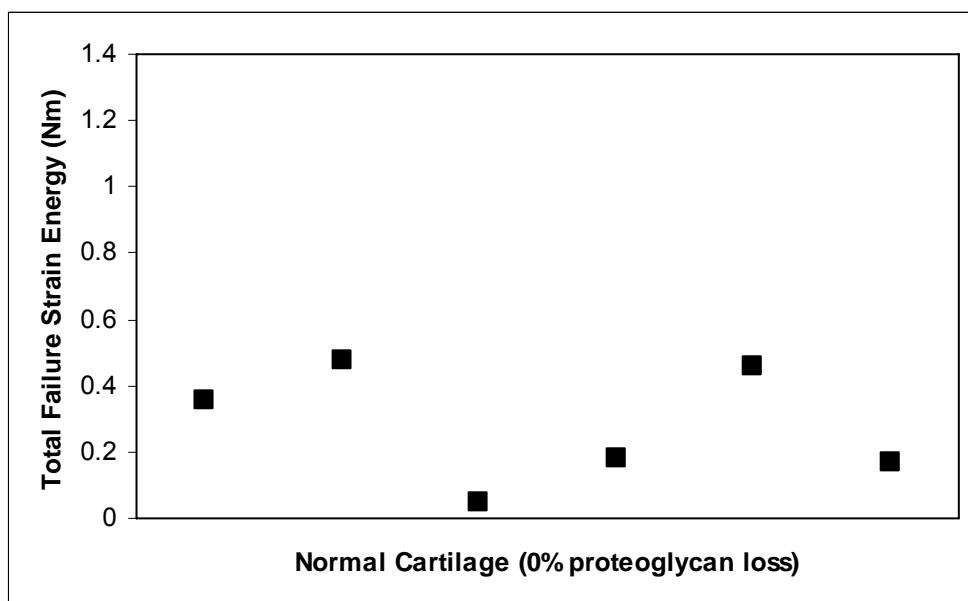
Figure 6.5 Total failure strain energy of normal cartilage

6.3 Influence of Proteoglycan Loss

Artificial degradation of proteoglycans with Trypsin for 1 hour produced varied loss in the total concentration of proteoglycans from different samples. The compressive hyperelastic curves reveal a stress value as high as 3.3MPa in some samples, and as low as 0.4MPa. The average stress for all samples at this strain was 1.3MPa (S.D. = 1.3MPa) as shown in Figure 6.6.
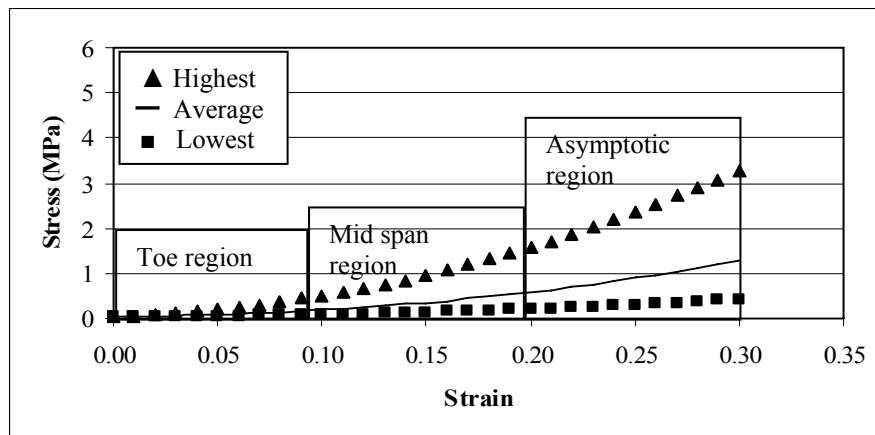
Figure 6.6 Representative compressive stress-strain curves showing highest and lowest levels and the average curve for Trypsin treated cartilage.

The tensile stress-strain curves also showed a large variation with a high stress value of 3.1MPa and a low value of 0.6MPa. The average stress for all samples at this strain was 1.8MPa (S.D. = 0.8MPa) as shown in Figure 6.7.
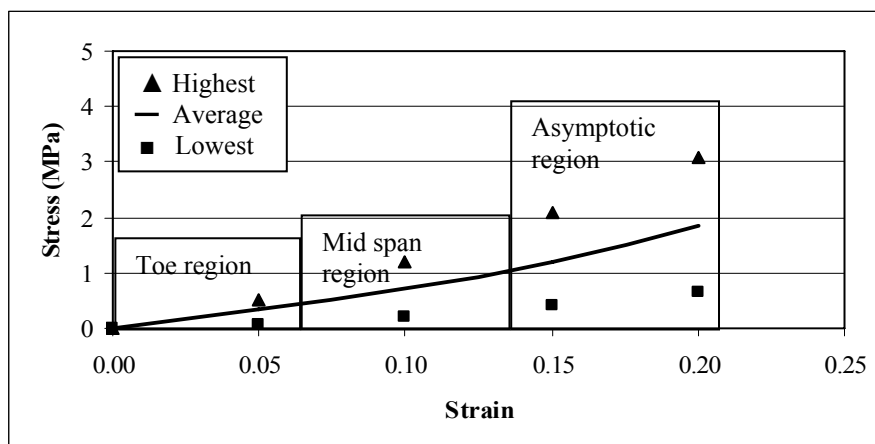
Figure 6.7 Representative tensile stress-strain curves showing highest and lowest levels and the average curve for normal cartilage.

For comparative analysis, the degradation of proteoglycans from each sample was converted to percentage loss (Figure 6.8) using the formula:

$$\frac{\text{Total proteoglycan content} - \text{Remaining proteoglycan content}}{\text{Total proteoglycan content}} \qquad \textbf{(6.1)}$$

The use of the expression (6.1) eliminated the effects of the variations in proteoglycan content relative to individual quantity thus enabling meaningful comparisons to be made between the samples tested.

Figure 6.8 shows Safranin O stained slides, alongside the optical absorbance slide for the same section of cartilage. The red staining represents presence of proteoglycan, intensifying in colour with increasing proteoglycan concentration. Increasing stain intensity results in black through to white shading, where black represents no proteoglycans and is assigned the value 0, while white represents high proteoglycan concentration, and is assigned the maximum value of 3.
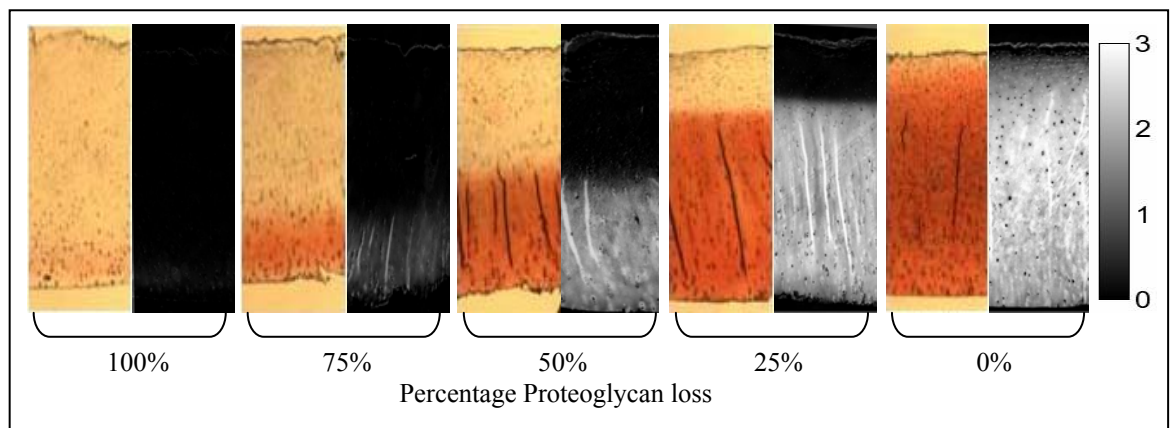
Figure 6.8 Safranin O stained articular cartilage (colour) and optical absorbance (greyscale) for varying levels of proteoglycan loss following Trypsin treatment.

The assignment of values to the optical absorbance slides can further be seen in Figure 6.9. A slide has been rotated on its side here, to show how the optical absorbance curves are created. The sum of absorbance values at each depth transect were calculated (Figure 6.9). These values were then plotted at each depth value, and

the total proteoglycan content determined by adding the absorbance value at each depth from the surface to the bone. In other words, the initial and remaining quantity of proteoglycans was determined by measuring the area under the curve of the optical absorbance verse depth curves (Figure 6.10).
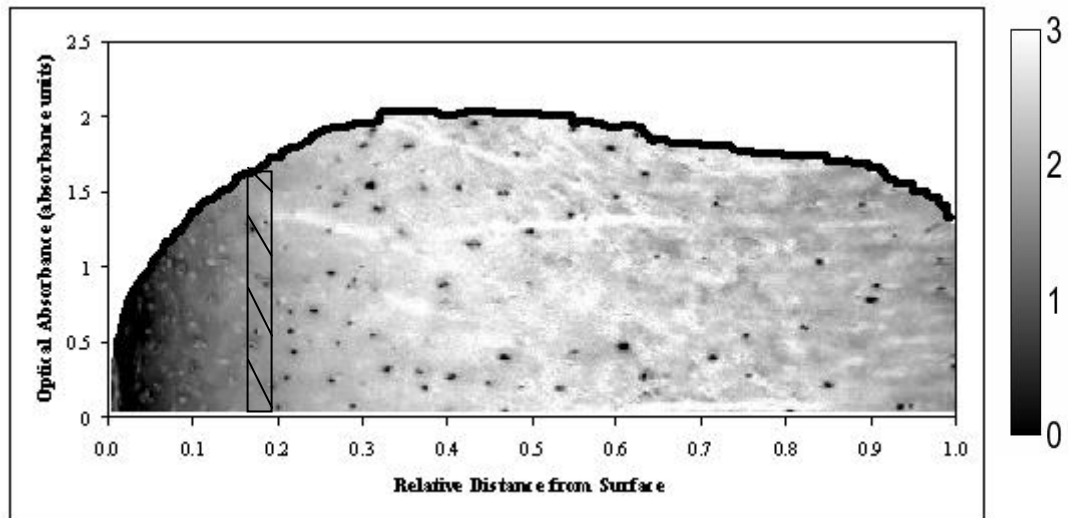
Figure 6.9 Schematic showing how optical absorbance versus depth curves are created from stained articular cartilage slides. The area of the curve is calculated by adding the areas of strips such as indicated in the figure from the surface to the bone.
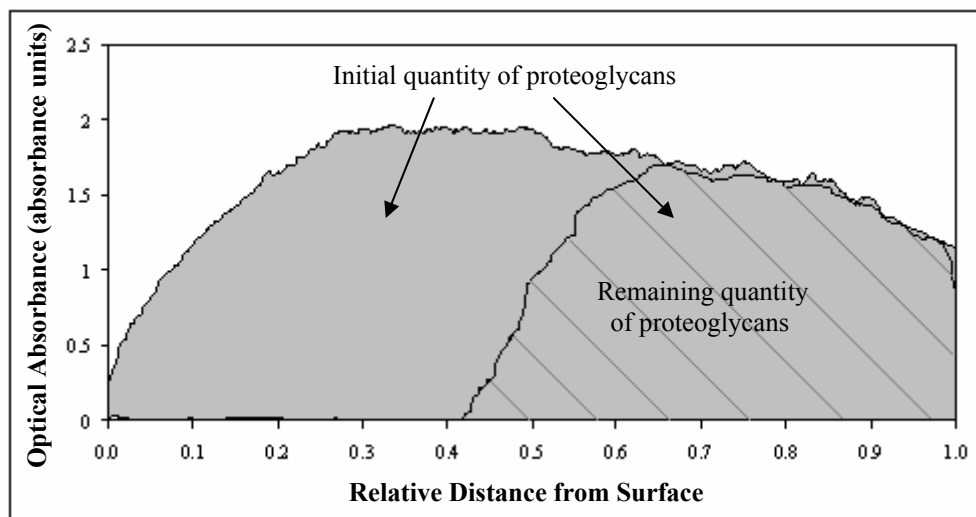
Figure 6.10 Optical absorbance versus depth curve showing determination of proteoglycan content. The area under the curve was measured for normal sample to determine the initial quantity of proteoglycans (entire plane grey area), while the degraded sample was measured to determine the remaining quantity of proteoglycans (shaded area).

For compression tests, stiffness was shown to decrease with increasing loss in proteoglycans (Figure 6.11). Because this analysis looks at percentage proteoglycan content and not the degradation time, samples degraded for 1 to 3 hours were included in order to be able to use a range of levels of degradation to determine a relationship, if any, between proteoglycan loss and compressive stiffness values. A close scrutiny of the data in Figure 6.11 demonstrates that compressive stiffness decreases after 30% loss, remaining constant between 50 and 70% proteoglycan loss, before exhibiting another decrease at 70% proteoglycan loss. This variation is plotted in Figure 6.11 below.
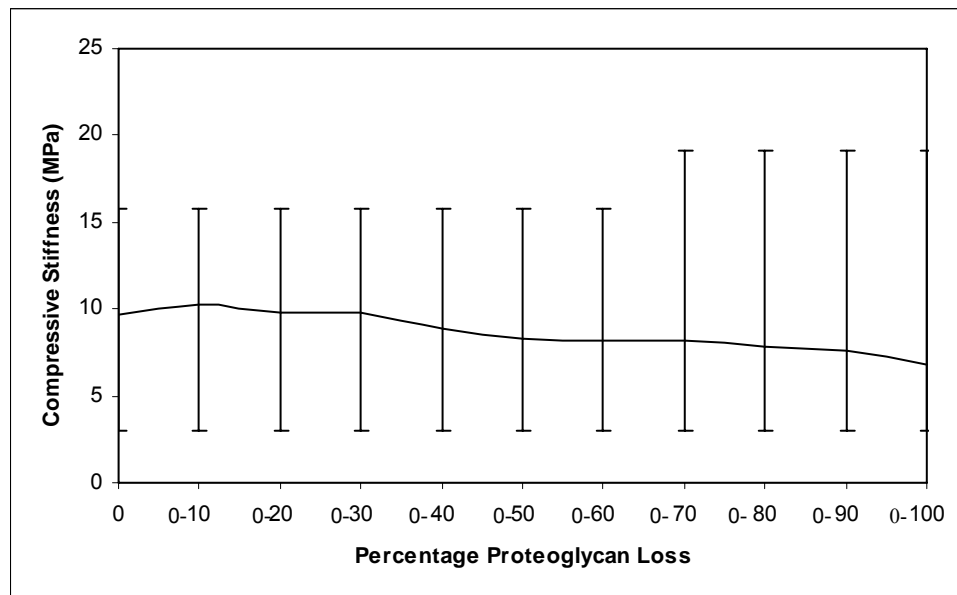
Figure 6.11 Mean compressive stiffness of cartilage versus cumulative proteoglycan loss. X-axis represents for example: 0-10 = loss between 0 to 10%; 0-20 = loss between 0 to 20% etc.

The tests conducted for tensile and fracture testing indicated that there was no significant variation among Trypsin treated cartilage (Figure 6.12) relative to the variation observed in their normal counterparts (Figure 6.3). The highest measure of strain in some samples for fracture initiation was 30.9 and 13.1 for the lowest, with

an average value of 19.0 (S.D. 6.2). The highest strain for final failure was 41.7 and

25.5 for the lowest measure, with an average value of 30.9 (S.D. 7.0).
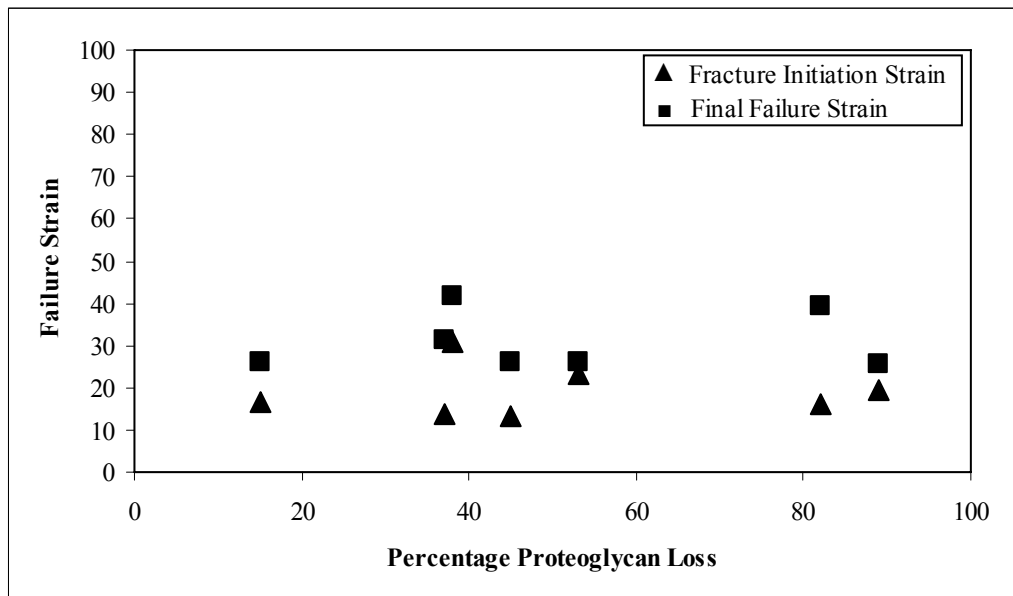
Figure 6.12 Crack initiation strain and Final failure strain versus proteoglycan loss.

The tensile stiffness of Trypsin treated cartilage showed a highest value of 1.3MPa at

45% proteoglycan loss and a lowest value of 0.2MPa at 37% proteoglycan loss

(Figure 6.13). Although the highest and lowest readings were within a matter of 8%

proteoglycan loss, there appeared to be a small trend of increasing tensile stiffness

with increasing proteoglycan loss.
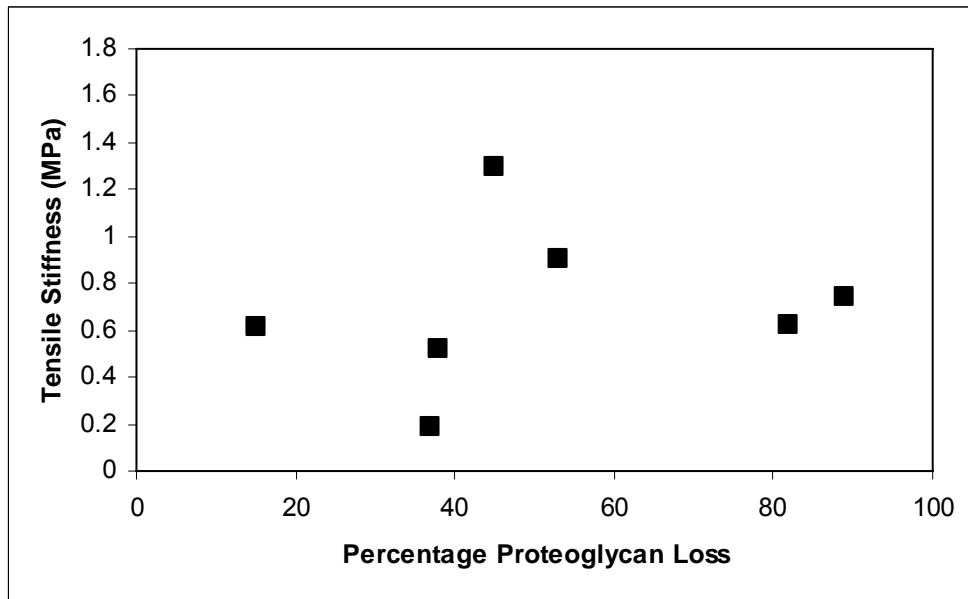
Figure 6.13 Tensile stiffness at 20% strain versus proteoglycan loss.

Figure 6.14 on the other hand shows very little correlation of proteoglycan loss to total failure strain energy. The highest and lowest total failure strain energy was measured to be 0.26Nm and 0.09Nm respectively. The average total failure strain energy for all samples was 0.14Nm (S.D. 0.06).
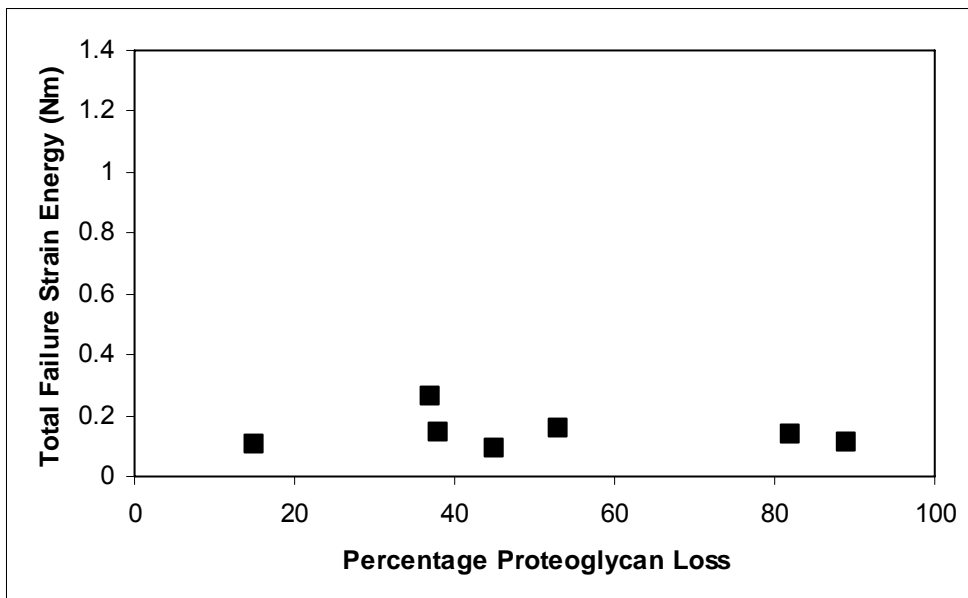
Figure 6.14 Total failure strain energy versus proteoglycan loss.

6.4 Influence of Collagen Disruption

Collagenase caused large variation in the compressive hyperelastic curves, for example, at 20% strain the value of stress in some samples was as high as 4.7MPa, while it was as low as 0.5MPa in other samples. The average stress for all samples at this strain was 2.8MPa (S.D. = 1.2MPa) as shown in Figure 6.15.
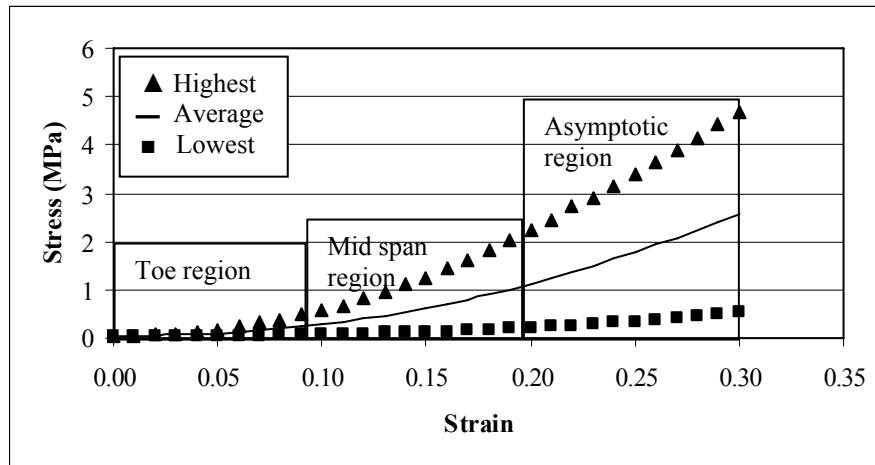
Figure 6.15 Representative compressive stress-strain curves showing highest and lowest levels and the average curve for Collagenase treated cartilage.

The tensile stress-strain curves also showed a large variation with some samples as high as 4.6MPa, and other samples as low as 1.0MPa. The average stress for all samples at this strain was 2.3MPa (S.D. = 1.4MPa) as shown in Figure 6.16.
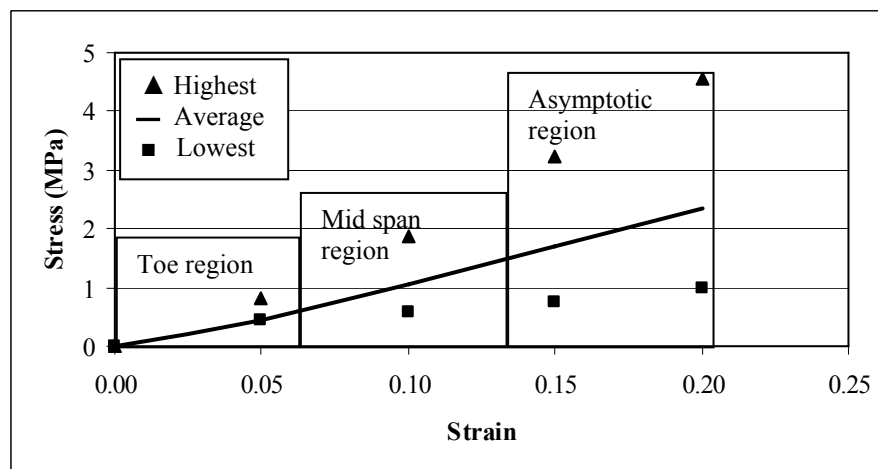
Figure 6.16 Representative tensile stress-strain curves showing highest and lowest levels and the average curve for Collagenase treated cartilage.

Unlike cartilage treated with Trypsin, Collagenase treated samples were unable to be measured in terms of disruption to the collagen network, due to insufficient methodology available for collagen assessment. Therefore the Collagenase treated cartilage was compared against the normal cartilage as two separate groups rather than by percentage degradation.

The compressive stiffness results for Collagenase treated cartilage were highly varied with values ranging from a 28% decrease in compressive stiffness, to a 211% increase (Figure 6.17). At 30% strain the compressive stiffness was as high as 23.3MPa, and as low as 3.7MPa for all Collagenase treated samples. The average compressive stiffness of all Collagenase treated samples was 11.7 (S.D. 7.4).
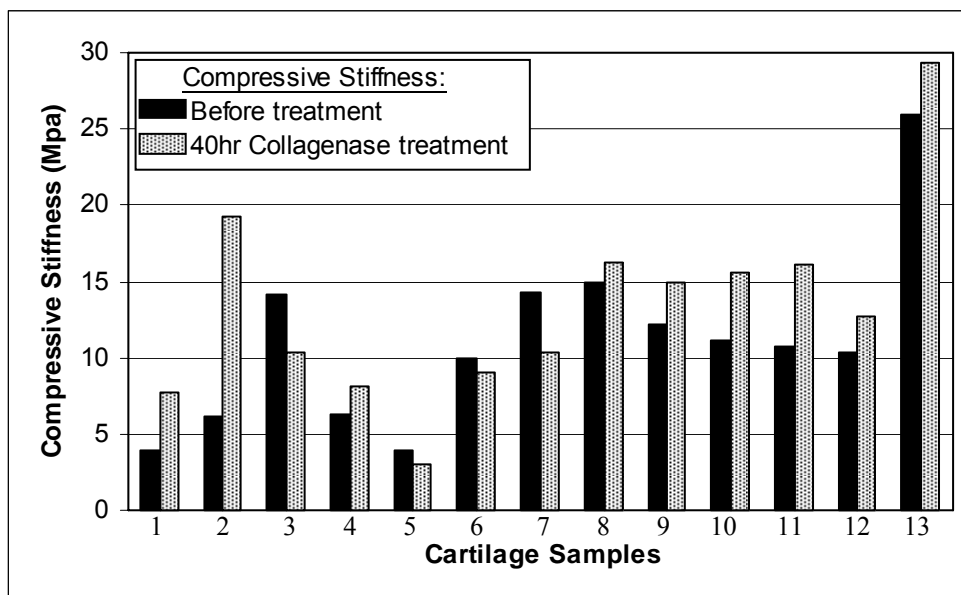
Figure 6.17 Compressive stiffness of cartilage at 30% strain before and after 40 hours Collagenase treatment.

The tests conducted for tensile and fracture testing, measured a highest strain of 46.2 and lowest of 17.1 for crack initiation strain, and 48.5 and 27.6 for the highest and lowest final failure strain (Figure 6.18). The average values were 28.6 (S.D. 10.7) and 42.4 (S.D. 8.9) respectively. Therefore Collagenase treated cartilage appeared to

withstand greater stretching than normal cartilage before the crack began to propagate, and before complete failure occurred.
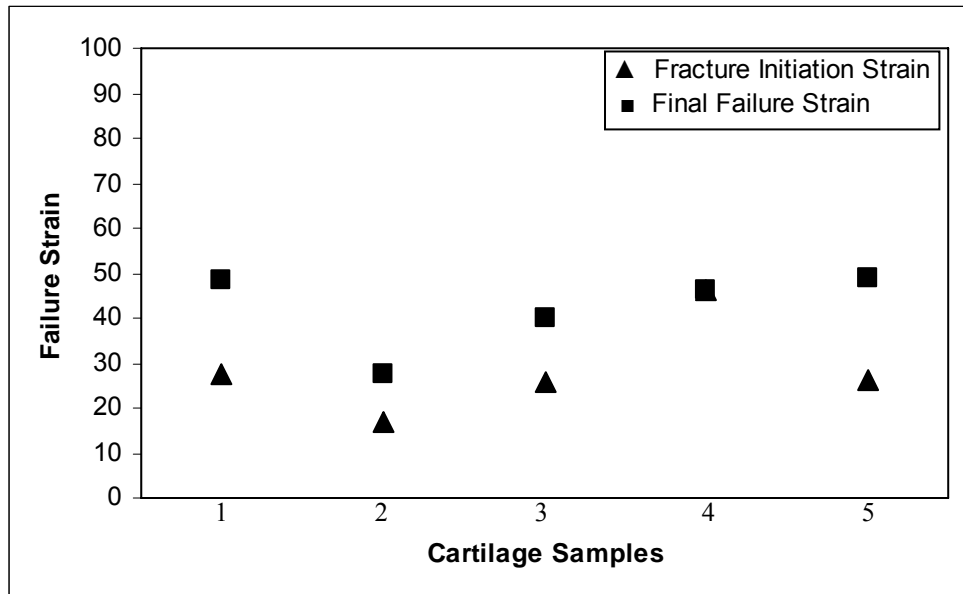
Figure 6.18 Crack initiation strain and Final failure strain for cartilage treated in Collagenase for 40 hours.

Tensile tests indicated that at 20% strain, Collagenase treated cartilage was measured with a high stiffness value of 1.67MPa for some samples, and a low stiffness of 0.1MPa in tension (Figure 6.19), demonstrating a large variation among the tensile stiffness of cartilage samples treated with collagenase. The average value for tensile stiffness was 0.7MPa (S.D. 0.6) at the same strain.
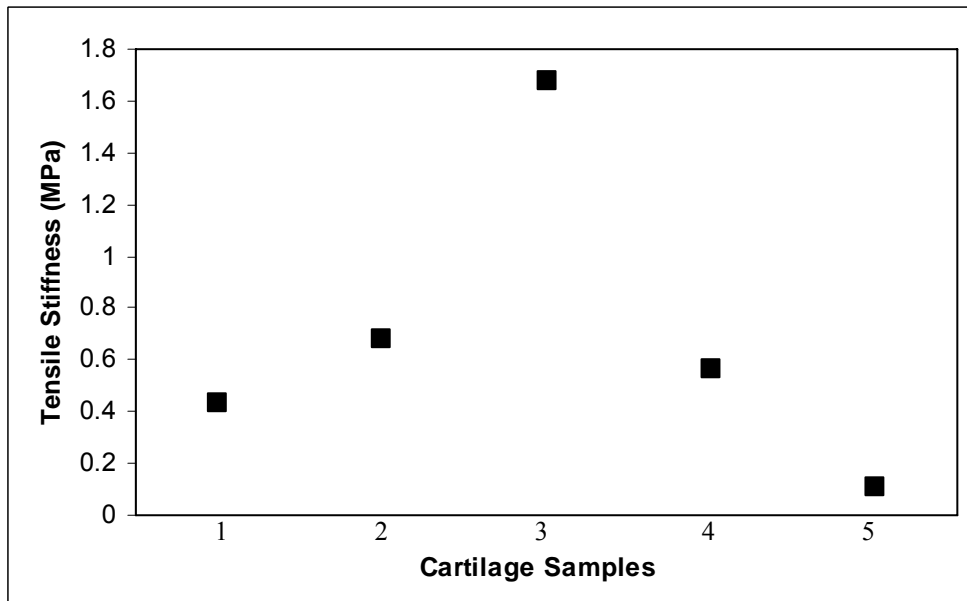
Figure 6.19 Tensile stiffness at 20% strain for cartilage treated in Collagenase for 40 hours.

Results for total failure strain energy were in keeping with aforementioned results, showing that Collagenase treated cartilage appeared to have a higher trend in total failure strain energy, with a high value of 1.23Nm and a low of 0.05MPa (Figure 6.20). The average value for all samples degraded in Collagenase was 0.62Nm (S.D. 0.45). These results again show a large variation in the results of samples degraded for the same time exposure in Collagenase.
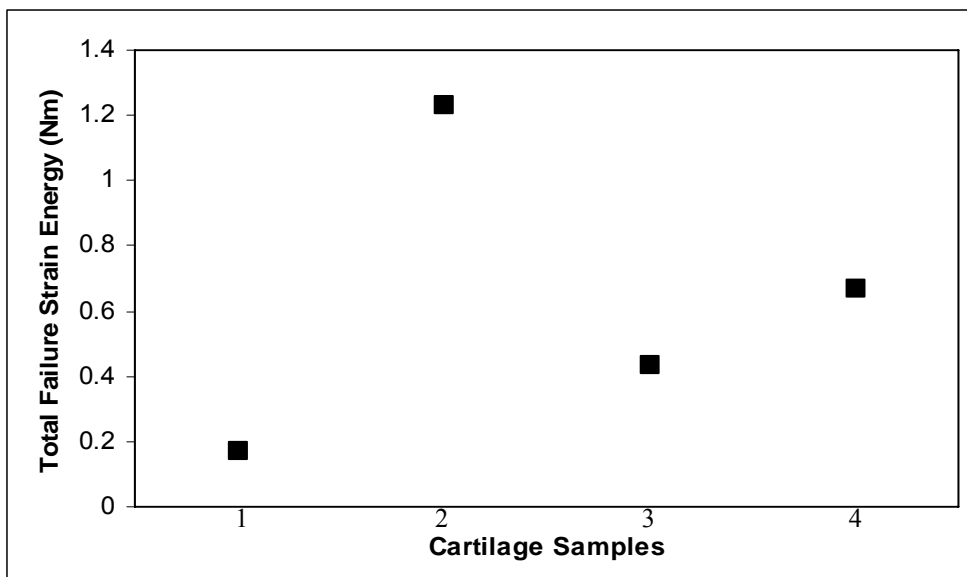
6.5 Relative Effects of Degradation Treatments on the Principal Mechanical Parameters

Test	Normal	Trypsin	Collagenase
Hyperelastic Curves	• Highest stress of 5.2MPa at 30% strain • Lowest stress of 0.4MPa at 30% strain • Average stress of 1.8MPa at 30% strain (S.D. 1.2MPa)	• Highest stress of 3.3MPa at 30% strain • Lowest stress of 0.4MPa at 30% strain • Average stress of 1.3MPa at 30% strain (S.D. 1.3MPa)	• Highest stress of 4.7MPa at 30% strain • Lowest stress of 0.5MPa at 30% strain Average stress of 2.8MPa at 30% strain (S.D. 1.2MPa)
Tensile stress-strain curves	• Highest stress of 3.0MPa at 20% strain • Lowest stress of 1.4MPa at 20% strain • Average stress of 1.9MPa at 20% strain (S.D. 0.6MPa)	• Highest stress of 3.1MPa at 20% strain • Lowest stress of 0.6MPa at 20% strain • Average stress of 1.8MPa at 20% strain (S.D. 0.8MPa)	• Highest stress of 4.6MPa at 20% strain • Lowest stress of 1.0MPa at 29% strain • Average stress of 2.3MPa at 20% strain (S.D. 1.4MPa)
Compressive Stiffness	• Highest stiffness of 30.5MPa at 30% strain • Lowest stiffness of 3.6MPa at 30% strain • Average stiffness of 9.7MPa (S.D. 7.8MPa) at 30% strain	• Highest stiffness of 29.2MPa at 30% strain • Lowest stiffness of 3.7MPa at 30% strain • Average stiffness of 10.0MPa (S.D. 8.1MPa) at 30% strain	• Highest stiffness of 23.3MPa at 30% strain • Lowest stiffness of 3.7MPa at 30% strain • Average stiffness of 11.7MPa (S.D. 7.4MPa) at 30% strain • Large variation in stiffness values, ranging from small decrease in stiffness, to very large increase in stiffness.
Failure Strain	• Fracture initiation strain varied from 9.3 to 32.1 for all samples, with average strain of 19.3 (S.D. 7.8) • Final failure strain varied from 22.9-50.5 (aberrant value 90.9) for all samples, with average strain of 33.5 (S.D. 10.2)	• Fracture initiation strain varied from 13.1 to 30.9 for all samples, with average strain of 19.0 (S.D. 6.2) • Final failure strain varied from 25.5 to 41.7 for all samples, with average strain of 30.9 (S.D. 7.0)	• Fracture initiation strain varied from 17.1 to 46.2 for all samples, with average strain of 28.6 (S.D. 10.7) • Final failure strain varied from 27.6 to 48.5 for all samples, with average strain of 42.2 (S.D. 8.9)
Tensile Stiffness	• Highest stiffness of 0.3MPa at 20% strain (aberrant value of 1.6MPa) • Lowest stiffness of 0.04MPa at 20% • average stiffness of 0.15MPa (S.D.	• Highest stiffness of 1.3MPa at 20% strain • Lowest stiffness of 0.2MPa at 20% strain • Average stiffness of 0.7MPa (S.D.	• Highest stiffness of 1.67MPa at 20% strain • Lowest stiffness of 0.1MPa at 20% strain • Average stiffness of 0.7MPa (S.D. 0.6MPa)

	0.12MPa)	0.34MPa) at 20% strain • Stiffness increased with increasing proteoglycan loss	
Total Failure Strain Energy	• Varied between 0.05Nm and 0.47Nm • Average of 0.28Nm (S.D. 0.18Nm)	• Varied between 0.09Nm and 0.26Nm • Average of 0.14Nm (S.D. 0.06Nm) • Decreasing total failure strain energy with increasing proteoglycan loss	• Varied between 0.05Nm and 1.23Nm • Average of 0.62Nm (S.D. 0.45Nm)

Table 6.1 Relative effects of degradation treatments on the principal mechanical parameters

7 Discussion and Conclusion

7.1 Discussion and Conclusion

Research into replacement biological and artificial materials for articular cartilage is an important step towards appeasing the physical and financial burden of cartilage related diseases. In order to validate the appropriate functional characteristics of cartilage, we need to systematically study and understand what constitutes normality and degradation in cartilage. This thesis provides a step in this direction.

The aim of the work presented here was to create artificial models of degradation to determine the influence of specific material constituents on the mechanical properties of articular cartilage. According to previous research into the anatomical and physiological changes that occur during diseases such as osteoarthritis, there is a combination of cascading events that occur throughout the tissue. It must therefore be reiterated that artificial degradation specifically targets single components with little to no collateral damage to other matrix components, although it has been noted that Trypsin may cause some collateral damage to collagen, and Collagenase may cause minor damage to proteoglycans. Furthermore, these specific components are disrupted or degraded without simultaneous cyclic loading, as would be the case in vivo. Therefore, the process of artificial degradation is merely an idealisation on

what can occur in vivo, and can only provide insight into the mechanical properties of single components by examining the subsequent behaviour of the tissue following its removal. It is for this reason that artificial degradation is a useful tool in understanding the individual components of cartilage.

The anatomical constitution of cartilage has been shown in this work, to vary from joint to joint, and more specifically, location to location (Chapter 3). The specific distribution and concentration of matrix components is dependent on the load share carried by a particular section of cartilage, and more globally by the shape of the surrounding bone, ligaments and tendons, maintenance of the tissue by the variable concentration of chondrocytes, and by the diet and lifestyle of the mammal. It is this change in the matrix components that determines how the tissue will function. Despite the variability in the tissues make-up and function, no published manuscript has demonstrated the enormity of the variability in the anatomy and subsequent mechanical performance of cartilage samples and therefore the impact on biomechanical research methodologies and results.

Normal cartilage was tested to form a benchmark from which artificially degraded cartilage could be compared and contrasted in order to determine the anatomical and mechanical changes occurring as a direct result of specific matrix disruption. Histological studies of the matrix showed a large variation in concentration and distribution of matrix components, specifically the proteoglycans (Figure 4.3 and Figure 4.4). As a direct result, the process of degradation with Trypsin resulted in greatly varied quantities of proteoglycan loss (Figure 4.4 and Figure 6.8). This finding was of great relevance to past, present and future research. Previously,

researchers would degrade cartilage for a specified amount of time, and use this time to analyse the change in mechanical properties resulting from the effects of the enzyme. However enzymes such as Trypsin are dependent on environmental factors including the concentration of their target protein. Therefore if cartilage begins with a high degree of variation before any testing takes place, it will result in greatly varied levels of degradation, which in turn would have large effects on the analysis of the mechanical results.

The results presented here have led toward a mathematical model which will help researchers to pre-determine, and apply Trypsin treatment of articular cartilage when modelling degeneration in vitro, with a better degree of certainty. To overcome the variability here, the level of proteoglycan loss was employed (Equation 6.1), to allow analysis of the effects of proteoglycan loss on the subsequent mechanical properties.

The mechanical loading tests also showed large variability possibly due to the anatomical inconsistencies (Figure 6.1). The average stiffness of cartilage samples appeared to decrease with increasing proteoglycan loss, with large decreases evident after 30% proteoglycan loss, and again at 70% proteoglycan (Figure 6.11). The loss of proteoglycans has been previously shown to decrease the stiffness of cartilage, due to the subsequent decrease in water, which acts to oppose the initial stages of driven loads (28, 59, 67). The constant stiffness value in the first 30% loss in proteoglycan therefore suggests that the water bound proteoglycans in the superficial zone provides little resistance to the initial load carriage in cartilage, with the mid to lower zones providing the greater resistance to load.

In contrast, the results presented in this study showed that the average stiffness of cartilage samples increased following Collagenase disruption to the collagen network (Figure 6.17). This result is in conflict to previous research, suggesting either discrepancies between research methodologies, or perhaps contrasting effects with increased collagen disruption, which could not be measured here. The increase in stiffness may be attributed to the disruption of the superficial collagen network, limiting the dispersion of stress to a larger surface area in the deeper matrix. This could lead to a localised concentration of stress under the indenter, increased osmotic pressure, and therefore a stiffer response at the larger strains, possibly indicative of local stiffening associated with early signs of osteoarthritis.

Decrease in stiffness following Collagenase treatment shown in some samples in this study, and commonly reported in previous research (59, 67), may be due to more severe collagen disruption, resulting in the loss of proteoglycans from the superficial to mid-zone, and therefore decrease in the load resisting water concentration. Another cause for the decrease may be due to an initial lower concentration of proteoglycans in the surface to midzone, decreasing the amount of available molecules available to swell with water.

Artificial degradation of cartilage in Trypsin and Collagenase cause very different effects on the compressive stiffness; however both have a common causative factor, of which is water. The loss in proteoglycans, result in a loss of available water binding constituents; while a disruption to the collagen network allows for the water binding proteoglycans to bind to larger volumes of water and swell. In vivo, osteoarthritis involves the combined degradation of proteoglycan and disruption to

the collagen network, which would reduce the water binding proteoglycans, and disrupt the swell restricting collagen network. We would therefore expect to see an overall decrease in the compressive stiffness of cartilage in response to collateral damage. Furthermore, the absence of water bound proteoglycans in the surface, in conjunction with damaged fibrils, would result in the localised stress directed immediately under the load, increasing the chance of damage to this tissue.

Although the results for Collagenase treated cartilage do not appear to represent disease processes in vivo, it may in fact contain insight into the early stages of disease. In a healthy matrix, there is a constant turnover of proteoglycans from the chondrocytes, which is increased during the early stages of disease to compensate the disruption to the proteoglycans. However, the collagen network cannot be repaired or replaced as readily, and so it could be possible that the early stages of disease are characterised by a constant proteoglycan concentration (due to increased turnover rate), and an increasingly disrupted collagen network. This process may be an attempt of the matrix to slow down the degrading process by increasing the lateral distribution of the stress, thereby decreasing the localised stress. As disruption to the network increases, the proteoglycans are lost through a decrease in cross linking to the network, resulting in an inability of the tissue to sufficiently transmit energy, further resulting in subsequent wearing away to the bone.

Despite the trends that emerged from the hyperelastic experiments, the range of stiffness values of the Trypsin and Collagenase treated samples (artificially degraded normal samples) fall within the range of the stiffness values for the normal cartilage samples, therefore indicating that these parameters are not dependable for

benchmarking. The wide range of stiffness from the normal cartilage samples and their resulting degraded states is due to the variation that occurs between different geographical locations on a patella, and between patellae from different individuals. Despite this large variation in the stiffness values for normal, Trypsin and Collagenase treated samples, all levels of degradation, and variation within these groups could be modelled by the same two hyperelastic laws, the Yeoh and the Polynomial.

The hyperelastic curves for tension demonstrated a slight decrease in the average stress-strain curve following Trypsin treatment (Figure 6.7), and an increase following Collagenase treatment (Figure 6.16), with both treatment groups showing increased variability in the hyperelastic curves, relative to the normal cartilage results. Tensile stiffness on the other hand was significantly increased following Trypsin (Figure 6.13) and Collagenase treatment (Figure 6.19), demonstrating an increase in resistance to the load as strain increased as seen in Table 6.2. This can be seen as an increased gradient (stiffness) on the stress-strain curves. For the Trypsin treated samples, this phenomenon may be due to a smaller resistance to stretch at lower strain due to decreased proteoglycan content, providing less resistance to the alignment of collagen fibrils in the direction of the load. Then as more collagen fibrils align, they form a sudden resistance to the load, resulting in an increased force required to displace the cartilage, and therefore increase gradient and stiffness. For the Collagenase treated samples, the increased stiffness may be due to the increase in water (due to decrease in restricting collagen network), providing resistance to the realignment of collagen fibrils. The smaller gradient in the toe region may be a result

of minor collagen disruption to part of the superficial region, resulting in a softening of the first layer of resistance to displacement.

The results for Trypsin and Collagenase treated samples show similar trends in the stiffening effect during tensile loading. However the reasoning here suggests that collateral damage to both the collagen network and the proteoglycans would result in a decrease in tensile stiffness, since there are no swollen proteoglycans to resist the realignment of collagen fibrils, and the fibrils themselves are disrupted and contain minimal cross-linkage.

The average hyperelastic curves for treated samples falls within the range of normal values (Figure 6.3), and therefore are not dependable parameters. However the stiffness values at greater strains, within the asymptotic region are higher, and well outside the normal tensile stiffness boundaries, and therefore may be used as benchmarking parameters. These results are in conflict with previously reported results, and should therefore be repeated before they become dependable. It should again be noted that the change in stiffness may have been influenced by an artifact of the zero strain position being difficult to define, particularly on degraded tissue which has been substantially softened, thereby increasing the error in measurement.

The failure strain indicates the toughness of the different regions of the matrix in fracture mechanics. Fracture initiation failure strain indicates at what point the superficial zone can withstand fracture propagation, and final failure is more dependent on the toughness of the mid to deeper zones. Comparison of the normal and treated samples (Figure 6.4 and Figure 6.12 respectively) showed that

proteoglycan loss had little to no effect on the fracture initiation strain or the final fracture strain, indicating that proteoglycans do not provide resistance to propagating fractures. Collagenase treated samples on the other hand showed larger strain levels at which fractures were initiated (Figure 6.18). This may have been due to the decrease in rigidity of the collagen fibrils, resulting from the digestion of bonds cross linking the fibrils. Rather than taut fibrils breaking under the strain, instead they pulled out from the tissue, allowing for greater stretch before the fibrils broke away from the remaining bonds. The final fracture strain for Collagenase samples fell within the normal range, suggesting that the treatment does not impact on the final fracture. Collagenase has been shown to disrupt only the superficial zone within 48 hours, so it is expected that collagen disruption is limited to the superficial zone, and therefore would only affect the fracture initiation strain.

The total failure strain energy is taken as the area under the stress-strain curve for fracture, and is therefore dependent on the fracture stiffness and the failure strain. Proteoglycan loss was shown to have little effect on fracture mechanics, and similarly on the total failure strain energy (Figure 6.14). However Collagenase was shown to result in an increase in fracture stiffness, and the fracture initiation strain (Figure 6.20). Consequently, the total failure strain energy was greater following Collagenase treatment.

The trends in artificial degradation presented in Table 6.1, and discussed above, suggest many opposing mechanical characteristics due to Trypsin treatment or Collagenase treatment. Although these singular trends are not indicative of the effects of disease in vivo, they do provide important insight into the individual

processes that occur towards creating a cascade of collateral damage to the tissue. For example, if the levels of proteoglycans begin to diminish, the collagen fibrils would undergo increasing stress to overcome the load carriage previously carried by the proteoglycans. Over time, this may lead to damage of the fibrils, resulting in their eventual disruption. Similarly, if the collagen fibrils are the first to be disrupted, the loss in the network that acts to bind and hold onto the molecules would eventually result in the loss of proteoglycans in the area of damage. Therefore, the results shown here may be reflective of the early signs of osteoarthritis and related diseases, where the mechanical characteristics appear to improve with the disruption to single components, before resulting in the collateral damage of all matrix constituents, and eventual wearing away to the underlying bone.

The results presented in this thesis show significant influences of Trypsin and Collagenase treatment on articular cartilage samples. Normal samples begin with large variations in the anatomical and consequently, the mechanical properties. Furthermore, degradation to the proteoglycan and collagen network results in large variations in the anatomical and mechanical properties. As a result, the average values of the treated cartilage samples fall within the normal range of results, and so cannot be used as dependable parameters for benchmarking articular cartilage.

7.2 Recommendations for future work

The analysis of this work would have been greatly improved upon if the measurement of the disruption to the collagen network was more reliable. This would have enabled greater insight into the effect of the collagen on the biomechanics of articular cartilage, and the relationship between the collagen network and the

117

proteoglycans, providing a more holistic representation of the tissue. Therefore, it would be largely beneficial if further work was conducted on the quantification and orientation of collagen fibrils, and following this, recreation of some of the mechanical tests presented here. A mathematical model similar to that of the Trypsin model may then be created to allow more controlled disruption to the collagen fibrils.

By decreasing the variability in the initial make-up of the cartilage matrix, thereby producing more cartilage samples of similar levels of degradation, it may be possible to more accurately identify the level of degradation of proteoglycans and collagenase at which significant changes occur in the biomechanical properties such as compression and tension. This would greatly advance the understanding of the mechanical response of cartilage in disease, and aid in the search for treatments and cartilage replacements.

Also following on from the development of a more reliable collagen assessment tool, would be the testing of articular cartilage samples degraded simultaneously with collagenase and Trypsin to examine the effects of collateral damage to the cartilage matrix. Osteoarthritis has also been shown to have decreased levels of lipids in the early stages, and affect the compressive properties of cartilage. Therefore the effects of delipidization on tension and fracture would be useful, in addition to the collateral damage with proteoglycan loss and collagen degradation. This may also provide a more realistic view of the behaviour of degenerate tissue in vivo, and produce more significant changes to the mechanical properties of cartilage to provide dependable benchmarking tools, hence closer to understanding osteoarthritic and diseased articular cartilage.

Appendix A MATLAB Results for Hyperelastic Curve Analysis

SIG2
MR
General model:
    $f(x) = 2*(x^2-1/x)*(C10+1/x*C01)$
Coefficients (with 95% confidence bounds):
    C01 = -9.866e+005 (-1.077e+006, -8.964e+005)
    C10 = 9.739e+005 (9.003e+005, 1.047e+006)

Goodness of fit:
  SSE: 3.299e+009
  R-square: 0.9928
  Adjusted R-square: 0.9926
  RMSE: 1.067e+004

Iterations - 12

YEOH
General model:
    $f(x) = 2*(x^2-1/x)*(C10+2*C20*(x^2-1)+3*C30*(x^2-1)^2)$
Coefficients (with 95% confidence bounds):
    C10 = 6.941e+004 (6.215e+004, 7.666e+004)
    C20 = 2.488e+004 (8487, 4.126e+004)
    C30 = 8.706e+004 (7.535e+004, 9.877e+004)

Goodness of fit:
  SSE: 1.475e+008
  R-square: 0.9997
  Adjusted R-square: 0.9997
  RMSE: 2295

Iterations - 6

Poly 2
General model:
    $f(x)$ = $2*(x^2-1/x)*(C10+C01*(1/x)+C11*(x^(-2)-1)+C11*((x^2-1)/x)+2*C20*(x^2-1)+2*C02*((x^(-2)-1)/x))$
Coefficients (with 95% confidence bounds):
    C01 = 4.782e+006 (1.256e+006, 8.308e+006)
    C02 = -2.127e+006 (-2.806e+006, -1.448e+006)
    C10 = -4.702e+006 (-8.244e+006, -1.16e+006)
    C11 =   1e+007 (fixed at bound)
    C20 = -9.492e+005 (-1.243e+006, -6.557e+005)

Goodness of fit:
  SSE: 1.277e+008
  R-square: 0.9997
  Adjusted R-square: 0.9997
  RMSE: 2175

Iterations - 60
SIG3
MR
General model:
    $f(x) = 2*(x^2-1/x)*(C10+1/x*C01)$
Coefficients (with 95% confidence bounds):
    C01 = -4.377e+006 (-4.592e+006, -4.161e+006)
    C10 = 4.283e+006 (4.107e+006, 4.459e+006)

Goodness of fit:
  SSE: 1.892e+010
  R-square: 0.9978
  Adjusted R-square: 0.9977
  RMSE: 2.554e+004

Iterations – 40

YEOH
General model:
  $f(x) = 2*(x^2-1/x)*(C10+2*C20*(x^2-1)+3*C30*(x^2-1)^2)$
Coefficients (with 95% confidence bounds):
  C10 = 1.185e+005 (1.087e+005, 1.282e+005)
  C20 = 4.909e+005 (4.689e+005, 5.129e+005)
  C30 =   1.06e+005 (9.026e+004, 1.217e+005)

Goodness of fit:
  SSE: 2.659e+008
  R-square: 1
  Adjusted R-square: 1
  RMSE: 3081

Iterations – 9

POLY 2
General model:
  $f(x)$ = $2*(x^2-1/x)*(C10+C01*(1/x)+C11*(x^{(-2)}-1)+C11*((x^2-1)/x)+2*C20*(x^2-1)+2*C02*((x^{(-2)}-1)/x))$
Coefficients (with 95% confidence bounds):
  C01 = -2.521e+006 (-2.464e+007, 1.96e+007)
  C02 = -6.379e+005 (-1.462e+007, 1.334e+007)
  C10 = 2.689e+006 (-1.945e+007, 2.483e+007)
  C11 =   9.99e+006 (-5.379e+007, 7.377e+007)
  C20 = -1.036e+006 (-9.368e+006, 7.296e+006)

Goodness of fit:
  SSE: 4.74e+007
  R-square: 1
  Adjusted R-square: 1
  RMSE: 1350

Iterations - 60
SIG4
MR
General model:
  $f(x) = 2*(x^2-1/x)*(C10+1/x*C01)$
Coefficients (with 95% confidence bounds):
  C01 = -9.689e+006 (-1.139e+007, -7.99e+006)
  C10 =   1e+007 (8.613e+006, 1.139e+007)

Goodness of fit:
  SSE: 1.173e+012
  R-square: 0.9848
  Adjusted R-square: 0.9843
  RMSE: 2.011e+005

Iterations – 138

YEOH

General model:
    f(x) = 2*(x^2-1/x)*(C10+2*C20*(x^2-1)+3*C30*(x^2-1)^2)
Coefficients (with 95% confidence bounds):
    C10 = 1.159e+005 (3.257e+004, 1.993e+005)
    C20 = 1.815e+006 (1.627e+006, 2.004e+006)
    C30 = 1.443e+005 (9855, 2.788e+005)

Goodness of fit:
  SSE: 1.944e+010
  R-square: 0.9997
  Adjusted R-square: 0.9997
  RMSE: 2.635e+004

Iterations - 19

POLY 2
General model:
    f(x)   =   2*(x^2-1/x)*(C10+C01*(1/x)+C11*(x^(-2)-1)+C11*((x^2-1)/x)+2*C20*(x^2-1)+2*C02*((x^(-2)-1)/x))
Coefficients (with 95% confidence bounds):
    C01 = -9.77e+006 (-9.867e+006, -9.674e+006)
    C02 = 1.005e+006 (5.907e+005, 1.42e+006)
    C10 =   1e+007 (fixed at bound)
    C11 =   1e+007 (fixed at bound)
    C20 = -1.838e+005 (-3.303e+005, -3.727e+004)

Goodness of fit:
  SSE: 1.504e+010
  R-square: 0.9998
  Adjusted R-square: 0.9998
  RMSE: 2.318e+004

Iterations - 92
SIG5
MR
General model:
    f(x) = 2*(x^2-1/x)*(C10+1/x*C01)
Coefficients (with 95% confidence bounds):
    C01 = -9.866e+005 (-1.077e+006, -8.964e+005)
    C10 = 9.739e+005 (9.003e+005, 1.047e+006)

Goodness of fit:
  SSE: 3.299e+009
  R-square: 0.9928
  Adjusted R-square: 0.9926
  RMSE: 1.067e+004

Iterations - 12

YEOH
General model:
    f(x) = 2*(x^2-1/x)*(C10+2*C20*(x^2-1)+3*C30*(x^2-1)^2)
Coefficients (with 95% confidence bounds):
    C10 = 6.941e+004 (6.215e+004, 7.666e+004)
    C20 = 2.488e+004 (8487, 4.126e+004)
    C30 = 8.706e+004 (7.535e+004, 9.877e+004)

Goodness of fit:
  SSE: 1.475e+008
  R-square: 0.9997

Adjusted R-square: 0.9997
RMSE: 2295

Iterations - 6

POLY 2
General model:
    f(x) = 2*(x^2-1/x)*(C10+C01*(1/x)+C11*(x^(-2)-1)+C11*((x^2-1)/x)+2*C20*(x^2-1)+2*C02*((x^(-2)-1)/x))
Coefficients (with 95% confidence bounds):
    C01 = 4.782e+006 (1.256e+006, 8.308e+006)
    C02 = -2.127e+006 (-2.806e+006, -1.448e+006)
    C10 = -4.702e+006 (-8.244e+006, -1.16e+006)
    C11 = 1e+007 (fixed at bound)
    C20 = -9.492e+005 (-1.243e+006, -6.557e+005)

Goodness of fit:
  SSE: 1.277e+008
  R-square: 0.9997
  Adjusted R-square: 0.9997
  RMSE: 2175

Iterations - 60
SIG6
MR
General model:
    f(x) = 2*(x^2-1/x)*(C10+1/x*C01)
Coefficients (with 95% confidence bounds):
    C01 = -2.884e+006 (-3.017e+006, -2.751e+006)
    C10 = 2.875e+006 (2.766e+006, 2.983e+006)

Goodness of fit:
  SSE: 7.17e+009
  R-square: 0.9983
  Adjusted R-square: 0.9983
  RMSE: 1.572e+004

Iterations - 27

YEOH
General model:
    f(x) = 2*(x^2-1/x)*(C10+2*C20*(x^2-1)+3*C30*(x^2-1)^2)
Coefficients (with 95% confidence bounds):
    C10 = 1.231e+005 (1.185e+005, 1.278e+005)
    C20 = 3.41e+005 (3.305e+005, 3.514e+005)
    C30 = 5.696e+004 (4.948e+004, 6.445e+004)

Goodness of fit:
  SSE: 6.026e+007
  R-square: 1
  Adjusted R-square: 1
  RMSE: 1467

Iterations - 8

POLY 2
General model:
    f(x) = 2*(x^2-1/x)*(C10+C01*(1/x)+C11*(x^(-2)-1)+C11*((x^2-1)/x)+2*C20*(x^2-1)+2*C02*((x^(-2)-1)/x))
Coefficients (with 95% confidence bounds):

$$C01 = 4.925e+006 \quad (-1.785e+007, 2.771e+007)$$
$$C02 = -2.266e+006 \quad (-1.666e+007, 1.213e+007)$$
$$C10 = -4.799e+006 \quad (-2.76e+007, 1.8e+007)$$
$$C11 = 9.998e+006 \quad (-5.568e+007, 7.568e+007)$$
$$C20 = -6.977e+005 \quad (-9.278e+006, 7.882e+006)$$

Goodness of fit:
  SSE: 5.027e+007
  R-square: 1
  Adjusted R-square: 1
  RMSE: 1391

Iterations - 63
SIG7
MR
General model:
  $f(x) = 2*(x^2-1/x)*(C10+1/x*C01)$
Coefficients (with 95% confidence bounds):
  $C01 = -7.912e+006 \quad (-8.129e+006, -7.695e+006)$
  $C10 = 8.096e+006 \quad (7.919e+006, 8.274e+006)$

Goodness of fit:
  SSE: 1.917e+010
  R-square: 0.9995
  Adjusted R-square: 0.9995
  RMSE: 2.571e+004

Iterations - 83

YEOH
General model:
  $f(x) = 2*(x^2-1/x)*(C10+2*C20*(x^2-1)+3*C30*(x^2-1)^2)$
Coefficients (with 95% confidence bounds):
  $C10 = 6.588e+004 \quad (3.469e+004, 9.706e+004)$
  $C20 = 2.142e+006 \quad (2.072e+006, 2.213e+006)$
  $C30 = -7.324e+005 \quad (-7.827e+005, -6.821e+005)$

Goodness of fit:
  SSE: 2.722e+009
  R-square: 0.9999
  Adjusted R-square: 0.9999
  RMSE: 9859

Iterations - 17

POLY 2
General model:
  $f(x) = 2*(x^2-1/x)*(C10+C01*(1/x)+C11*(x^(-2)-1)+C11*((x^2-1)/x)+2*C20*(x^2-1)+2*C02*((x^(-2)-1)/x))$
Coefficients (with 95% confidence bounds):
  $C01 = -1e+007 \quad (-2.78e+007, 7.798e+006)$
  $C02 = -2.256e+006 \quad (-5.683e+006, 1.171e+006)$
  $C10 = 9.973e+006 \quad (-7.904e+006, 2.785e+007)$
  $C11 = 1e+007 \quad (fixed\ at\ bound)$
  $C20 = -2.13e+006 \quad (-3.612e+006, -6.489e+005)$

Goodness of fit:
  SSE: 3.255e+009
  R-square: 0.9999
  Adjusted R-square: 0.9999

RMSE: 1.098e+004

Iterations - 99
SIG8
MR
General model:
    f(x) = 2*(x^2-1/x)*(C10+1/x*C01)
Coefficients (with 95% confidence bounds):
    C01 = -8.416e+005 (-9.075e+005, -7.757e+005)
    C10 = 8.565e+005 (8.027e+005, 9.103e+005)

Goodness of fit:
  SSE: 1.763e+009
  R-square: 0.9959
  Adjusted R-square: 0.9958
  RMSE: 7798

Iterations - 11

YEOH
General model:
    f(x) = 2*(x^2-1/x)*(C10+2*C20*(x^2-1)+3*C30*(x^2-1)^2)
Coefficients (with 95% confidence bounds):
    C10 =   7.59e+004 (7.065e+004, 8.116e+004)
    C20 = 4.371e+004 (3.185e+004, 5.558e+004)
    C30 = 5.769e+004 (4.921e+004, 6.617e+004)

Goodness of fit:
  SSE: 7.732e+007
  R-square: 0.9998
  Adjusted R-square: 0.9998
  RMSE: 1662

Iterations - 6

POLY 2
General model:
    f(x)   =   2*(x^2-1/x)*(C10+C01*(1/x)+C11*(x^(-2)-1)+C11*((x^2-1)/x)+2*C20*(x^2-1)+2*C02*((x^(-2)-1)/x))
Coefficients (with 95% confidence bounds):
    C01 = -4.549e+005 (-2.857e+007, 2.766e+007)
    C02 = 1.822e+006 (-1.595e+007, 1.959e+007)
    C10 = 5.317e+005 (-2.76e+007, 2.866e+007)
    C11 = -9.993e+006 (-9.104e+007, 7.106e+007)
    C20 = 1.743e+006 (-8.845e+006, 1.233e+007)

Goodness of fit:
  SSE: 7.651e+007
  R-square: 0.9998
  Adjusted R-square: 0.9998
  RMSE: 1715

Iterations - 57
SIG9
MR
General model:
    f(x) = 2*(x^2-1/x)*(C10+1/x*C01)
Coefficients (with 95% confidence bounds):
    C01 = -2.976e+006 (-3.125e+006, -2.828e+006)
    C10 = 2.955e+006 (2.834e+006, 3.076e+006)

Goodness of fit:
  SSE: 8.938e+009
  R-square: 0.998
  Adjusted R-square: 0.9979
  RMSE: 1.756e+004

Iteration - 28

YEOH
General model:
    $f(x) = 2*(x^2-1/x)*(C10+2*C20*(x^2-1)+3*C30*(x^2-1)^2)$
Coefficients (with 95% confidence bounds):
    C10 = 1.248e+005 (1.191e+005, 1.305e+005)
    C20 = 3.291e+005 (3.163e+005, 3.419e+005)
    C30 = 7.556e+004 (6.64e+004, 8.473e+004)

Goodness of fit:
  SSE: 9.034e+007
  R-square: 1
  Adjusted R-square: 1
  RMSE: 1796

Iteration - 8

Poly 2
General model:
    $f(x)$ = $2*(x^2-1/x)*(C10+C01*(1/x)+C11*(x^(-2)-1)+C11*((x^2-1)/x)+2*C20*(x^2-1)+2*C02*((x^(-2)-1)/x))$
Coefficients (with 95% confidence bounds):
    C01 = 1.986e+006 (-1.429e+004, 3.986e+006)
    C02 = -1.627e+006 (-2.012e+006, -1.242e+006)
    C10 = -1.84e+006 (-3.848e+006, 1.693e+005)
    C11 =   1e+007 (fixed at bound)
    C20 = -9.052e+005 (-1.072e+006, -7.387e+005)

Goodness of fit:
  SSE: 4.109e+007
  R-square: 1
  Adjusted R-square: 1
  RMSE: 1234

Iterations - 56
SIG10
MR
General model:
    $f(x) = 2*(x^2-1/x)*(C10+1/x*C01)$
Coefficients (with 95% confidence bounds):
    C01 = -7.058e+006 (-7.247e+006, -6.869e+006)
    C10 = 7.175e+006 (7.021e+006, 7.329e+006)

Goodness of fit:
  SSE: 1.448e+010
  R-square: 0.9995
  Adjusted R-square: 0.9995
  RMSE: 2.235e+004

Iteration - 71

YEOH

General model:

$$f(x) = 2*(x^2-1/x)*(C10+2*C20*(x^2-1)+3*C30*(x^2-1)^2)$$

Coefficients (with 95% confidence bounds):

    C10 = 2.987e+005 (2.633e+005, 3.341e+005)
    C20 = 1.192e+006 (1.113e+006, 1.272e+006)
    C30 = -1.242e+005 (-1.813e+005, -6.709e+004)

Goodness of fit:
  SSE: 3.509e+009
  R-square: 0.9999
  Adjusted R-square: 0.9999
  RMSE: 1.119e+004

Iteration - 11

POLY 2

General model:

$$f(x) = 2*(x^2-1/x)*(C10+C01*(1/x)+C11*(x^{(-2)}-1)+C11*((x^2-1)/x)+2*C20*(x^2-1)+2*C02*((x^{(-2)}-1)/x))$$

Coefficients (with 95% confidence bounds):

    C01 = -9.662e+006 (-9.705e+006, -9.618e+006)
    C02 = -7.594e+004 (-2.638e+005, 1.119e+005)
    C10 =   1e+007 (fixed at bound)
    C11 =   1e+007 (fixed at bound)
    C20 = -1.503e+006 (-1.57e+006, -1.437e+006)

Goodness of fit:
  SSE: 3.091e+009
  R-square: 0.9999
  Adjusted R-square: 0.9999
  RMSE: 1.051e+004

Iterations - 88
SIG11
MR
General model:

$$f(x) = 2*(x^2-1/x)*(C10+1/x*C01)$$

Coefficients (with 95% confidence bounds):

    C01 = -9.866e+005 (-1.077e+006, -8.964e+005)
    C10 = 9.739e+005 (9.003e+005, 1.047e+006)

Goodness of fit:
  SSE: 3.299e+009
  R-square: 0.9928
  Adjusted R-square: 0.9926
  RMSE: 1.067e+004

Iterations - 12

YEOH
General model:

$$f(x) = 2*(x^2-1/x)*(C10+2*C20*(x^2-1)+3*C30*(x^2-1)^2)$$

Coefficients (with 95% confidence bounds):

    C10 = 6.941e+004 (6.215e+004, 7.666e+004)
    C20 = 2.488e+004 (8487, 4.126e+004)
    C30 = 8.706e+004 (7.535e+004, 9.877e+004)

Goodness of fit:
  SSE: 1.475e+008
  R-square: 0.9997

Adjusted R-square: 0.9997
RMSE: 2295

Iterations - 6

POLY 2
General model:
    f(x) = 2*(x^2-1/x)*(C10+C01*(1/x)+C11*(x^(-2)-1)+C11*((x^2-1)/x)+2*C20*(x^2-1)+2*C02*((x^(-2)-1)/x))
Coefficients (with 95% confidence bounds):
    C01 = 4.782e+006 (1.256e+006, 8.308e+006)
    C02 = -2.127e+006 (-2.806e+006, -1.448e+006)
    C10 = -4.702e+006 (-8.244e+006, -1.16e+006)
    C11 = 1e+007 (fixed at bound)
    C20 = -9.492e+005 (-1.243e+006, -6.557e+005)

Goodness of fit:
  SSE: 1.277e+008
  R-square: 0.9997
  Adjusted R-square: 0.9997
  RMSE: 2175

Iterations – 60
SIG12
MR
General model:
    f(x) = 2*(x^2-1/x)*(C10+1/x*C01)
Coefficients (with 95% confidence bounds):
    C01 = -3.044e+006 (-3.238e+006, -2.849e+006)
    C10 = 2.963e+006 (2.804e+006, 3.121e+006)

Goodness of fit:
  SSE: 1.533e+010
  R-square: 0.9961
  Adjusted R-square: 0.9959
  RMSE: 2.299e+004

Iterations - 28

YEOH
General model:
    f(x) = 2*(x^2-1/x)*(C10+2*C20*(x^2-1)+3*C30*(x^2-1)^2)
Coefficients (with 95% confidence bounds):
    C10 = 1.053e+005 (9.813e+004, 1.124e+005)
    C20 = 2.452e+005 (2.291e+005, 2.613e+005)
    C30 = 1.445e+005 (1.33e+005, 1.56e+005)

Goodness of fit:
  SSE: 1.421e+008
  R-square: 1
  Adjusted R-square: 1
  RMSE: 2253

Iterations - 8

POLY 2
General model:
    f(x) = 2*(x^2-1/x)*(C10+C01*(1/x)+C11*(x^(-2)-1)+C11*((x^2-1)/x)+2*C20*(x^2-1)+2*C02*((x^(-2)-1)/x))
Coefficients (with 95% confidence bounds):

```
C01 =  3.875e+006  (1.481e+006, 6.269e+006)
C02 = -1.738e+006  (-2.199e+006, -1.277e+006)
C10 = -3.742e+006  (-6.146e+006, -1.338e+006)
C11 =      1e+007  (fixed at bound)
C20 = -6.573e+005  (-8.566e+005, -4.581e+005)
```

Goodness of fit:
  SSE: 5.887e+007
  R-square: 1
  Adjusted R-square: 1
  RMSE: 1477

Iterations - 41
SIG13
MR
General model:
    $f(x) = 2*(x^2-1/x)*(C10+1/x*C01)$
Coefficients (with 95% confidence bounds):
    C01 = -5.57e+006 (-6.064e+006, -5.076e+006)
    C10 = 5.256e+006 (4.853e+006, 5.659e+006)

Goodness of fit:
  SSE: 9.919e+010
  R-square: 0.9899
  Adjusted R-square: 0.9895
  RMSE: 5.848e+004

Iterations - 49

YEOH
General model:
    $f(x) = 2*(x^2-1/x)*(C10+2*C20*(x^2-1)+3*C30*(x^2-1)^2)$
Coefficients (with 95% confidence bounds):
    C10 = 1.397e+005 (1.08e+005, 1.715e+005)
    C20 = 1.648e+005 (9.321e+004, 2.364e+005)
    C30 = 4.737e+005 (4.225e+005, 5.248e+005)

Goodness of fit:
  SSE: 2.815e+009
  R-square: 0.9997
  Adjusted R-square: 0.9997
  RMSE: 1.003e+004

Iterations - 8

POLY 2
General model:
    $f(x) = 2*(x^2-1/x)*(C10+C01*(1/x)+C11*(x^(-2)-1)+C11*((x^2-1)/x)+2*C20*(x^2-1)+2*C02*((x^(-2)-1)/x))$
Coefficients (with 95% confidence bounds):
    C01 = -1.464e+006 (-1.162e+008, 1.132e+008)
    C02 = 5.189e+005 (-7.197e+007, 7.301e+007)
    C10 = 1.73e+006 (-1.131e+008, 1.165e+008)
    C11 = 9.999e+006 (-3.207e+008, 3.407e+008)
    C20 = -3.383e+005 (-4.354e+007, 4.286e+007)

Goodness of fit:
  SSE: 1.274e+009
  R-square: 0.9999
  Adjusted R-square: 0.9998

RMSE: 6999

Iterations - 58
SIG14
MR
General model:
    $f(x) = 2*(x^2-1/x)*(C10+1/x*C01)$
Coefficients (with 95% confidence bounds):
    C01 = -1.422e+006 (-1.556e+006, -1.288e+006)
    C10 = 1.353e+006 (1.244e+006, 1.462e+006)

Goodness of fit:
  SSE: 7.277e+009
  R-square: 0.9894
  Adjusted R-square: 0.9891
  RMSE: 1.584e+004

Iterations - 15

YEOH
General model:
    $f(x) = 2*(x^2-1/x)*(C10+2*C20*(x^2-1)+3*C30*(x^2-1)^2)$
Coefficients (with 95% confidence bounds):
    C10 = 5.404e+004 (4.702e+004, 6.107e+004)
    C20 = 2.362e+004 (7751, 3.948e+004)
    C30 = 1.345e+005 (1.232e+005, 1.458e+005)

Goodness of fit:
  SSE: 1.382e+008
  R-square: 0.9998
  Adjusted R-square: 0.9998
  RMSE: 2222

Iterations - 7

POLY 2
General model:
    $f(x) = 2*(x^2-1/x)*(C10+C01*(1/x)+C11*(x^{(-2)}-1)+C11*((x^2-1)/x)+2*C20*(x^2-1)+2*C02*((x^{(-2)}-1)/x))$
Coefficients (with 95% confidence bounds):
    C01 = 6.945e+006 (3.648e+006, 1.024e+007)
    C02 = -2.371e+006 (-3.006e+006, -1.736e+006)
    C10 = -6.88e+006 (-1.019e+007, -3.569e+006)
    C11 =   1e+007 (fixed at bound)
    C20 = -6.509e+005 (-9.253e+005, -3.766e+005)

Goodness of fit:
  SSE: 1.116e+008
  R-square: 0.9998
  Adjusted R-square: 0.9998
  RMSE: 2033

Iterations - 75
SIG15
MR
General model:
    $f(x) = 2*(x^2-1/x)*(C10+1/x*C01)$
Coefficients (with 95% confidence bounds):
    C01 = -6.83e+006 (-7.048e+006, -6.612e+006)
    C10 = 6.62e+006 (6.442e+006, 6.798e+006)

Goodness of fit:
  SSE: 1.937e+010
  R-square: 0.999
  Adjusted R-square: 0.999
  RMSE: 2.584e+004

Iterations - 65

YEOH
General model:
    $f(x) = 2*(x^2-1/x)*(C10+2*C20*(x^2-1)+3*C30*(x^2-1)^2)$
Coefficients (with 95% confidence bounds):
    C10 =   3666 (-2.557e+004, 3.29e+004)
    C20 = 1.059e+006 (9.931e+005, 1.125e+006)
    C30 = -5.028e+004 (-9.744e+004, -3125)

Goodness of fit:
  SSE: 2.392e+009
  R-square: 0.9999
  Adjusted R-square: 0.9999
  RMSE: 9243

Iterations - 11

POLY 2
General model:
    $f(x)$ = $2*(x^2-1/x)*(C10+C01*(1/x)+C11*(x^{(-2)}-1)+C11*((x^2-1)/x)+2*C20*(x^2-1)+2*C02*((x^{(-2)}-1)/x))$
Coefficients (with 95% confidence bounds):
    C01 = -9.935e+006 (-9.963e+006, -9.907e+006)
    C02 = 2.676e+005 (1.471e+005, 3.881e+005)
    C10 =   1e+007 (fixed at bound)
    C11 =   1e+007 (fixed at bound)
    C20 = -1.465e+006 (-1.508e+006, -1.423e+006)

Goodness of fit:
  SSE: 1.271e+009
  R-square: 0.9999
  Adjusted R-square: 0.9999
  RMSE: 6739

Iterations - 93
SIG16
MR
General model:
    $f(x) = 2*(x^2-1/x)*(C10+1/x*C01)$
Coefficients (with 95% confidence bounds):
    C01 = -9.792e+006 (-1.047e+007, -9.112e+006)
    C10 =   1e+007 (9.445e+006, 1.056e+007)

Goodness of fit:
  SSE: 1.879e+011
  R-square: 0.9972
  Adjusted R-square: 0.9971
  RMSE: 8.049e+004

Iterations - 150

YEOH

General model:
    $f(x) = 2*(x^2-1/x)*(C10+2*C20*(x^2-1)+3*C30*(x^2-1)^2)$
Coefficients (with 95% confidence bounds):
    C10 = -6.867e+004 (-1.312e+005, -6175)
    C20 = 2.593e+006 (2.452e+006, 2.734e+006)
    C30 = -6.81e+005 (-7.818e+005, -5.802e+005)

Goodness of fit:
  SSE: 1.093e+010
  R-square: 0.9998
  Adjusted R-square: 0.9998
  RMSE: 1.976e+004

Iterations - 16

POLY 2
Fit computation did not converge: General model:
    $f(x)$ = $2*(x^2-1/x)*(C10+C01*(1/x)+C11*(x^{(-2)}-1)+C11*((x^2-1)/x)+2*C20*(x^2-1)+2*C02*((x^{(-2)}-1)/x))$
Coefficients (with 95% confidence bounds):
    C01 =   -1e+007 (fixed at bound)
    C02 = -1.939e+006 (-2.383e+006, -1.494e+006)
    C10 = 9.877e+006 (9.777e+006, 9.976e+006)
    C11 =   1e+007 (fixed at bound)
    C20 = -1.508e+006 (-1.652e+006, -1.365e+006)

Goodness of fit:
  SSE: 1.591e+010
  R-square: 0.9998
  Adjusted R-square: 0.9997
  RMSE: 2.384e+004

Iterations - 99
SIG17
MR
General model:
    $f(x) = 2*(x^2-1/x)*(C10+1/x*C01)$
Coefficients (with 95% confidence bounds):
    C01 = -8.6e+005 (-9.751e+005, -7.449e+005)
    C10 = 8.552e+005 (7.613e+005, 9.492e+005)

Goodness of fit:
  SSE: 5.385e+009
  R-square: 0.9856
  Adjusted R-square: 0.9851
  RMSE: 1.363e+004

Iterations - 11

YEOH
General model:
    $f(x) = 2*(x^2-1/x)*(C10+2*C20*(x^2-1)+3*C30*(x^2-1)^2)$
Coefficients (with 95% confidence bounds):
    C10 = 9.64e+004 (8.368e+004, 1.091e+005)
    C20 = -5.22e+004 (-8.092e+004, -2.347e+004)
    C30 = 1.302e+005 (1.097e+005, 1.507e+005)

Goodness of fit:
  SSE: 4.531e+008
  R-square: 0.9988

Adjusted R-square: 0.9987
RMSE: 4023

Iterations - 6

POLY 2
General model:
$$f(x) = 2*(x^2-1/x)*(C10+C01*(1/x)+C11*(x^{(-2)}-1)+C11*((x^2-1)/x)+2*C20*(x^2-1)+2*C02*((x^{(-2)}-1)/x))$$
Coefficients (with 95% confidence bounds):
C01 = 1e+007 (fixed at bound)
C02 = 5.099e+004 (-3765, 1.057e+005)
C10 = -9.94e+006 (-9.952e+006, -9.927e+006)
C11 = -1e+007 (fixed at bound)
C20 = 2.693e+006 (2.675e+006, 2.71e+006)

Goodness of fit:
SSE: 2.416e+008
R-square: 0.9994
Adjusted R-square: 0.9993
RMSE: 2938

Iterations - 94
SIG18
MR
General model:
$$f(x) = 2*(x^2-1/x)*(C10+1/x*C01)$$
Coefficients (with 95% confidence bounds):
C01 = -4.038e+006 (-4.22e+006, -3.855e+006)
C10 = 4.006e+006 (3.856e+006, 4.155e+006)

Goodness of fit:
SSE: 1.358e+010
R-square: 0.9983
Adjusted R-square: 0.9983
RMSE: 2.164e+004

Iterations - 37

YEOH
General model:
$$f(x) = 2*(x^2-1/x)*(C10+2*C20*(x^2-1)+3*C30*(x^2-1)^2)$$
Coefficients (with 95% confidence bounds):
C10 = 1.48e+005 (1.36e+005, 1.6e+005)
C20 = 4.917e+005 (4.647e+005, 5.188e+005)
C30 = 6.918e+004 (4.986e+004, 8.85e+004)

Goodness of fit:
SSE: 4.015e+008
R-square: 1
Adjusted R-square: 0.9999
RMSE: 3787

Iterations - 10

POLY 2
General model:
$$f(x) = 2*(x^2-1/x)*(C10+C01*(1/x)+C11*(x^{(-2)}-1)+C11*((x^2-1)/x)+2*C20*(x^2-1)+2*C02*((x^{(-2)}-1)/x))$$
Coefficients (with 95% confidence bounds):

C01 = -5.049e+006 (-4.46e+007, 3.45e+007)
C02 = -2.833e+005 (-2.528e+007, 2.471e+007)
C10 = 5.251e+006 (-3.433e+007, 4.483e+007)
C11 = 9.992e+006 (-1.04e+008, 1.24e+008)
C20 = -1.338e+006 (-1.623e+007, 1.356e+007)

Goodness of fit:
  SSE: 1.515e+008
  R-square: 1
  Adjusted R-square: 1
  RMSE: 2414

Iterations - 63
SIG19
MR
General model:
    $f(x) = 2*(x^2-1/x)*(C10+1/x*C01)$
Coefficients (with 95% confidence bounds):
    C01 = -4.216e+006 (-4.344e+006, -4.089e+006)
    C10 = 4.53e+006 (4.426e+006, 4.633e+006)

Goodness of fit:
  SSE: 6.561e+009
  R-square: 0.9996
  Adjusted R-square: 0.9996
  RMSE: 1.504e+004

Iterations - 41

YEOH
General model:
    $f(x) = 2*(x^2-1/x)*(C10+2*C20*(x^2-1)+3*C30*(x^2-1)^2)$
Coefficients (with 95% confidence bounds):
    C10 = 2.673e+005 (2.356e+005, 2.991e+005)
    C20 = 1.098e+006 (1.026e+006, 1.17e+006)
    C30 = -3.581e+005 (-4.094e+005, -3.069e+005)

Goodness of fit:
  SSE: 2.826e+009
  R-square: 0.9998
  Adjusted R-square: 0.9998
  RMSE: 1.005e+004

Iterations - 11

POLY 2
General model:
    $f(x) = 2*(x^2-1/x)*(C10+C01*(1/x)+C11*(x^{(-2)}-1)+C11*((x^2-1)/x)+2*C20*(x^2-1)+2*C02*((x^{(-2)}-1)/x))$
Coefficients (with 95% confidence bounds):
    C01 = -9.739e+006 (-9.783e+006, -9.694e+006)
    C02 = -8.982e+005 (-1.091e+006, -7.055e+005)
    C10 =   1e+007 (fixed at bound)
    C11 =   1e+007 (fixed at bound)
    C20 = -2.191e+006 (-2.259e+006, -2.123e+006)

Goodness of fit:
  SSE: 3.253e+009
  R-square: 0.9998
  Adjusted R-square: 0.9998

RMSE: 1.078e+004

Iterations - 94

Bibliography

1. SCHERING-PLOUGH ANIMAL HEALTH (2003. Retrieved on 8/12/2005 from the World Wide Web:) Osteoarthritis: The Inside Story.

2. AUSTRALIAN BUREAU OF STATISTICS (2002) National Health Survey 2001, Summary of Results Cat. No. 4364.0 (Canberra).

3. ACCESS ECONOMICS (2005) Arthritis - the bottom line: The economic impact of arthritis in Australia, *Prepared for Arthritis Australia*.

4. MEACHIM, G. & STOCKWELL, R. A. (1973) The Matrix, in: Freeman, M. A. R. (Ed.) *Adult Articular Cartilage*, pp. 1-50 (London, Pitman Medical).

5. THIBAULT, M., POOLE, A. R. & BUSCHMANN, M. D. (2002) Cyclic compression of cartilage/bone explants In vitro leads to physical weakening, mechanical breakdown of collagen and release of matrix fragments, *Journal of Orthopaedic Research*, 20, 1265-1273.

6. PRIZM DEVELOPMENT INC (2005. Retrieved on 23/11/2005 from the World Wide Web:) Durango Orthopedics.

7. FREEMAN, M. A. R. & KEMPSON, G. E. (1973) Load Carriage, in: Freeman, M. A. R. (Ed.) *Adult Articular Cartilage*, pp. 228-246 (London, Pitman Medical).

8. BETH ISRAEL DEACONESS MEDICAL CENTER (2005. Retrieved on 8/12/05 from the World Wide Web) Functional Imaging of Cartilage.

9. GLENISTER, T. W. (1976) An embryological view of cartilage, *J. Anat*, 122, 323-330.

10. KAMALANATHAN, S. & BROOM, N. D. (1993) The biomechanical ambiguity of the articular surface, *J. Anat.*, 183, 567-578.

11. MINNS, R. J. & STEVEN, F. S. (1977) The collagen fibril organization in human articular cartilage, *J. Anat.*, 123, 437-457.

12. SLOMIANKA, L. (2004. Retrieved on 8/12/2005 from the World Wide Web:) Blue histology - skeletal tissues - cartilage. School of Anatomy and Human Biology, The University of Western Australia.

13. BENNINGHOFF, A. (1925) Form und brau der gelenknorpel in ihren bezeihungen zur funktion, *Zeitschrift fur Zellforschung und mikroskopische Anatomie*, 2, 783-825.

14. MEACHIM, G. & STOCKWELL, R. A. (1973) The Matrix, in: Freeman, M. A. R. (Ed.) *Adult Articular Cartilage*, pp. 100-130 (Carlton, Pitman Medical).

15. UNIVERSITAT STUTTGART (2004. Retrieved on the 7/12/2005 from the World Wide Web:) Der bewegungsapparat: form und funktionsbeziehung-das skelettsystem-gelenknorpel.

16. REDLER, I. (1974) A scanning electron microscopic study of human normal and osteoarthritic articular cartilage, *Clinical Orthopaedics and Related Research*, 103, 262-268.

17. HEINEGARD, D., BAYLISS, M. & LORENZO, P. (2003) Biochemistry and metabolism of normal and osteoarthritis cartilage, in: Brandt, K. D., Doherty, M. & Lohmander, L. S. (Eds.) *Osteoarthritis* (New York, Oxford University Press).

18. VOET, D. & VOET, J. G. (2004) *Biochemistry* (New York, J. Wiley and Sons).

19. VAN DER REST, M. & GARRONE, R. (1990) Collagens as multidomain proteins, *Biochemie*, 72, 473-484.

20.	SHINGLETON, W. D., HODGES, D. J., BRICK, P. & CAWSTON, T. E. (1996) Collagenase: a key enzyme in collagen turnover, *Biochemistry and Cell Biology*, 74, 759-775.

21.	BROOM, N., CHEN, M.-H. & HARDY, A. (2001) A Degeneration-based hypothesis for interpreting fibrillar changes in the osteoarthritic cartilage matrix, *J. Anat.*, 199, 683-698.

22.	MEACHIM, G., DENHAM, D., EMERY, I. H. & WILKINSON, P. H. (1974) Collagen alignments and artificial splits at the surface of human articular cartilage, *J. Anat.*, 118, 101-118.

23.	BROOM, N. D. (1984) Further insight into the structural principles governing the function of articular cartilage, *J. Anat.*, 139, 275-294.

24.	KIRALY, K., HYTTINEN, M. M., LAPVETELAINEN, T. et al. (1997) Specimen preparation and quantification of collagen birefringence in unstained sections of articular cartilage using image analysis and polarizing light microscopy, *Histochemical Journal*, 29, 317-327.

25.	HUANG, C., STANKIEWICZ, A., ATESHIAN, G. A. & MOW, V. C. (2005) Anisotropy, inhomogeneity, and tension-compression nonlinearity of human glenohumeral cartilage in finite deformation, *Journal of Biomechanics*, 38, 799-809.

26.	KEMPSON, G. E., MUIR, H., POLLARD, C. & TUKE, M. (1973) The Tensile Properties of the cartilage of human femoral condyles related to the content of collagen and glycosaminoglycans, *Biochimica et Biophysica Acta*, 297, 456-472.

27. WOO, S. L., AKESON, W. H. & JEMMOTT, G. F. (1976) Measurements of nonhomogenous, directional mechanical properties of articular cartilage in tension, *J. Biomechanics*, 9, 785-791.

28. KEMPSON, G. E., MUIR, H., SWANSON, S. A. V. & R, F. M. A. (1970) Correlations between stiffness and the chemical constituents of cartilage on the human femoral head, *Biochim. Biophys. Acta*, 215, 70-77.

29. TESCHE, F. & MIOSGE, N. (2004) Perlecan in late stages of osteoarthritis of the human knee joint, *Osteoarthritis and Cartilage*, 12, 852-862.

30. BRANDT, K. D. & MUIR, H. (1971) Heterogeneity of protein-polysaccharides of porcine articular cartilage. The sequential extraction of chondroitin sulphate-proteins with iso-osmotic neutral sodium acetate, *The Biochemical journal*, 121, 261-270.

31. PEPROTECH INC (2005. Retrieved on the 8/12/2005 from the World Wide Web:) Cartilage, related cytokines, and osteoarthritis.

32. BONNER, W. M., JONSSON, H., MALANOS, C. & BRYANT, M. (1975) Changes in the lipids of human articular cartilage with age, *Arthritis and Rheumatism*, 18, 461-473.

33. STOCKWELL, R. A. (1967) Lipid content of human costal and articular cartilage, *Annals of the Rheumatic Diseases*, 26, 481-486.

34. SARMA, A. V., POWELL, G. L. & LABERG, M. (2001) Phospholipid composition of articular cartilage boundary lubricant, *J. Orthopaedic Research*, 19, 671-676.

35. BALLANTINE, G. C. & STACHOWIAK, G. W. (2002) The effects of lipid depletion on osteoarthritic wear, *Wear*, 253, 385-393.

36. HILLS, B. A. (1996) Synovial surfactant and the hydrophobic articular surface, *The Journal of Rheumatology*, 23, 1323-1325.

37. OLOYEDE, A., GUDIMETLA, P., CRAWFORD, R. & HILLS, B. A. (2004) Consolidation responses of delipidized articular cartilage, *Clinical Biomechanics*, 19, 534-542.

38. OLOYEDE, A., GUDIMETLA, P., CRAWFORD, R. & HILLS, B. A. (2004) Biomechanical responses of normal and delipidized articular cartilage subjected to varying rates of loading, *Connective Tissue Research*, 45, 86-93.

39. WONG, M. & HUNZIKER, E. B. (1998) Articular cartilage biology and mechanics, *Sports Medicine and Arthroscopy Review*, 6, 4-12.

40. STOK, K. & OLOYEDE, A. (2003) A qualitative analysis of crack propagation in articular cartilage at varying rates of tensile loading, *Connective Tissue Research*, 44, 109-120.

41. OLOYEDE, A., FLACHSMANN, R. & BROOM, N. D. (1992) The dramatic influence of loading velocity on the compressive response of articular cartilage, *Connective Tissue Research*, 27, 211-224.

42. SILVER, F. H., BRADICA, G. & TRIA, A. (2002) Elastic energy storage in human articular cartilage: estimation of the elastic modulus for type II collagen and changes associated with osteoarthritis, *Matrix Biology*, 21, 129-137.

43. ANDERSON, T. L. (1995) *Fracture Mechanics: fundamentals and applications* (Boca Raton, CRC Press).

44. ASPDEN, R. M., SCHEVEN, B. A. A. & HUTCHISON, J. D. (2001) Osteoarthritis as a systematic disorder including stromal cell differentiation and lipid metabolism, *The Lancet*, 357, 1118-1120.

45.   JURVELIN, J. S., BUSCHMANN, M. D. & HUNZIKER, E. B. (1997) Optical and mechanical determination of poisson's ratio of adult bovine humeral articular cartilage, *Journal of Biomechanics*, 30, 235-241.

46.   PURSLOW, P. P. (1983) Positional variations in fracture toughness, stiffness and strength of descending thoracic pig aorta, *J. Biomechanics*, 16, 947-953.

47.   PURSLOW, P. P. (1983) Measurement of the fracture toughness of extensible connective tissues, *Journal of Material Science*, 18, 3591-3598.

48.   PRICE, J. S., TILL, S. H., BICKERSTAFF, D. R., BAYLISS, M. T. & HOLLANDER, A. P. (1999) Degradation of cartilage type II collagen precedes the onset of osteoarthritis following anterior cruciate ligament rupture, *Arthritis & Rheumatism*, 42, 2390-2398.

49.   LEWIS, J. L., DELORIA, L. B., OYEN-TIESMA, M. et al. (2003) Cell death after cartilage impact occurs around matrix cracks., *Journal of orthopaedic research : official publication of the Orthopaedic Research Society*, 21, 881-887.

50.   SMITH, J. O., OREFFO, R. O. C., CLARKE, N. M. P. & ROACH, H. I. (2003) Changes in the antiangiogenic properties of articular cartilage in osteoarthritis, *J. Orthop. Sci.*, 8, 849-857.

51.   DODGE, G. R. & POOLE, A. R. (1989) Immunohistochemical detection and immunochemical analysis of type II collagen degradation in human normal, rheumatoid, and osteoarthritic articular cartilages and the explants of bovine articular cartilage cultured with interleukin 1, *J. Clin. Invest.*, Volume 83, 647-661.

52.   GOLDRING, M. (2000) The role of the chondrocyte in osteoarthritis, *Arthritis & Rheumatism*, 43, 1916-1926.

53. BANK, R. A., KRIKKEN, M., BEEKMAN, B. et al. (1997) A simplified measurement of degraded collagen in tissues: Application in healthy, fibrillated and osteoarthritic cartilage, *Matrix Biology*, 16, 233-243.

54. SCHMIDT, M. B., MOW, V. C., CHUN, L. E. & EYRE, D. R. (1990) Effects of proteoglycan extraction on the tensile behavior of articular cartilage, *Journal of Orthopaedic Research*, 8, 353-363.

55. RIEPPO, J., TOYRAS, J., NIEMINEN, M. T. et al. (2003) Structure-function relationships in enzymatically modified articular cartilage, *Cells Tissues Organs*, 175, 121-132.

56. KORHONEN, R. K., LAASANEN, M. S., TOYRAS, J. et al. (2003) Fibril reinforced poroelastic model predicts specifically mechanical behaviour of normal, proteoglycan depleted and collagen degraded articular cartilage, *Journal of Biomechanics*, 36, 1373-1397.

57. NIEMINEN, H. J., TOYRAS, J., RIEPPO, J. et al. (2002) Real-time ultrasound analysis of articular cartilage degradation in vitro, *Ultrasound in Medicine and Biology*, 28, 519-525.

58. KEMPSON, G. E., TUKE, M. A., DINGLE, J. T., BARRETT, A. J. & HORSFIELD, P. H. (1976) The effects of proteolytic enzymes on the mechanical properties of adult human articular cartilage, *Biochimica et Biophysica Acta*, 428, 741-760.

59. HARRIS, E. D., PARKER, H. G., RADIN, E. L. & KRANE, S. M. (1972) Effects of proteolytic enzymes on structural and mechanical properties of cartilage, *Arthritis & Rheumatism*, 15, 497-503.

60. OLOYEDE, A., GUDIMETLA, P., CRAWFORD, R. & HILLS, B. A. (2003) Consolidation responses of delipidized articular cartilage, *Clinical Biomechanics*, 19. 534-542.

61.   DISILVESTRO, M. R. & SUH, J. K. F. (2002) Biphasic poroviscoelastic characteristics of proteoglycan-depleted articular cartilage: simulation and degeneration, *Annals of Biomedical Engineering*, 30, 792-800.

62.   LYYRA, T., AROKOSKI, J. P. A., OKSALA, N. et al. (1999) Experimental validation of arthroscopic cartilage stiffness measurement using enzymatically degraded cartilage samples, *Physics in Medicine and Biology*, 44, 525-535.

63.   QIN, L., ZHENG, Y., LEUNG, C. et al. (2002) Ultrasound detection of trypsin-treated articular cartilage: its association with cartilaginous proteoglycans assessed by histological and biochemical methods, *Journal of Bone and Mineral Metabolism*, 20, 281-287.

64.   CAMPLEJOHN, K. L. & ALLARD, S. A. (1988) Limitations of safranin O staining in proteoglycan-depleted cartilage demonstrated with monoclonal antibodies, *Histochemistry*, 89, 185-188.

65.   BORTHAKUR, A., SHAPIRO, E. M., BEERS, J. et al. (2000) Sensitivity of MRI to proteoglycan depletion in cartilage: comparison of sodium and proton MRI, *Osteoarthritis and Cartilage*, 8, 288-293.

66.   ZHENG, Y. P., SHI, J., QIN, L. et al. (2004) Dymanic depth-dependent osmotic swelling and solute diffusion in articular cartilage monitored using real-time ultrasound, *Ultrasound in Medicine and Biology*, 30, 841-849.

67.   LAASANEN, M. S., TOYRAS, J., HIRVONEN, J. et al. (2002) Novel mechano-acoustic technique and instrument for diagnosis of cartilage degeneration, *Physiological Measurement*, 23, 491-503.

68. PRATTA, M. A., YAO, W., DECICCO, C. et al. (2003) Aggrecan protects cartilage collagen from proteolytic cleavage, *The Journal of Biological Chemistry*, 278, 45539-45545.

69. ZHENG, Y. P., DING, C. X., BAI, J., MAK, A. F. T. & QIN, L. (2001) Measurement of the layered compressive properties of trypsin-treated articular cartilage: an ultrasound investigation, *Medical and Biological Engineering and Computing*, 39, 534-541.

70. LAURENT, D., WASVARY, J., YIN, J. et al. (2001) Quantitative and qualitative assessment of articular cartilage in the goat knee with magnetization transfer imaging, *Magnetic resonance imaging*, 19, 1279-1286.

71. REGATTE, R. R., KAUFMAN, J. H., NOYSZEWSKI, E. A. & REDDY, R. (1999) Sodium and proton MR properties of cartilage during compression, *Journal of Magnetic Resonance Imaging*, 10, 961-967.

72. INSKO, E. K., KAUFMAN, J. H., LEIGH, J. S. & REDDY, R. (1999) Sodium NMR evaluation of articular cartilage degradation, *Magnetic Resonance in Medicine*, 41, 30-34.

73. DUVVURI, U., KUDCHODKAR, S., REDDY, R. & LEIGH, J. S. (2002) T(1rho) relaxation can assess longitudinal proteoglycan loss from articular cartilage in vitro, *Osteoarthritis and Cartilage*, 10, 838-844.

74. NIEMINEN, M. T., TOYRAS, J., RIEPPO, J. et al. (2000) Quantitative MR microscopy of enzymatically degraded articular cartilage, *Magnetic Resonance in Medicine*, 43, 676-681.

75. CATERSON, B., FLANNERY, C. R., HUGHES, C. E. & LITTLE, C. B. (2000) Mechanisms involved in cartilage proteoglycan catabolism, *Matrix Biology*, 19, 333-344.

76. KIRALY, K., LAPVETELAINEN, T., AROKOSKI, J. et al. (1996) Application of selected cationic dyes for the semiquantitative estimation in histological sections of srticular cartilage by microspectrophotometry, *Histochemical Journal*, 28, 577-590.

77. ROSENBERG, L. (1971) Chemical Basis for the histological use of safranin O in the study of articular cartilage, *The Journal of Bone and Joint Surgery*, 53-A, 69-82.

78. CAMPLEJOHN, K. L. & ALLARD, S. A. (1987) Limitations of safranin O staining in proteoglycan-depleted cartilage demonstrated with monoclonal antibodies, *Histochemistry*, 89, 185-188.

79. KIVIRANTA, I., JURVELIN, J., TAMMI, M., SAAMANEN A, M. & HELMINEN, H. J. (1985) Microspectrophotometric quantitation of glycosaminoglycans in articular cartilage sections stained with Safranin O, *Histochemistry*, 82, 249-255.

80. PANULA, H. E., HYTTINEN, M. M., AROKOSKI, J. P. A. et al. (1998) Articular cartilage superficial zone collagen birefringence reduced and cartilage thickness increased before surface fibrillation in experimental osteoarthritis, *Annals of the Rheumatic Diseases*, 57, 237-245.

81. AROKOSKI, J. P. A., HYTTINEN, M. M., LAPVETELAINEN, T. et al. (1996) Decreased Birefringence of the superficial zone collagen network in the canine knee (stifle) articular cartilage after long distance running training, detected by quantitative polarised light microscopy, *Annals of the Rheumatic Diseases*, 55, 253-264.

82. XIA, Y., MOODY, J. B., BURTON-WURSTER, N. & LUST, G. (2001) Quantitative in situ correlation between microscopic MRI and polarised light

microscopy studies of articular cartilage, *Osteoarthritis and Cartilage*, 9, 393-406.

83.   SIPOS, T. & MERKEL, J. R. (1970) An effect of calcium ions on the activity, heat stability, and structure of trypsin, *Biochemistry*, 9, 2766-2775.

84.   SPILKER, R. L., SUH, J. K. & MOW, V. C. (1992) A finite element analysis of the indentation stress-relaxation response of linear biphasic articular cartilage, *Journal of Orthopaedic Research*, 8, 353-363.

85.   KIVIRANTA, I., TAMMI, M., JURVELIN, J., SAAMANEN A, M. & HELMINEN, H. (1984) Fixation, decalcification, and tissue processing effects on articular cartilage sections stained with Safranin O, *Histochemistry*, 82, 249-255.

86.   (2001) ABAQUS/Standard Theory Manual (Pawtucket, RI, USA, HKS Inc.).

87.   KEMPSON, G. E. (1973) Mechanical properties of articular cartilage, in: Freeman, M. A. R. (Ed.) *Adult Articular Cartilage*, pp. 171-227 (London, Pitman Medical).

88.   TRELOAR, L. R. G. (1970) *Introduction to polymer science* (London, Wykeham Publications).

89.   NGUYEN, T. (2005) Mathematical modelling of the biomechanical parameters of articular cartilage (Brisbane, QUT).

90.   BROOM, N. D. & POOLE, C. (1983) Articular cartilage collagens and proteoglycans, *Arthritis & Rheumatism*, 29, 1111-1119.

91.   CHIN-PURCELL, M. V. & LEWIS, J. L. (1996) Fracture of articular cartilage, *Journal of Biomechanical Engineering*, 118, 545-556.